

**Understanding the Causes of Streamflow Changes in the
Eurasian Arctic**

Jennifer C. Adam

A dissertation submitted in partial fulfillment of the requirements for the degree of

Doctor of Philosophy

University of Washington

2007

Program Authorized to Offer Degree:
Department of Civil and Environmental Engineering

UMI Number: 3293452

INFORMATION TO USERS

The quality of this reproduction is dependent upon the quality of the copy submitted. Broken or indistinct print, colored or poor quality illustrations and photographs, print bleed-through, substandard margins, and improper alignment can adversely affect reproduction.

In the unlikely event that the author did not send a complete manuscript and there are missing pages, these will be noted. Also, if unauthorized copyright material had to be removed, a note will indicate the deletion.

UMI[®]

UMI Microform 3293452

Copyright 2008 by ProQuest Information and Learning Company.

All rights reserved. This microform edition is protected against unauthorized copying under Title 17, United States Code.

ProQuest Information and Learning Company
300 North Zeeb Road
P.O. Box 1346
Ann Arbor, MI 48106-1346


University of Washington
Graduate School

This is to certify that I have examined this copy of a doctoral dissertation by

Jennifer C. Adam

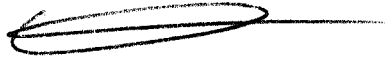
and have found that it is complete and satisfactory in all respects, and that any and all
revisions by the final examining committee have been made.

Chair of the Supervisory Committee:

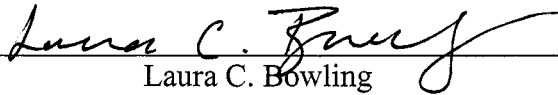


Dennis P. Lettenmaier

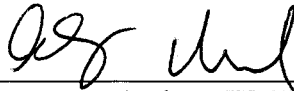
Reading Committee:



Dennis P. Lettenmaier



Laura C. Bowling



Andrew W. Wood

Date: 12/5/07

In presenting this dissertation in partial fulfillment of the requirements for the doctoral degree at the University of Washington, I agree that the Library shall make its copies freely available for inspection. I further agree that extensive copying of the dissertation is allowable only for scholarly purposes, consistent with "fair use" as prescribed in the U.S. Copyright Law. Requests for copying or reproduction of this dissertation may be referred to ProQuest Information and Learning, 300 N. Zeeb Rd, Ann Arbor, MI 48106-1346, 1-800-521-0600, to whom the author has granted "the right to reproduce and sell a) copies of the manuscript in microform and/or b) printed copies of the manuscript made from microform".

Signature: J. A. Selman

Date: 12/2/07

University of Washington

Abstract

Understanding the Causes of Streamflow Changes in the Eurasian Arctic

Jennifer C. Adam

Chair of the Supervisory Committee:
Professor Dennis P. Lettenmaier
Department of Civil and Environmental Engineering

Since the 1930s, streamflow from Eurasian rivers discharging to the Arctic Ocean has been increasing. Much of this change has been attributed to increased precipitation, but recent studies show inconsistencies in long-term streamflow and precipitation trends. Alternatively, these inconsistencies may imply a release of water from storage via permafrost degradation. For many of the Eurasian rivers, an increase in annual streamflow volume has been accompanied by a shift in seasonality. However, the signature of these changes in forcings and/or internal hydrologic dynamics are potentially confounded by the construction and operation of large reservoirs on many of the region's major rivers. A combination of data analysis and macroscale hydrological modeling are used to explore the controls on observed changes in annual and seasonal streamflow for several basins in the Eurasian Arctic. This work comprises three related studies. First, by comparing trends in observed streamflow and precipitation for a number of periods between 1936 and 2000, we find that streamflow trends generally exceeded precipitation trends for the permafrost basins (likely due to permafrost degradation), whereas precipitation trends generally exceeded streamflow trends over the non-permafrost basins (likely due to increased summer evapotranspiration). Second, using a physically-based reservoir model coupled to the Variable Infiltration Capacity (VIC) macroscale hydrology model, we find that, while reservoir construction and operation apparently had

little effect on long-term annual streamflow trends, they are responsible for much of the observed increases in winter and early spring streamflow from the regulated basins.

Third, by applying the VIC model over the Eurasian Arctic, we explored the roles of evapotranspiration, snowpack storage, and soil moisture storage (both liquid and frozen) in contributing to discrepancies between monthly precipitation and streamflow trends. Evapotranspiration influenced streamflow trends between May and September, while the effects of snowpack dynamics (the greatest contributor to seasonal streamflow changes) were greatest during the spring snowmelt and the fall onset of snowpack accumulation. The effects of soil moisture dynamics on streamflow changes were dominant during the snow-free season, although for some permafrost basins, an increase in active layer depth likely resulted in greater baseflow into the fall and early winter.

Table of Contents

	Page
List of Figures	iv
List of Tables	vi
1. Introduction.....	1
2. Strategy	5
3. Study Domain and Period	7
4. Application of New Precipitation and Reconstructed Streamflow Products to Streamflow Trend Attribution.....	10
4.1. Background and Chapter Goals	10
4.1.1. Potential Controls on Observed Northern Eurasian Streamflow Trends ...	10
4.1.1.1. Reservoir Construction and Operation.....	10
4.1.1.2. Precipitation Changes	11
4.1.1.3. Permafrost Changes	12
4.1.1.4. Evapotranspiration Changes	13
4.1.2. Problems with Precipitation Data used for Trend Attribution.....	14
4.1.3. Goals and New Contributions of this Chapter	14
4.2. Data Sources and Development of a New Precipitation Product	15
4.2.1. Data Sources	15
4.2.2. Development of Long-Term Precipitation Data	17
4.2.2.1. Choose Data Sources (Step 1).....	19
4.2.2.2. Process High-Quality Station Data (Step 2)	19
4.2.2.3. Combine High-Quality and High-Density Data Sets (Step 3).....	20
4.2.2.4. Incorporate Monthly Climatology (Step 4).....	21
4.2.3. Comparison of Precipitation and Streamflow Data Sets.....	22
4.3. Streamflow Trend Attribution: Methods	25
4.3.1. Overview of Analyses.....	25
4.3.2. Hypothesis Formulation via Temperature/Streamflow Correlation	28

4.3.3.	Trend Analysis.....	28
4.3.3.1.	Selection of Trend Test.....	28
4.3.3.2.	Multi-Period Trend Analysis of Individual Variables	32
4.4.	Streamflow Trend Attribution: Results and Discussion	34
4.4.1.	Hypothesis Formulation via Temperature/Streamflow Correlation	34
4.4.2.	Multi-Period Trend Analysis of Individual Variables	35
4.4.3.	Comparison of Precipitation and Streamflow Trends.....	39
4.5.	Conclusions.....	46
5.	Simulation of Reservoir Influences on Annual and Seasonal Changes.....	49
5.1.	Background and Chapter Goals	49
5.2.	Methods.....	51
5.2.1.	Selection of Reservoirs for Analysis.....	51
5.2.2.	Modeling Framework.....	54
5.2.2.1.	Hydrology and Routing Models.....	55
5.2.2.2.	Bias Correction	58
5.2.2.3.	Reservoir Model.....	59
5.2.3.	Development of the Reconstructed Product	65
5.2.4.	Trend Analysis.....	66
5.2.5.	Reservoir Model Error Propagation.....	67
5.3.	Results and Discussion	70
5.3.1.	Comparison of Simulated and Observed Reservoir Signatures.....	70
5.3.2.	Comparison to Other Reconstructed Streamflow Products	74
5.3.2.1.	Descriptions of Other Products.....	74
5.3.2.2.	Comparison of Reservoir Effects on Flow Seasonality	75
5.3.2.3.	Comparison of Reservoir Effects on Annual Flows	77
5.3.3.	Effect of Reservoirs on Streamflow Trends.....	81
5.3.4.	Reservoir Model Error Propagation.....	88
5.4.	Conclusions.....	94
6.	Application of a Macroscale Hydrologic Model to Streamflow Trend Attribution ..	96
6.1.	Background and Chapter Goals	96

6.1.1.	Observed Changes to Snow and Frozen Soils in the Eurasian Arctic	97
6.1.2.	The Importance of Snow and Frozen Soils to Hydrology	98
6.1.3.	Snow and Permafrost as Linkages between Climate and Hydrology	99
6.1.4.	Chapter Goal	100
6.2.	Data and Model.....	100
6.2.1.	Data Sources	100
6.2.2.	Modeling Framework.....	101
6.3.	Analytical Methods.....	104
6.3.1.	Water Balance Approach	104
6.3.2.	Trend Analysis	105
6.3.3.	Description of Tasks Performed	106
6.4.	Results and Discussion	108
6.4.1.	Initialization of Ground Ice Concentrations	108
6.4.2.	Selection of Periods and Basins for Trend Analysis.....	116
6.4.3.	Spatial Distributions of Annual Trends	120
6.4.4.	Monthly Trends in Each Water Balance Component	126
6.5.	Conclusions.....	133
7.	Conclusions.....	136
	References.....	142

List of Figures

Figure Number	Page
Figure 2.1 Potential relationships between the hypothesized controls on annual and seasonal streamflow changes and the “modulators”	5
Figure 3.1 Brown et al. (1998) permafrost distribution	9
Figure 4.1 High quality, long-term Groisman precipitation stations used for the trend adjustment procedure.....	18
Figure 4.2 Development of the UW data set.....	22
Figure 4.3 For each of the eleven study basins, basin-mean annual anomaly time-series and monthly climatologies for precipitation and streamflow.....	23
Figure 4.4 1931 to 2000 precipitation trend slope	26
Figure 4.5 Pearson product-moment correlation coefficient between basin-average time-series of streamflow and UDel temperature.	29
Figure 4.6 Histograms of the differences D_{ij}	33
Figure 4.7 Streamflow trend plots	38
Figure 4.8 Trend plots for UDel temperature and UW precipitation.....	40
Figure 4.9 UW precipitation trend plots.	41
Figure 4.10 Scatter-plots of trend slopes between streamflow and UW precipitation	43
Figure 5.1 Locations of operational reservoirs	52
Figure 5.2 Model coupling schematic.....	55
Figure 5.3 Theoretical shape used for the reservoir storage-area-depth relationships.	63
Figure 5.4 Comparison of observed and simulated monthly reservoir signatures.....	72
Figure 5.5 Comparison of simulated monthly reservoir signatures to the reservoir signatures inferred from three reconstructed streamflow products.....	76
Figure 5.6 Comparison of seasonal flows for four reconstructed streamflow products.....	78
Figure 5.7 Comparison of annual flows for four reconstructed streamflow products	79
Figure 5.8 Annual and mean monthly potential reservoir evaporation	80
Figure 5.9 Trends in annual basin-outlet streamflow	82
Figure 5.10 Trends in winter (DJF) basin-outlet streamflow.	85
Figure 5.11 Trends in spring (MAM) basin-outlet streamflow.	86
Figure 6.1 Excess ground ice concentrations.....	110
Figure 6.2 Scatter-plots of trend slopes between observed and simulated annual streamflow	113
Figure 6.3 Basin-mean annual anomaly time-series and monthly climatologies for observed and simulated streamflow.....	115
Figure 6.4 Observed streamflow trend plots.....	118
Figure 6.5 Simulated streamflow trend plots.....	119

Figure 6.6 1936 to 1999 trend slopes.....	122
Figure 6.7 1949-1999 trend slopes.....	123
Figure 6.8 1979-1999 trend slopes.....	124
Figure 6.9 Monthly and annual trend-test results for two “cold” basins and two “threshold” basins	127
Figure 6.10 Monthly and annual trend-test results for one “threshold” basin and three “warm” basins.....	128

List of Tables

Table Number	Page
Table 3.1 Attributes for the study basins	8
Table 3.2 Percent area coverage by each permafrost category	9
Table 4.1 Climate and streamflow data used for the trend attribution study	16
Table 4.2 Seasonal Mann-Kendall 1931 to 2000 trend significance and slope for precipitation.	25
Table 4.3 The number of periods for which trends are significant.....	37
Table 4.4 Summary of Section 4.4 results and hypothesized primary controls.....	42
Table 5.1 Characteristics of the large (> 1 km ³) operational reservoirs	53
Table 5.2 The ratio of the characteristic length to the depth of the reservoir	54
Table 5.3 Streamflow gauging stations used for bias correction of inflow	59
Table 5.4 Minimum flow released from each reservoir.....	61
Table 5.5 The calibration parameters for the monthly pricing distribution	66
Table 5.6 Streamflow gauging stations used for evaluation of the simulated reservoir signature on streamflow seasonality.....	67
Table 5.7 Comparison of observed and simulated mean annual streamflow	73
Table 5.8 Annual reservoir evaporation estimates.....	81
Table 5.9 The number of periods for which trends are significant.....	83
Table 5.10 Analysis details for the longest period with a trend significant at 99% for annual, seasonal, and monthly observed streamflows at the outlet of the Lena basin	87
Table 5.11 Analysis details for the longest period with a trend significant at 99% for annual, seasonal, and monthly observed streamflows at the outlet of the Yenisei basin.....	88
Table 5.12 Analysis details for the longest period with a trend significant at 99% for annual, seasonal, and monthly observed streamflows at the outlet of the Ob' basin.....	89
Table 5.13 RMSE values between simulated and SWMSA stage height.....	90
Table 5.14 Analysis of the error in reconstructed Yenisei River streamflow due to uncertainties in the reservoir simulations	91
Table 5.15 Analysis of the error in reconstructed Ob' River streamflow due to uncertainties in the reservoir simulations	92
Table 5.16 Analysis of the error in reconstructed Lena River streamflow due to uncertainties in the reservoir simulations	93
Table 6.1 Brown et al. (1998) permafrost classifications	107
Table 6.2 Multi-period trend-slope error statistics for each simulation.....	111
Table 6.3 The number of periods for which annual trends are significant at 90% for observed streamflow	112

Table 6.4 Error statistics for annual and monthly simulated streamflow.	114
Table 6.5 Thee period in which simulated streamflow captures the trends in observed streamflow	117

Acknowledgements

The author would like to thank the supervisory committee, Laura Bowling of Purdue University, Jessica Lundquist of the University of Washington, Gerard Roe of the University of Washington, Andy Wood of the University of Washington, and Daqing Yang of the University of Alaska, with special thanks to Dennis Lettenmaier for many years of support and mentoring. Thanks also to Svetlana Berezovskaya of the University of Alaska for her careful reading of the first paper, Ming Pan of Princeton University for his work on the implicit solver for the VIC frozen soils algorithm, Steve Burges of the University of Washington, Eric Wood of Princeton University, Ed Maurer of Santa Clara University, and Alan Hamlet of the University of Washington for thoughtful mentoring and advice. Thanks to the entire Land Surface Hydrology Group, especially Xiaogang Shi and Amanda Tan for their work in testing the sensitivity of the VIC model to changes in the frozen soils algorithm, Ted Bohn and George Thomas for support related to the VIC model, and Kostas Andreadis for help with programming and statistical techniques. Also thanks to Ingjerd Haddeland of the Norwegian Water Resources and Energy Directorate for support with the reservoir model. A final thanks to Patrick Adam for his gentle and unfailing support over the years.

1. Introduction

Annual average temperatures over the Arctic have increased at nearly twice the rate observed for the rest of the globe over the last few decades (ACIA 2005), and paleoclimate records indicate that recent temperatures in the Arctic are the highest they have been in the last 400 years (Overpeck et al. 1997). In response, system-wide changes have already occurred in the Arctic hydrological cycle (Hinzman et al. 2005). Changes in the terrestrial hydrologic cycle that are generally (but not uniformly) observed in the Arctic include increasing precipitation, increasing annual streamflow (for the Eurasian Arctic) and earlier spring snowmelt runoff, declining snow cover extent, negative glacier mass balances, thawing permafrost, changes to the volume and extent of wetlands and lakes, and shortening of the freeze season (ACIA 2005; Frauenfeld et al. 2004; Hinzman et al. 2005; Peterson et al. 2002; Serreze et al. 2000; Smith et al. 2005; Yoshikawa and Hinzman 2003).

Research interest in Arctic regions derives partly because of the region's sensitivity to global change, and partly because climate-induced changes in the Arctic have the potential to feed back to the global climate system. Several mechanisms have been identified, including the following that are particularly related to land surfaces processes. First, increasing freshwater flux to the Arctic Ocean (via increasing riverine inflow, increasing moisture convergence over the ocean, or glacier melt (Dyurgerov and Carter 2004)) may cause a weakening of the world ocean's thermohaline circulation (THC) by inhibiting deep water formation in the North Atlantic (Broecker 1997; Clark et al. 2002; Curry et al. 2003). Implications of THC changes include slowing the rate of warming (and perhaps even cooling) over the North Atlantic and northern Europe, and slowing of CO₂ transport to the deep ocean leading to increased global warming (ACIA 2005). Second, decreasing snow cover and sea ice extent, the northward migration of the tree-line, and deposition of soot on ice and snow all contribute towards decreasing the surface albedo, thus increasing the absorption of incoming radiation (ACIA 2005). The result is

an increase in the Earth's net radiation, a positive feedback response to a warming climate. Third, degradation of organic-rich permafrost in the high latitudes releases high concentrations of CH₄, a potent greenhouse gas, thereby intensifying the greenhouse effect (Walter et al. 2006).

Streamflow is an effective indicator of hydrologic change because it responds to the effects of climate change spatially over areas up to several million km², in the case of the largest Arctic rivers (White et al. 2007). The three largest Siberian watersheds (the Lena, Yenisei, and Ob') are responsible for more than 45% of the total freshwater discharge into the Arctic Ocean (Shiklomanov et al. 2000). Therefore, analysis of streamflow from these three basins alone can provide insight into how climate has affected and may continue to affect large-scale hydrological processes in the pan-Arctic basin. Combined annual streamflow volumes from the six largest Eurasian basins (of which the Lena, Yenisei, and Ob' are the largest) increased by approximately 7% (or $2.0 \pm 0.4 \text{ km}^3 \text{ year}^{-2}$) between 1936 and 1999 (Peterson et al. 2002; Shiklomanov et al. 2006) and by approximately 10% (or $5.34 \text{ km}^3 \text{ year}^{-2}$) between 1964 and 2000 (McClelland et al. 2006). Changes in annual runoff volume have been accompanied by shifts in seasonal runoff timing. In general, the most significant increases have been observed during the cold season, which is also the season of low flow (October to April), while the spring snowmelt peak has shifted earlier (Georgievsky et al. 1996; Yang et al. 2004a; Yang et al. 2004b; Yang et al. 2002), although this is not the case for all rivers. Changes in other seasons are generally less pronounced; for the Lena and Ob' river basins, summer discharges have slightly increased, whereas fall discharges have slightly decreased (Yang et al. 2004a; Yang et al. 2002; Ye et al. 2003).

Notwithstanding the potential for observed Arctic river discharge changes to affect global climate, there is little current understanding of the primary controls on Arctic river streamflow change and variability, as evidenced by conflicting explanations for observed historical changes (Adam and Lettenmaier 2007b; Berezovskaya et al. 2004;

Berezovskaya et al. 2005; McClelland et al. 2004; Nijssen et al. 2001; Pavelsky and Smith 2006; Rawlins et al. 2006; Smith et al. 2007; Wu et al. 2005; Yang et al. 2003; Ye et al. 2004). Potential controls on streamflow trends include changes in precipitation; changes in permafrost, soil moisture storage, snowpack storage, and evapotranspiration in response to climatic change; and direct human influences, such as the construction and operation of hydropower reservoirs (see discussion in Section 4.1.1). Knowledge of these controls would arguably facilitate better parameterization of key physical processes in land surface models that represent runoff generation processes in global and regional climate models, and in turn should improve the predictability of climate feedback processes.

The overarching goal of this research is to evaluate the ways that precipitation and temperature changes have affected long-term changes in annual and seasonal streamflow over the Eurasian Arctic, and to identify the roles that evapotranspiration, soil moisture storage, and snowpack storage have played in modulating these effects. The specific science questions related to this goal are:

- To what extent are long-term trends in annual and seasonal streamflow due to the construction and operation of reservoirs for hydropower production? Over what seasons and periods have observed streamflow changes been a result of direct human influence versus climatic change?
- To what extent can long-term trends in Eurasian Arctic annual streamflow be explained by changes in precipitation and what are the most likely explanations for discrepancies between streamflow and precipitation trends, e.g. changes in evapotranspiration (ET) and/or changes in soil moisture dynamics (such as permafrost degradation)?

- Over what regions of the Eurasian Arctic is streamflow most sensitive to temperature versus precipitation changes and how does this relate to regional climatic regime and the extent of permafrost in the basin?
- What are the roles of frozen ground processes in modulating the effects of climate change on streamflow generation? In particular, how does the presence of permafrost affect long-term trends in annual and seasonal streamflow, and how does this relate to the type of permafrost in a basin (continuous vs. discontinuous)?
- How have snow processes modulated the interactions between climate and streamflow generation, particularly via effects of snowpack accumulation and melt? In what seasons have precipitation versus temperature changes most influenced the effects of snowpack storage on streamflow generation?

We focus our study on the Eurasian portion of the pan-Arctic drainage basin because the most significant increases in river discharge to the Arctic Ocean have been observed there (McClelland et al. 2006; Peterson et al. 2002), because there is a relatively consistent and long-term set of in-situ observations (for streamflow, climate, and ground conditions) for the region, and because of a large east-west temperature gradient and corresponding gradient in permafrost fraction across the region (Adam and Lettenmaier 2007b; Brown et al. 1998).

2. Strategy

Figure 2.1 summarizes what we hypothesize to be the most important contributors to observed streamflow changes. The “controls” on annual and seasonal streamflow changes are divided into two groups, climate and human. For climate, we explore the roles of precipitation and surface air temperature, whereas for human, we explore only the effects of reservoirs. We also consider the influences of evapotranspiration, the snowpack, and near-surface groundwater storage in modulating the effects of the “controls” on streamflow. For example, changes in air temperature only affect streamflow via the “modulators”, i.e. by affecting snowpack accumulation and melt, the freeze and thaw of groundwater, and evapotranspiration.

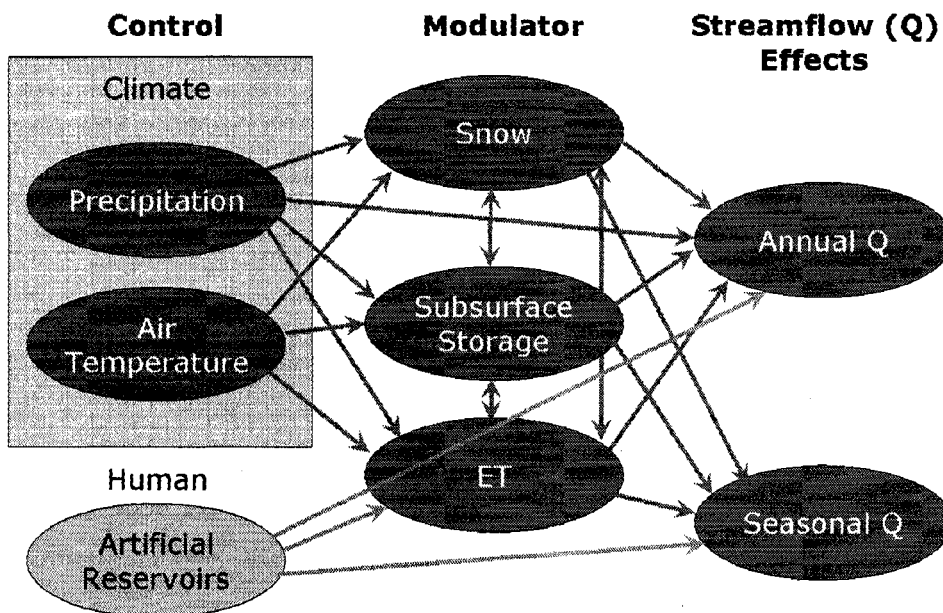


Figure 2.1 Potential relationships between the hypothesized controls (left column) on annual and seasonal streamflow changes (right column) and the “modulators” (middle column), i.e. elements of the terrestrial water balance that may influence how streamflow is affected by the controls. The arrows related only to reservoirs are shaded in gray.

In Chapter 4 (Adam and Lettenmaier 2007b), we apply newly developed reconstructed streamflow and precipitation data over the Eurasian Arctic to evaluate, for a comprehensive range of time periods basins, the extent to which long-term changes in annual streamflow can be explained by changes in precipitation. We then use these results to develop a set of hypotheses explaining the mechanisms that would cause streamflow trends to be inconsistent with precipitation trends given the observed increases in air temperature. We document the development of the new gridded precipitation product over the Eurasian Arctic, for which several adjustments have been made to improve the monthly averages and the long-term variability of existing gridded products.

In Chapter 5 (Adam et al. 2007), we apply a physically-based reservoir model to investigate the effects of reservoirs on streamflow over the Lena, Yenisei, and Ob' River basins, including the effects of initial reservoir filling, reservoir operations, and increased evaporation – i.e., the arrows shaded in gray in Figure 2.1. Also, we develop reconstructed streamflow time series, in which the effects of the reservoirs are minimized, for the outlets of the regulated basins.

In Chapter 6 (Adam and Lettenmaier 2007a), we apply the Variable Infiltration Capacity (VIC) macroscale hydrologic model (Cherkauer and Lettenmaier 1999; Liang et al. 1994) to explore the climate-induced changes to annual and seasonal streamflow and the roles of the modulators, particularly those of the snowpack and frozen ground. We document several new developments to the VIC model frozen soils algorithm to improve simulation of permafrost dynamics.

3. Study Domain and Period

Figure 3.1 shows our northern Eurasian study basins, all of which discharge to the Arctic Ocean. We selected three primary study basins (outlined in black in Figure 3.1) and eight secondary basins (outlined in red in Figure 3.1). Basin attributes are listed in Table 3.1. Each basin is assigned an ID and reference name (columns 1 and 3, respectively, in Table 3.1), and hereafter the basins are indicated by these identifiers. The basins were selected according to the following criteria: (1) significant streamflow changes observed at the basin outlet, (2) the availability of a long-term stream gauge record, and (3) a basin area exceeding 10^5 km². Furthermore, we sought to choose an even distribution of basins across the study domain. Note that there is a strong east to west temperature gradient across northern Eurasia which is reflected in the permafrost distribution -- i.e., continuous permafrost in the east, threshold (discontinuous, sporadic, and isolated) permafrost in central Siberia, and seasonally frozen soil in the west (Figure 3.1 and Table 3.2). The basins are categorized into one of three temperature regimes (column 10 of Table 3.1), “cold” for basins with mean temperatures less than -8 °C and underlain by at least 80% continuous permafrost, “threshold” for basins with mean annual temperatures greater than -8 °C and less than -2 °C and underlain by between 30% and 80% continuous permafrost, and “warm” for basins with mean temperatures greater than -2 °C and underlain by less than 30% continuous permafrost. Each basin’s response to climatic changes will be assessed in the context of these temperature regimes, to determine whether basin response to climatic change can be predicted according to mean climate and permafrost state.

Changes across these basins have been documented and studied most often between 1936 and 2000 (Berezovskaya et al. 2004; McClelland et al. 2004; Peterson et al. 2002). To develop an understanding of how the controls on streamflow trends vary in time, we analyze the consistency between precipitation and streamflow trends for a large number of periods between these years. These periods vary with start year and period length.

Selection of the analysis periods is discussed in Section 4.3.3.2, Section 5.2.4, and Section 6.3.2, for Chapters 4, 5, and 6, respectively.

Table 3.1 Attributes for the three primary study basins (basins 1 through 3) and the eight secondary basins and sub-basins (basins 8 through 11). Note that most of the secondary basins are nested inside the primary basins, i.e. as indicated by the basin reference name in column 3. Also, note that sub-basin 6 is nested inside sub-basin 5). Period of gauging record, basin area, and mean annual streamflow (for the period of gauging record) are from the R-ArcticNET v3.0 data set (Lammers and Shiklomanov 2000); reservoir information is from McClelland et al. (2004). Basin-average 1930-2000 mean-annual precipitation and temperature are from the Adam and Lettenmaier (2007b) (Chapter 4) and Willmott and Matsuura (2005) data sets, respectively. The temperature regime of each basin relates to the type of permafrost in the basin, primarily continuous permafrost in “cold” basins, non-continuous permafrost in “threshold” basins, and seasonally frozen soil in “warm” basins.

ID	Streamflow Gauging Station	Basin Reference Name	Period of Record	Area (10 ⁶ km ²)	Large Dams	Streamflow (mm year ⁻¹)	Precipitation (mm year ⁻¹)	Temperature (°C)	Regime
1	Lena At Kusun	Lena	1934-2000	2.43	1	217	432	-9.98	Cold
2	Yenisei At Igarka	Yeni	1936-1999	2.44	8	238	570	-5.83	Threshold
3	Ob At Salekhard	Ob	1930-1999	2.43	3	163	533	-0.93	Warm
4	Aldan At Verkhoyanskiy Perevoz	Lena1	1942-1999	0.70	0	240	479	-10.52	Cold
5	Lena At Tabaga	Lena2	1936-1999	0.90	0	247	485	-7.5	Threshold
6	Lena at Krestovskoe	Lena3	1936-1999	0.44	0	299	529	-7.06	Threshold
7	Selenga At Novoselenginsk	Yeni1	1932-1997	0.36	0	65	422	-2.94	Threshold
8	Yenisei at Kyizyil	Yeni2	1926-1999	0.12	0	280	752	-7.3	Threshold
9	Chulym At Baturino	Ob1	1936-2000	0.13	0	189	514	-0.46	Warm
10	Irtish At Tobol'sk	Ob2	1891-1999	0.96	2	70	462	0.66	Warm
11	Severnaya Dvina At Ust'-Pinega	SDvina	1881-1999	0.35	0	290	653	0.43	Warm

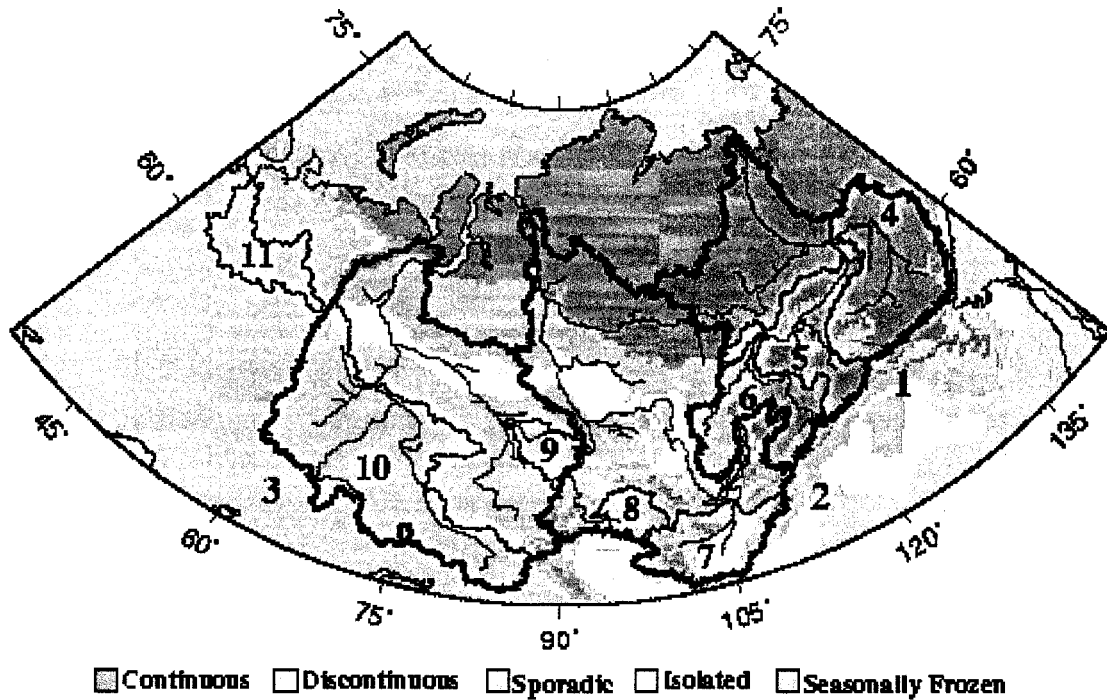


Figure 3.1 Brown et al. (1998) permafrost distribution. Permafrost category is defined by the percent of area underlain by permafrost, i.e. continuous: 90-100%, discontinuous: 50-90%, sporadic: 10-50%, and isolated: less than 10%. Primary study basins are outlined in black while the secondary basin and sub-basins are outlined in red. Note that basin 6 is nested inside basin 5 (which is nested inside basin 1). Basin attributes are listed in Table 3.1. Basins delineations are according to the HYDRO1k digital data set.

Table 3.2 Percent area coverage by each permafrost category (calculated using the Brown et al. (1998) data set) for each study basin. Permafrost category definitions are listed in the Figure 3.1 caption.

ID	Basin Reference Name	Permafrost				
		All Types	Continuous	Discontinuous	Sporadic	Isolated
1	Lena	100%	80%	11%	6%	3%
2	Yeni	89%	33%	12%	18%	26%
3	Ob	27%	2%	4%	9%	11%
4	Lena1	100%	89%	10%	1%	0%
5	Lena2	100%	55%	23%	16%	7%
6	Lena3	100%	45%	15%	30%	10%
7	Yeni1	100%	30%	10%	21%	39%
8	Yeni2	100%	32%	55%	6%	6%
9	Ob1	11%	0%	0%	0%	11%
10	Ob2	3%	0%	0%	2%	1%
11	SDvina	0%	0%	0%	0%	0%

4. Application of New Precipitation and Reconstructed Streamflow Products to Streamflow Trend Attribution

This chapter summarizes and excerpts research submitted to Journal of Climate as:

Adam, J.C., and D.O. Lettenmaier, 2007: Application of new precipitation and reconstructed streamflow products to streamflow trend attribution in northern Eurasia, *J. of Climate* (accepted).

4.1. Background and Chapter Goals

4.1.1. Potential Controls on Observed Northern Eurasian Streamflow Trends

Recent research has focused on any or a combination of the following potential controls on observed Eurasian Arctic streamflow trends: (a) human effects (primarily through reservoir construction and regulations); (b) increased northward transport of moisture (as a result of an intensification of the hydrologic cycle); (c) release of stored frozen ground water via permafrost degradation; and (d) factors affecting evapotranspiration (*ET*).

Recent work in each of these areas is reviewed briefly below.

4.1.1.1. Reservoir Construction and Operation

Beginning in the mid-1950s, the former Soviet Union constructed several major hydroelectric dams in the large northern Eurasian basins (McClelland et al. 2004). For maximum hydropower production throughout the year, the reservoirs act to diminish the differences in streamflow between seasons by storing streamflow during the spring and summer high flow seasons and releasing additional flow during the winter low-flow season. The effects of reservoirs on long-term trends at the basin outlets have been analyzed using a variety of approaches. McClelland et al. (2004), Ye et al. (2003), and Yang et al. (2004b) used statistical techniques to develop reconstructed streamflow data,

in which the effects of reservoirs were removed from basin-outlet streamflow. Using these products, they concluded that estimates of natural river discharge trends at the outlets of these river basins tend to be underestimated in the summer and overestimated in the fall and winter as a result of reservoir operations. Furthermore, McClelland et al. (2004) conclude that reservoir operations cannot be responsible for the observed increases in annual streamflow, and may have even reduced annual streamflow volume, either through groundwater storage dynamics or increases in evaporation due to increased surface water storage. Using a reservoir system model that determines reservoir releases by maximizing hydropower production for each operational year, Adam et al. (2007) (Chapter 5) show similar effects of reservoirs on long-term streamflow trends. Although the annual effects are small, seasonal effects are large. For instance, Adam et al. (2007) (Chapter 5) show that at the outlet of the Lena basin, reservoirs account for approximately 80% and 30% of the observed 1938 to 1998 winter and spring streamflow trends, respectively. At the outlet of the Yenisei basin, reservoirs account for 100%, 40%, and 60% to 100% of the observed winter, spring, and late summer to early fall streamflow trends, respectively, and at the outlet of the Ob' basin, reservoirs account for 25% to 100% of the observed streamflow trends in the winter and early spring.

4.1.1.2. Precipitation Changes

Various coupled and uncoupled land-atmosphere modeling studies have predicted increased Arctic river discharge due to increased northward atmospheric moisture transport (Arnell 2005; Lawrence and Slater 2005; Manabe and Stouffer 1980; Miller and Russell 1992; Nijssen et al. 2001; Wu et al. 2005). Although precipitation exerts a primary control on streamflow, there is little observational evidence that precipitation is the sole or even primary driver of observed trends for many of the basins. Berezovskaya et al. (2004) compared basin-outlet discharge to basin-average precipitation for the largest basins (the Ob', Yenisei, and Lena) for the period of 1950 to 2000. Their results show little consistency between precipitation and streamflow trends. A positive trend in Lena streamflow is accompanied by only a weak precipitation increase; Yenisei

discharge increases are accompanied by mostly negative precipitation trends; and insignificant trends in both discharge and precipitation are observed for the Ob'. Pavelsky and Smith (2006) performed a similar analysis but at a finer spatial resolution, examining the compatibility of long-term streamflow and precipitation trends for 66 river basins in northern Eurasia. Of these basins, 40 exhibited statistically significant streamflow trends, and 29 of these also exhibited statistically significant precipitation trends (22 increasing, and 7 decreasing). For these 29 basins, agreement between precipitation and discharge trends was between 35% and 62%. Pavelsky and Smith (2006) conclude that precipitation does play an important role for many of the basins, but not all of them, and may or may not be the sole mechanism.

4.1.1.3. Permafrost Changes

Russian soil temperature observations indicate that permafrost active layer depth has deepened by approximately 20 cm on average throughout Siberian permafrost regions between 1956 and 1990 (Frauenfeld et al. 2004). Zhang et al. (2003) hypothesize that climate-induced changes to permafrost could lead to changes in both streamflow seasonality and annual volumes. Thickening of the active layer leads to an increase in potential summer and fall liquid ground water storage while the delaying of active layer freeze-up leads to the potential for subsurface water to contribute to streamflow into the winter (Serreze et al. 2002; Yang et al. 2002; Ye et al. 2004; Zhang et al. 2003). Annual streamflow is augmented by the thawing and release of excess ground ice (Frauenfeld et al. 2004; Zhang et al. 2003). Although the sensitivity of winter streamflow to permafrost thaw has been demonstrated by both models and observed data (Savelieva et al. 2000; Van der Linden et al. 2003; Zhang et al. 2003), the sensitivity of annual streamflow to permafrost thaw is unresolved. McClelland et al. (2004) argue that, even if the seasonality of streamflow is affected by permafrost thaw, melting of ground ice cannot produce enough excess water to account for the observed increase in annual streamflow. They demonstrate this by back-calculating the depth of permafrost thaw needed to

produce the observed annual streamflow increase (by allowing all melted ice to drain completely from the soil and contribute to runoff). They conclude that permafrost, as the only agent of change, would have needed to thaw a minimum of four meters uniformly across the six largest Eurasian Arctic watersheds, which they argue is unrealistic. In contrast, Zhang et al. (2003) used ground ice data to estimate that an increase in active layer depth of 30 cm would produce sufficient water to account for the apparent imbalance in the water budget (precipitation minus streamflow minus *ET*). One possible explanation for the discrepancy in these two estimates is that Zhang et al. (2003) considered the potential of ground ice melt to account for this water budget imbalance, whereas McClelland et al. (2004) evaluated the ability of ground ice melt to account for all of the streamflow increase.

4.1.1.4. Evapotranspiration Changes

The role of *ET* changes is, perhaps, the least understood factor, largely because direct *ET* observations are essentially non-existent in the region. Observations that may yield insight into *ET* trends, such as pan evaporation estimates, lead to further uncertainties. (For example, see Barnett et al. (2005) for a discussion of the "evaporation paradox". In general, evaporation measured using evaporation pans has been decreasing over the last few decades, but this may be indicative either of decreasing actual evaporation or it could be indicative of increasing actual evaporation, which alters the humidity regime surrounding the evaporation pan). Although increased precipitation and temperature would result in an increase in *ET*, the possibility exists that, even with warming, annual *ET* trends could be negative, i.e. greatest warming occurs during the winter when there is less liquid water available for evaporation. McClelland et al. (2004) speculate that thawing permafrost could reduce *ET*, if lower water tables are a result of a thickening active layer. Also, Rawlins et al. (2006) suggest that an increase in solid precipitation with respect to liquid precipitation (as occurred over much of the region between the mid-1930s and late-1950s) could result in less *ET* because a larger proportion of solid precipitation will contribute directly to runoff (during the snowmelt period when the

ground is saturated), especially in regions underlain by permafrost where infiltration is limited. They document large solid precipitation increases, which are accompanied by liquid precipitation decreases, from the mid-1930s to the late-1950s primarily across north-central Eurasia, areas that are predominantly underlain by permafrost.

4.1.2. Problems with Precipitation Data used for Trend Attribution

Trend attribution for northern Eurasian rivers is complicated by the paucity, sparseness, and poor quality of observation data in Arctic areas, particularly that of precipitation. Berezovskaya et al. (2004) suggest that inconsistencies between observed precipitation and streamflow trends could be a result of data quality, primarily that of the gridded precipitation data. Known problems include: sparse and non-uniform station networks (Adam and Lettenmaier 2003; Serreze et al. 2003), temporally inhomogeneous measurement and pre-processing techniques (Groisman 2005; Groisman and Rankova 2001; Groisman et al. 1991; Mekis and Hogg 1999), orographic effects which are not well represented in station data (Adam et al. 2006), large precipitation gauge measurement biases (Adam and Lettenmaier 2003; Groisman et al. 1991; Yang et al. 2005), effects of climate on under-catch adjustments (Forland and Hanssen-Bauer 2000; Yang et al. 2005), temporally inconsistent station networks (Hamlet and Lettenmaier 2005; Rawlins et al. 2006), and a decline in observing stations since 1990 due to station closure (Serreze et al. 2003; Shiklomanov et al. 2002). These biases are discussed in more detail in Section 4.2.2.

4.1.3. Goals and New Contributions of this Chapter

The goals of this study are twofold. The first is to describe a new gridded precipitation product for the Eurasian Arctic which includes adjustments that make it more suitable for evaluation of long-term trends. The second is to apply the new precipitation product as well as observed temperature, observed streamflow, and new reconstructed streamflow data to investigate the most probable contributors to observed streamflow trends over the

Eurasian Arctic. More specifically, we apply the new reconstructed streamflow data to isolate the effects of reservoir operations on long-term trends in streamflow from other causes. Following this, we apply the new precipitation data to identify when and where precipitation trends are inconsistent with streamflow trends, and we develop a hypothesis to explain how temperature changes may account for these inconsistencies.

This study builds upon previous work, particularly that of Berezovskaya et al. (2004) and Pavelsky and Smith (2006), in which we evaluate the extent to which precipitation changes can account for observed streamflow trends. In doing so, this paper makes the following contributions:

- 1) We introduce and utilize a new gridded precipitation product for the Eurasian Arctic with adjustments to improve our estimation of long-term trends.
- 2) We utilize the reconstructed streamflow data of Adam et al. (2007) (Chapter 5) to isolate the effects of reservoirs on long-term streamflow trends.
- 3) We analyze the consistency between precipitation and streamflow trends on a temporally-varying basis, which allows us to define periods when precipitation is the likely cause of streamflow changes and periods when other factors are also likely playing a role.

4.2. Data Sources and Development of a New Precipitation Product

4.2.1. Data Sources

Precipitation, temperature, and streamflow data used in this study are summarized in Table 4.1. Hereafter, the data sets will be referenced using their respective data set IDs (see column 2 of Table 4.1). Among these are two new products: (1) our bias-adjusted gridded precipitation product (UW), the development of which is described in Section 4.2.2 (and compared to existing products in Section 4.2.3); and (2) the Adam et al. (2007) (Chapter 5) reconstructed streamflow product (Recon), for which the effects of manmade reservoirs have been removed. This product was created by running a coupled

Table 4.1 Climate and streamflow data used for the trend attribution study. All gridded products are in 0.5° geographic projection.

Variable	Data Set ID	Reference	Period	Adjustments	Application
Gridded Precipitation and Temperature Monthly Time-Series	UDeI	Willmott and Matsuura (2005)	1930-2004	none	(1) precipitation: used for development of UW data (Section 4.2); (2) temperature: streamflow/temperature correlation analysis (Section 4.4.1); (3) temperature: temperature trend analysis (Section 4.4.2)
Bias-Adjusted Daily Precipitation Station Data	Groisman	Groisman (2005)	varying periods between 1891 and 2001	(1) homogenized for wetting bias correction changes and rain gauge changes (Groisman and Rankova 2001); (2) temporally-varying gauge under-catch corrections (Bogdanova et al. 2002a; 2002b)	(1) used for development of UW data (Section 4.2)
Gridded Precipitation Climatology	AdamClim	Adam and Lettenmaier (2003); Adam et al. (2006)	1979-1999	(1) mean monthly adjustments for gauge under-catch; (2) mean annual adjustments for orographic effects on gridding	(1) used for development of UW data (Section 4.2)
Bias-Adjusted Gridded Precipitation Monthly Time-Series	UW	(this paper, described in Section 4.2)	1930-2000	(1) low frequency variability constrained by Groisman station data; (2) climatology adjustments of AdamClim	(1) precipitation trend analysis (Section 4.4.2); (2) precipitation/streamflow comparison (Section 4.4.3)
Observed Monthly Streamflow	Obs	Lammers and Shiklomanov (2000)	(see Table 3.1)	none	(1) streamflow trend analysis (Section 4.4.2); (2) precipitation/streamflow comparison (Section 4.4.3)
Reconstructed Monthly Streamflow	Recon	Adam et al. (2007) (Chapter 5)	1936-2000	effects of reservoirs removed	for regulated basins only: (1) streamflow trend analysis (Section 4.4.2); (2) precipitation/streamflow comparison (Section 4.4.3)

hydrology/river channel model with and without a coupled reservoir model, wherein the reservoir model calculates historical reservoir storage and release by maximizing

hydropower production (Haddeland et al. 2006a; Haddeland et al. 2006b; Haddeland et al. 2007). At the outlet of each of the regulated basins (see column 6 of Table 3.1), simulated streamflow without the reservoir model was subtracted from simulated streamflow with the reservoir model. This produced a time-series of reservoir influences which were then subtracted from the observed basin-outlet discharge, constraining the reconstructed flow to be identical to observed flow before reservoir construction. Adam et al. (2007) (Chapter 5) document this product and compare it to other reconstructed streamflow products (McClelland et al. 2004; Yang et al. 2004b; Ye et al. 2003).

4.2.2. Development of Long-Term Precipitation Data

The inconsistency between precipitation and streamflow trends may partly be a result of temporal biases in the gridded precipitation products. Trend biases can result from biases in the station data themselves or from the gridding procedure. Trend biases in the source station data may be a result of a change in precipitation gauge type, a change in the environment surrounding the station, or a change in the way the data were processed and archived, such as occurred in the way that the Soviet Government handled wetting biases in the mid-1960s (Groisman and Rankova 2001). A change in climate can also incur a bias in the temporal homogeneity of station precipitation because the degree to which a gauge underestimates precipitation is a function of climate (Forland and Hanssen-Bauer 2000; Yang et al. 2005). Temporal biases in gridded precipitation can also be caused by changes in the station network, i.e. over the Eurasian Arctic, station density increased up to about 1970 and decreased in the 1990s (Shiklomanov et al. 2002). Rawlins et al. (2006) suggest that, averaged over the Eurasian Arctic, gridded precipitation bias is well over $+10 \text{ mm yr}^{-1}$ in the 1930s network as compared to the 1972 network when station density was greatest and, therefore, most representative of true spatially-averaged precipitation.

Using the method of Hamlet and Lettenmaier (2005), we produce the UW monthly gridded precipitation product for the Eurasian Arctic domain (defined as Eurasian land

areas that discharge freshwater to the Arctic Ocean; the shaded regions in Figure 4.1). The Hamlet and Lettenmaier method combines the best features of three existing products: (1) the high-frequency spatial and temporal variability of the UDel gridded data set that uses all available stations for each month; (2) the low-frequency spatial and temporal variability of long-term stations selected from the Groisman bias-adjusted precipitation data set; and (3) the mean monthly climatology of the AdamClim data set that incorporates bias-adjustments for gauge under-catch and orographic effects. The steps in the bias adjustment procedure are outlined below.

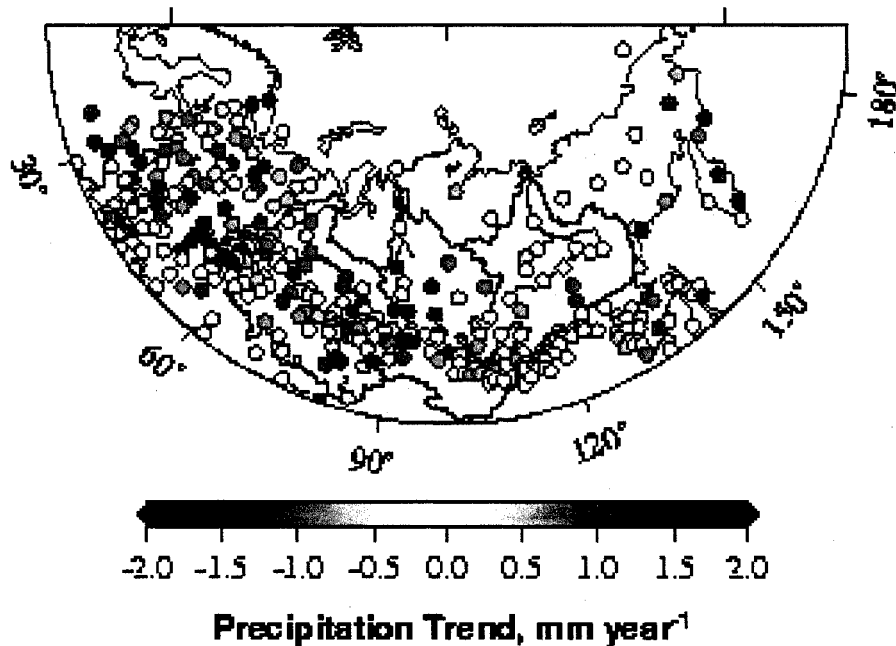


Figure 4.1 High quality, long-term Groisman precipitation stations used for the Hamlet and Lettenmaier (2005) trend adjustment procedure. The station color represents the 1931 to 2000 precipitation trend slope (calculated according to Hirsch et al. (1982) for the seasonal Mann-Kendall test, see Section 4.3.3.1). The spatial domain of our gridded precipitation product is given by the areas shaded in gray, e.g. the regions that discharge streamflow to the Arctic Ocean. Of the 410 stations shown, 210 fall within this domain.

4.2.2.1. Choose Data Sources (Step 1)

The data set is a combination of three products:

(1) *High-density gridded product for short-term variability.* We selected the UDel monthly time-series, a data set that makes use of most of the available station data (and therefore is associated with a relatively high-density station network, but is also susceptible to spurious trends due to changes in the gauging network).

(2) *High-quality station data for long-term variability.* We used the Groisman daily station data, aggregated to monthly for this analysis. These station data have been temporally homogenized for changes in precipitation gauge type as well as a change in the way that wetting biases were accounted for by the Soviet Government using the method of Groisman and Rankova (2001). Furthermore, these data incorporate temporally-varying corrections for wind-induced precipitation under-catch using the method of Bogdanova et al. (2002a; 2002b). Because we only select stations from the Groisman data set that cover the majority of the period, we effectively remove the spurious trends incurred by changes in station density with time. A further consequence of this procedure is that the Groisman adjustments made for temporal inhomogeneities are also incorporated into the low-frequency variability of the final gridded UW product.

(3) *Monthly climatology (AdamClim).* We used the climatology of Adam et al. (2006) in which the 0.5° grids have been adjusted for orographic effects. This data set incorporates the mean monthly adjustments of Adam and Lettenmaier (2003) for gauge under-catch biases.

4.2.2.2. Process High-Quality Station Data (Step 2)

The trend adjustment method is dependent on the high-quality station network (data set #2 above) being consistent for the entire study period, therefore it would be ideal to choose stations that have 100% temporal coverage between 1930 and 2000.

Unfortunately considerable gaps exist in many of the stations, so we relaxed the coverage requirement, choosing stations that had 75% temporal coverage between 1937 and 1996. This resulted in a total of 410 Russian stations, 210 of which were within our domain.

Figure 4.1 shows the distribution of the selected stations and the 1931 to 2000 precipitation trend magnitude for each station (see Section 4.3.3.1 for a description of the trend calculation). The results of this analysis may be questionable over regions with sparse station density, such as over north-eastern Siberia, although these are the regions where there are few inferred long-term changes in precipitation. Therefore, although there is a sparse distribution of Groisman stations over these regions, the observed spatial coherency in long-term trends suggests that the large-scale features of low-frequency precipitation variability will be captured by the UW data set.

We filled record gaps, using data from nearest neighbor stations, via the maintenance of variance extension type two method (MOVE.2) (Hirsch 1982). The objective of MOVE.2 is to maintain sample mean and variance, and is an alternative to linear regression. Linear regression has the objective of minimizing the square of the errors of the estimated values, but underestimates sample variance (Hirsch 1982). This approach is reasonable if the gaps are distributed throughout the record period, but is problematic if used for record extension. Following gap filling, the stations were gridded to 0.5° using the Synagraphic Mapping System (SYMAP) of Shepard (1984).

4.2.2.3. Combine High-Quality and High-Density Data Sets (Step 3)

The motivation of our approach is to maintain as much spatial information from the high-density gridded product as possible while constraining the long-term variability to match that of the less dense high-quality gridded data (Hamlet and Lettenmaier 2005). Using a Butterworth filter (Hamming 1989), the time-series for both the high-quality and high-density gridded data were temporally smoothed for each month individually (e.g. all Januaries between 1930 and 2000). We rescaled the unsmoothed high-density series by the ratios of the smoothed high-quality series to the smoothed high-density series.

4.2.2.4. *Incorporate Monthly Climatology (Step 4)*

For the period overlapping with the AdamClim monthly climatology (1979-1999), mean monthly differences were computed between the monthly AdamClim climatology and the product from step 3, and these differences were added to the full-length monthly time-series of the product from step 3. In cases where the adjusted monthly value was negative, the value was set to zero. We found that adding the difference of the climatologies, rather than rescaling by the ratio of the climatologies, allowed for the preservation of the desired long-term variability in the final product. This is because this method preserves the variance of the precipitation time series from the high-quality gridded product.

The final UW product is a 1930 to 2000 monthly precipitation time-series that includes adjustment for spurious trends due to a changing gauge network in time, as well as climatological adjustments for orographic effects on gridding and gauge-catch biases. The UW product has the low-frequency spatial and temporal characteristics of the low-density high-quality gridded product and the high-frequency spatial and temporal characteristics of the high-density low-quality UDel product. The results of this approach are summarized in Figure 4.2 which shows the unsmoothed and smoothed annual time-series for the high-density (black line), high-quality (dotted line), and final (dashed line) precipitation products, averaged over the three primary study basins. As desired, the smoothed time-series of the final product matches that of the smoothed high-quality product and the final amounts reflect adjustments for biases in gauge under-catch and orographic effects on gridding (both of which can result in considerable underestimation of precipitation in cold and/or mountainous regions, see Adam and Lettenmaier (2003) and Adam et al. (2006)).

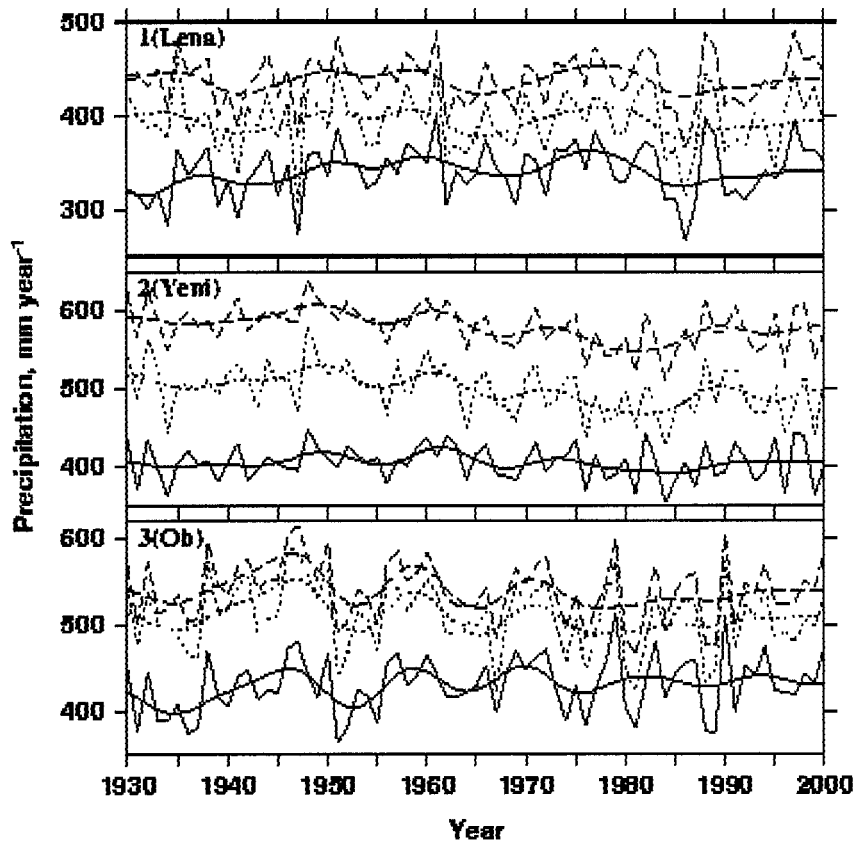


Figure 4.2 Development of the UW data set (dashed line) is via combination of three other gridded products: (1) the UDel product for short-term variability (solid line), (2) the gridded Groisman station data for long-term variability (dotted line), and (3) the AdamClim monthly climatology (not shown). For each data set are shown both the smoothed (using a Butterworth Filter; Hamming (1989)) and unsmoothed annual time-series. Although the procedure was performed on a grid-cell basis, results shown here are basin averages over the Lena, Yenisei, and Ob'.

4.2.3. Comparison of Precipitation and Streamflow Data Sets

Figure 4.3 shows the annual anomaly time-series and monthly climatologies for the UDel and UW precipitation products and the observed and reconstructed streamflow products. The water year, defined as October to September, was used to calculate annual amounts. The reconstructed streamflow is shown only for the basins with upstream reservoirs (i.e. Lena, Yenisei, Ob', and Ob2 sub-basin). There is close agreement in the inter-annual variability among all data sets, with the damped variability in the streamflow with respect

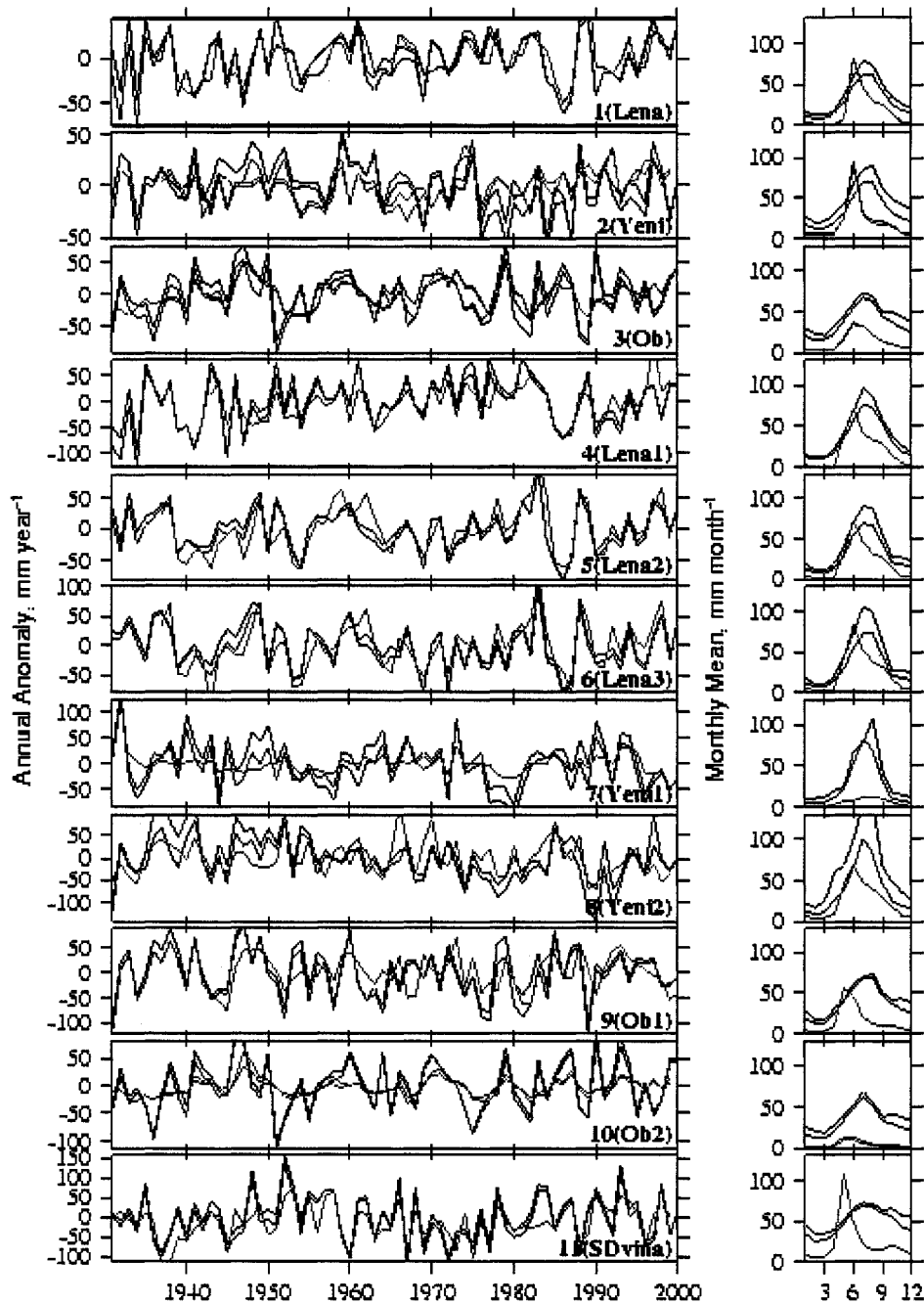


Figure 4.3 For each of the eleven study basins (see Table 3.1), basin-mean annual anomaly time-series (left) and monthly climatologies (right) for the UDel precipitation data set (black line) and the UW precipitation data set (red line). Also shown are the annual anomaly time-series (left) and monthly climatologies (right) for the observed streamflow product (blue line) and the Adam et al. (2007) (Chapter 5) reconstructed streamflow product (green line). The monthly climatologies for all products were calculated for the common period of 1943 to 1997.

to precipitation in the Yen1 and Ob2 sub-basins reflecting a lower runoff ratio (0.15 as compared to 0.3 to 0.5 for the other basins). For streamflow, the largest differences between the observed and reconstructed streamflows are for the Yenisei, due to the high degree of regulation in that basin. For precipitation, differences in the mean monthly data reflect the adjustments for gauge under-catch (the largest effect during the winter season) and orographic effects (the largest effect during the summer season). Differences in low-frequency variability between the precipitation products reflect the procedure used to constrain the long-term UW trends to match those of the gridded Groisman station data.

To explore this further, we used the seasonal Mann-Kendall test (see Section 4.3.3.1) to calculate the 1931 to 2000 trends in UDel and UW basin-average precipitation (Table 4.2) as well as for each 0.5° grid cell in the Eurasian Arctic domain (Figure 4.4). Generally, over the Eurasian Arctic, trend adjustment caused the precipitation trends to become less positive. These results are contrary to the findings of Rawlins et al. (2006), who suggested that adjusting for spurious trends due to a changing station network would result in precipitation trends that are more positive. An explanation is that, by constraining our low frequency variability to match that of the Groisman station data, we are adjusting for spurious trends that are a result of not only a changing station network but also for the change in the way the data were pre-processed for wetting biases as well as a change in the under-catch of precipitation as a function of a changing climate. Note that in regions with little or no coverage of Groisman stations (e.g. Scandinavia, northern Mongolia, and the Chukchi region of Russia), the trend adjustment procedure had the least effect (compare Figure 4.1 and Figure 4.4), therefore the long-term trends in these regions generally match those in UDel precipitation.

Table 4.2 Seasonal Mann-Kendall 1931 to 2000 trend significance and slope (see Section 4.3.3.1 for description of trend test) for precipitation before (UDel) and after (UW) trend adjustment for each of the study basins. "NA" indicates the trend did not pass statistical significance at the lowest level tested, i.e. tested levels were 99%, 98%, 95%, 90%, 80%, and 60%. See Figure 4.4 for spatial distributions of trend slope.

ID	Basin Reference Name	Precipitation (mm year ⁻¹)			
		UDel		UW	
1	Lena	98%	0.35	60%	0.12
2	Yeni	60%	0.14	80%	-0.26
3	Ob	90%	0.49	NA	-0.16
4	Lena1	95%	0.53	90%	0.34
5	Lena2	90%	0.24	NA	-0.06
6	Lena3	NA	0.06	90%	-0.26
7	Yeni1	NA	-0.10	80%	-0.20
8	Yeni2	80%	-0.42	95%	-0.52
9	Ob1	NA	0.12	NA	0.00
10	Ob2	90%	0.46	NA	0.13
11	SDvina	60%	0.38	NA	-0.22

4.3. Streamflow Trend Attribution: Methods

4.3.1. Overview of Analyses

The continuity equation applied to a watershed is

$$P = Q + ET + \frac{dS}{dt}, \quad (4.1)$$

where P , ET , and Q are the basin-average precipitation, evapotranspiration, and runoff, respectively, and dS is the net change in water stored in the basin (including surface and subsurface moisture) over the time increment, dt . In Section 4.1.1, we discussed numerous factors that may have contributed to the observed Q trends: (1) changes in dS/dt and/or ET due to reservoir construction and operation, (2) increase in P due to intensification of the hydrologic cycle (and/or increased northward moisture transport),

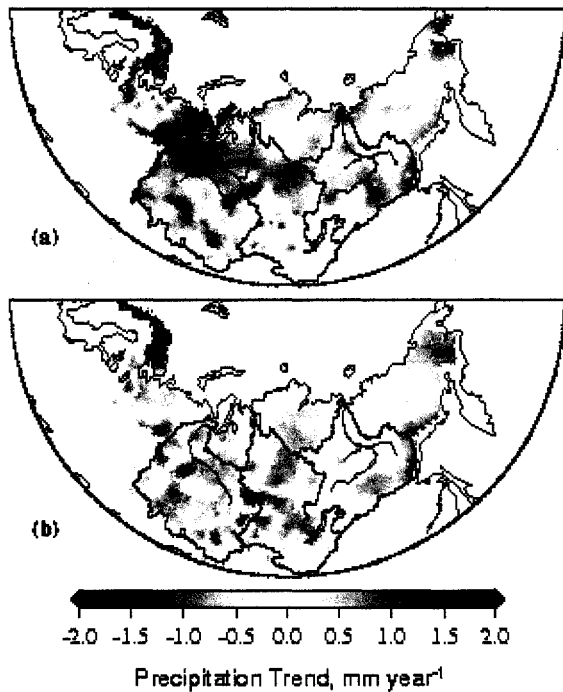


Figure 4.4 1931 to 2000 precipitation trend slope (calculated according to Hirsch et al. (1982) for the seasonal Mann-Kendall test, see Section 4.3.3.1) for (a) the UDel data set (i.e. before trend adjustment), and (b) the UW data set (i.e. after trend adjustment).

(3) decrease in dS/dt due to warming-induced permafrost degradation or changes in surface water storage, and (4) changes in ET due to changes in P and/or temperature (T). The contributions of the reservoirs to Q trends can be analyzed by examining the differences in long-term trends between observed and reconstructed Q (see Section 4.4.2; also see Adam et al. (2007) (Chapter 5) for a more exhaustive analysis). The remaining factors are induced by changes in P and/or T as follows. Changes in P will translate, to some degree, directly into changes in Q , i.e. increasing P results in increasing Q and vice versa. Furthermore, P changes will affect Q via changes in ET for the moisture-limited basins. Finally, T changes affect Q either through changes in ET (for the energy-limited basins) or in dS/dt (via permafrost degradation or other moisture storage dynamics). Our objective (as related to goal 2 in Section 4.1.3) is to evaluate when and where Q trends diverge from P trends, and to develop a set of most-likely warming-induced mechanisms that may explain these divergences.

Using the data products described in Table 4.2, we performed the following analyses:

(1) *Temperature/streamflow correlation analysis.* The purpose of this analysis was to develop a hypothesis to explain inconsistencies between observed precipitation and streamflow trends. This was done by examining the correlation between streamflow and UDel temperature for each of the basins on an annual basis and for the summer and winter seasons. This allowed us to comment on when and where streamflow is most sensitive to variations in temperature, and therefore to improve our understanding of how temperature-induced changes may have caused streamflow trends to diverge from precipitation trends. Reconstructed streamflow data were used for the regulated basins and observed streamflow data were used for the other basins. This method is described in Section 4.3.2 and the results are discussed in Section 4.4.1.

(2) *Multi-period trend analysis of individual variables.* Trend analysis was performed for each of the following products: UW precipitation, UDel temperature, and observed and reconstructed streamflow. The purpose of this analysis was twofold: (1) to document the significant trends in historical climate and streamflow, and (2) to comment on the role of reservoirs in observed streamflow changes by comparing significant trends in observed and reconstructed streamflow. The trend analysis techniques are described in Section 4.3.3.1 and the multi-period analysis is described in Section 4.3.3.2. The results are presented and discussed in Section 4.4.2.

(3) *Trend compatibility analysis between UW precipitation and observed and reconstructed streamflow.* Trends in precipitation and streamflow were compared for periods in which streamflow trends were statistically significant. The purpose of this analysis was to explore the most probable causes for inconsistencies between precipitation and streamflow trends, based on the hypothesis developed according to the temperature/streamflow correlation analysis (Section 4.4.1). The results are presented and discussed in Section 4.4.3.

4.3.2. Hypothesis Formulation via Temperature/Streamflow Correlation

Formulation of the hypothesis to explain inconsistencies between precipitation and streamflow trends was aided by correlation of basin-average temperature and streamflow time-series between 1943 and 1997 (the period common to all streamflow records). We investigated the relationships between temperature and streamflow by plotting the Pearson product-moment correlation coefficients, " T/Q ", against basin-average mean annual temperature (Figure 4.5; left panel) and percent continuous permafrost (Figure 4.5; right panel). T/Q correlations were calculated for the following time aggregations: (1) annual, defined as April 1 to March 31 in order to include the effects of summer permafrost thaw on winter discharge; (2) summer, defined as April 1 to September 31; (3) winter, defined as October 1 to March 31; and (4) summer/winter, in which the correlation was calculated between summer T and the following winter Q . Note that a correlation coefficient of +1 (-1) indicates a perfect increasing (decreasing) linear relationship, whereas a correlation of zero indicates that the data are not linearly dependent. The dotted lines in Figure 4.5 indicate statistical significance at the 99% level. Although most of the results shown in the figure are not statistically significant, the general patterns are robust. Furthermore, we use these results only as a framework to develop a hypothesis to explain observed streamflow changes, rather than as a basis to form conclusions. The results from this analysis are described in section 4.4.1.

4.3.3. Trend Analysis

4.3.3.1. Selection of Trend Test

To examine trends in annual time-series, we considered two non-parametric tests: Mann-Kendall on the annual sums (MK; Mann (1945)) and the seasonal Mann-Kendall test (SMK; Hirsch et al. (1982); Lettenmaier et al. (1994)). We opted to use SMK because it is sensitive to seasonal differences (the annual test statistic is calculated by summing the statistics for each of the seasonal flows). This is contrary to MK for which the annual statistic is calculating using annual flow (sum of seasonal flows) with no consideration for seasonal differences in trend (Hirsch et al. 1982). This is particularly important for

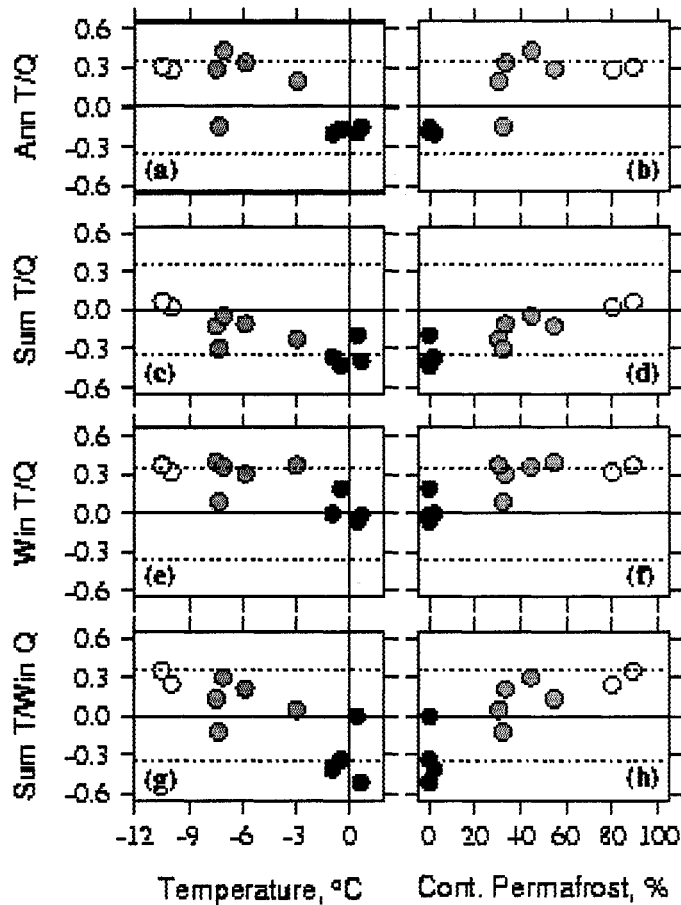


Figure 4.5 For each of the eleven study basins (see Table 3.1) and for the streamflow record common period of 1943 to 1997, the Pearson product-moment correlation coefficient between basin-average time-series of streamflow and UDel temperature plotted against basin-average mean-annual UDel temperature (left panel) and Brown et al. (1998) percent of continuous permafrost (right panel). Observed streamflow was used for the basins with no large upstream reservoirs, whereas the Adam et al. (2007) (Chapter 5) reconstructed streamflow product was used for basins with upstream reservoirs. The correlation coefficient is between (a/b) annual streamflow and annual temperature, (c/d) summer streamflow and summer temperature, (e/f) winter streamflow and winter temperature, and (g/h) summer temperature and winter streamflow (for which annual in this case is defined as April 1 to March 31, summer is defined as April 1 to September 30, and winter is defined as October 1 to March 31). Basins are sorted into three temperature regimes according to basin-average mean annual temperature, i.e. “cold” is for temperatures less than -8°C (white circles), “threshold” is for temperatures between -2 and -8°C (gray circles), and “warm” is for temperatures greater than -2°C (black circles). Dotted lines indicate the value for which the Pearson product-moment correlation is statistically significant at 99%.

applications in the Arctic because the most significant changes are occurring during the cold season when the variance is lowest, particularly for river discharge. In this context, an advantage of SMK is that trends occurring during the low-flow season are not obscured by the large variability of the high-flow season (Lettenmaier et al. 1994). SMK (as well as MK) is non-parametric with no linearity assumption. The null hypothesis is that the data, X , are independently identically distributed random variables, and therefore have no trend in time. Following Hirsch et al. (1982), the test statistic is expressed as the sum of the statistics for each season, i.e.

$$S_s = \sum_{k=1}^{n_s} S_k, \quad (4.2)$$

in which n_s is the number of seasons (i.e. 12 months). The statistic S_k , which represents the net direction of change over time, for each season is calculated as

$$S_k = \sum_{i=1}^{n_k-1} \sum_{j=i+1}^{n_k} \text{sgn}(X_{ik} - X_{jk}) \quad (4.3)$$

in which n_k is the number of observations for season k , and “sgn” is the sign function. S_s is approximately normally distributed, especially if a continuity correction is made by subtracting $\text{sgn}(S_s)$ (Hirsch et al. 1982). Therefore, the statistic Z , which is computed as

$$Z = \frac{S_s - \text{sgn}(S_s)}{\sqrt{\text{var}(S_s)}}, \quad (4.4)$$

is normally distributed with a mean of zero (under the null hypothesis) and a variance of 1, and a standard normal distribution table can be used to determine the probability P that the trend was falsely identified, i.e. if $|Z| > Z_{1-P/2}$, then the series displays a trend

significant at the level of $1-P/2$. The variance of the statistic is determined by summing over the variance of the statistics for each season, then adding a term to account for dependence between seasons, as follows:

$$\text{var}(S_s) = \sum_{k=1}^{n_s} \frac{n_k(n_k-1)(2n_k+5)}{18} + 2 \sum_{i=1}^{n_s-1} \sum_{j=i+1}^{n_s} \sigma_{ij}, \quad (4.5)$$

in which σ_{ij} is the covariance of the test statistic in seasons i and j .

We estimated the slope of the trend, B , for the data, X , according to the idea of Hirsch et al. (1982) as the median value of all D_{ijk} , which are determined by

$$D_{ijk} = \frac{X_{ik} - X_{jk}}{i - j} \text{ for all pairs } (X_{ik}, X_{jk}), \text{ where } 1 \leq k \leq n_s, \text{ and } 1 \leq i < j \leq n_k, \quad (4.6)$$

in which i and j are indices for year, k is an index for season, n_s is the number of seasons (i.e. 12 months, in our case), and n_k is the number of observations for season k (note that D is positive for a positive trend and vice versa). Therefore B is sensitive to changes occurring in a particular season because the differences are always computed between values that are multiples of n_s seasons apart (Lettenmaier et al. 1994). Throughout this manuscript, we refer to B as the “seasonal Mann-Kendall trend slope”. Note that, if $n_s = 1$, the formulation for SMK (equations 4.2 through 4.6) collapses to MK (equations 4.3 through 4.6, i.e. omitting k and the last term in equation 4.5).

We demonstrate the behavior of MK versus SMK by plotting histograms of the differences, D , for an example with especially strong winter changes, 1937 to 1998 Yenisei observed streamflow (Figure 4.6). Histograms are plotted for individual month MKs, annual MK, and SMK (note that combining all of the histograms for the individual months produces the histogram shown for SMK). Annual MK is unable to capture the

large December to April trend slope, whereas SMK is (i.e. the center of mass is shifted to the right).

Trend tests were performed for the hydrological “water year”, October through September. Trend slope units for the moisture flux variables are given as $\text{mm month}^{-1} \text{ year}^{-1}$ (for monthly series) or mm year^{-2} (for annual series). To be consistent with the literature, we use the short-hand unit of mm year^{-1} for both cases (i.e. this should be interpreted as $\text{mm month}^{-1} \text{ year}^{-1}$ for monthly data and mm year^{-2} for annual data). Because the SMK trend slope is calculated using monthly data, we convert the final trend slope to the proper annual units by multiplying by twelve (for moisture flux variables only and unless stated otherwise, as in Figure 4.6).

4.3.3.2. Multi-Period Trend Analysis of Individual Variables

Because the controls on streamflow variability operate at varying time-scales and in different periods, we determined trend significance and slope for a range of start and end dates. The periods were selected systematically: for every start year between 1936 and 2000, a set of end years was selected for period lengths greater or equal than twenty years in increments of five years. Therefore, trends were tested for the following periods: 1936-1956, 1936-1961, 1936-1966, ..., 1937-1957, 1937-1962, 1937-1967, etc... This results in a total of 225 potential periods, although many of the analyses utilize a subset of these periods, depending on the period of record for the data set under consideration. Following Lettenmaier (1976) and Ziegler et al. (2003), we selected the minimum period length of twenty years as the number of years needed to detect a 2% per year streamflow trend for a significance level of 99% given the mean variance in streamflow from these basins (cf. equation 3, Ziegler et al. (2003)). Trend testing was performed for precipitation, temperature, and streamflow using the SMK method (Section 4.3.3.1) for a significance level of 99%.

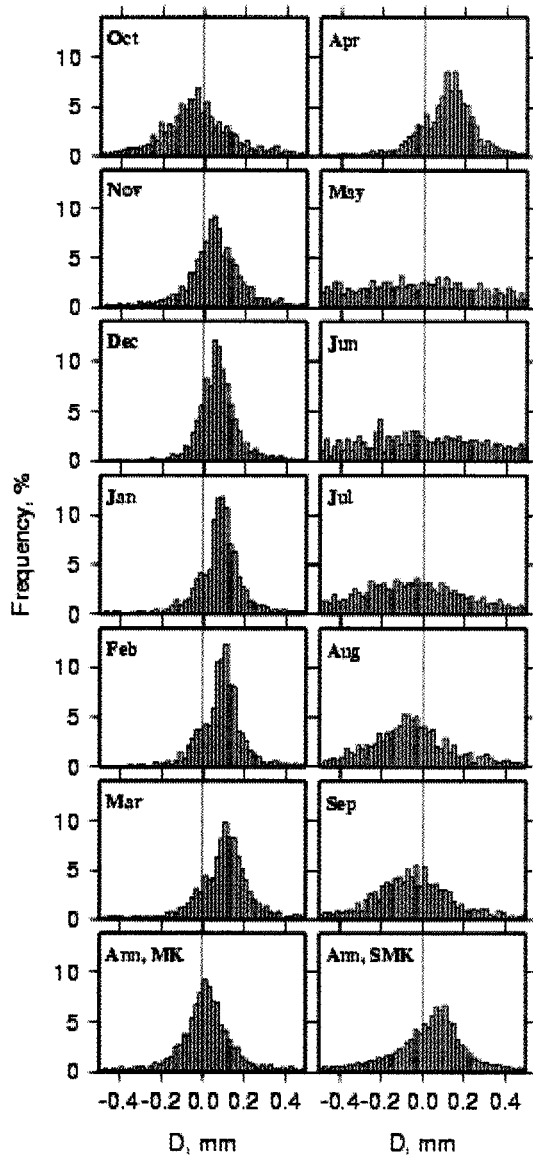


Figure 4.6 Histograms of the differences D_{ij} (MK statistics for individual months: "Oct" to "Sep"; and the MK statistic for annual streamflow: "Ann, MK") and D_{ijk} (for the SMK statistic: "Ann, SMK") used to determine the Mann-Kendall slope estimator B according to Hirsch et al. (1982), i.e. B is the median of the D_{ij} for MK and the D_{ijk} for SMK (see text for details). Results are shown for observed streamflow at the outlet of the Yenisei for the period of 1937 to 1998. Units are mm month^{-1} .

4.4. Streamflow Trend Attribution: Results and Discussion

4.4.1. Hypothesis Formulation via Temperature/Streamflow Correlation

Figures 4.5a and 4.5b suggest that the basins can be segregated into one of three temperature regimes using thresholds of approximately $-8\text{ }^{\circ}\text{C}$ and $-2\text{ }^{\circ}\text{C}$. First, the open circles are the “cold” basins (the Lena basin and the Lena1 sub-basin), the only basins with at least 80% continuous permafrost coverage. Second, the gray circles are the “threshold” basins (the Lena2 and Lena3 sub-basins and the Yenisei basin and its sub-basins) that are underlain by a minimum of 30% continuous permafrost. Third, the black circles are the “warm” basins (the Ob’ basin and sub-basins and the Severnaya Dvina basin) that are primarily in the region of seasonally frozen soil. The cold and threshold basins generally have positive correlation coefficients, indicating that as temperature increases, streamflow also increases, likely due to the melting of ground ice. The warm basins generally have negative T/Q correlations, indicating that as temperature increases, streamflow decreases, likely due to increased ET .

During the summer (Figures 4.5c and 4.5d), T/Q correlations are negative for the warm basins (as a result of temperature effects on ET); and increase with percent continuous permafrost for the permafrost basins, such that the T/Q correlations are negligible for the coldest basins (possibly due to less moisture available for ET in the thinner active layers). Winter streamflow from the warm basins is minimally affected by winter temperature variations and inversely affected by summer temperature variations, possibly due to drier soil conditions at the beginning of the winter (Figures 4.5e-h). Winter streamflow from the permafrost basins is positively affected by both winter and summer temperature, varying linearly with percent continuous permafrost (Figures 4.5e-h). This suggests that, in basins with extensive permafrost, warming effects on discharge are manifested primarily during the winter, consistent with Serreze et al. (2002) and Zhang et al. (2003) who hypothesized that a delayed active layer freeze-up (partially due to a deepening active layer) leads to a delay in the release of soil moisture storage into the winter. In fact, permafrost degradation should cause an increase in baseflow starting during the

summer season and lasting through the winter, although the effects of the baseflow increase would be most apparent during the winter low-flow season.

Overall, these results indicate that the way each region responds to precipitation and temperature changes is at least partially dependent on the region's mean climate and permafrost state. Based on our results we formulated the following hypothesis. We expect the regions with extensive continuous permafrost (the "cold" regions) to be sensitive to warming via the melt and release of excess ground ice (according to the degree of ice richness of the permafrost); therefore, streamflow increase may exceed precipitation increase. Furthermore, we expect that the release of this melt-water is sensitive to both winter and summer temperature variations and the impact of this melt should be felt primarily during the winter. We expect the *ET* in "warm" regions to increase with warming and/or increased precipitation; therefore, precipitation increases may exceed streamflow increases. Streamflow from the "threshold" basins, especially in regions with less extensive permafrost, is most likely affected by both the melting of ground ice and *ET* changes, as well as increased drainage, leading to less moisture available near the surface for *ET*. Therefore, it is difficult to predict the effects of temperature and precipitation changes on "threshold" basin streamflow.

4.4.2. Multi-Period Trend Analysis of Individual Variables

A summary of the multi-period trend analysis is given in Table 4.3. The table shows the number of periods with significant trends for each basin and data set, and qualitative descriptions of the signs of the trends. In general, there is no clear regional signature of precipitation trends, but temperature generally increased across the domain, as did streamflow. The trend results for the observed and reconstructed streamflow are plotted in Figure 4.7. Each line in the figure represents a period for which the trend is statistically significant; the trend slope is given by the line color. This plot can be thought of as an alternate way to view a time-series, wherein the objective is to view the significant changes in a noisy series. The results demonstrate that for the longest periods

with significant trends, the trends have been positive and that the largest positive trends occurred during the later part of the record, starting around the 1970s, indicating that streamflow increases accelerated up until the end of the last century. Streamflow increases have not been monotonic since the 1930s; many of the basins display negative trends during the 1960s and 1970s, and a few of the basins show negative trends beginning prior to the 1960s.

By comparing the observed and reconstructed panels, Figure 4.7 gives an indication of how the reservoirs have affected streamflow trends. For all four of the regulated basins (Lena, Yenisei, Ob', and Ob2), observed streamflow trends were positive for all periods; furthermore the number of periods with significant changes was larger for observed streamflow than for reconstructed streamflow. Recall that the SMK test (Section 4.3.3.1) is sensitive to significant changes occurring during individual months. The relative abundance of positive trends for the observed flows (as compared to the reconstructed flows) in the regulated basins is due to large increases in the winter low-flows as a result of reservoir operations. Adam et al. (2007) (Chapter 5) demonstrate that winter flows at the outlets of the Lena, Yenisei, and Ob' basins increased by 20-70% as a result of reservoir operations. For example, although there exists only one large reservoir in the Lena basin, the effects of this regulation caused a $500 \text{ m}^3 \text{ s}^{-1}$ winter flow increase at the outlet of the Lena basin, corresponding to a 50% increase in late winter streamflow (Adam et al. 2007). The reconstructed streamflow trends produced the same general features as observed streamflow for the unregulated basins, with negative trends occurring during the beginning or middle parts of the record and positive trends occurring during the later part of the record. The exception is for the Ob' basin, in which there were no periods with significant changes in reconstructed streamflow, indicating that the significant changes in observed streamflow were entirely due to reservoirs. Adam et al. (2007) (Chapter 5) present a more thorough comparison of observed to reconstructed streamflow trends, using the traditional MK test on annual and seasonal streamflow, in

contrast to the results presented here using the SMK statistic (see summary in Section 4.1.1.1). Recall from Section 4.3.3.1 that the SMK statistic may capture some trends that

Table 4.3 The number of periods for which trends are significant at 99% and a qualitative description of the sign of these trends for UW precipitation, UDel temperature, observed streamflow, and reconstructed streamflow for each of the study basins. The total number of tested periods for precipitation, temperature, and reconstructed streamflow is 225. The total number of tested periods for observed streamflow depends on the period of record for each basin. This number is given after the number of significant trends in the “Count” column for observed streamflow. “NA” indicates no major reservoirs for that basin (Table 3.1) or no periods with significant trends. See Figures 4.7 and 4.8 for visualizations of these trends.

ID	Basin Reference Name	Regime	UW Precipitation		UDeI Temperature		Obs Streamflow		Recon Streamflow	
			Count	Sign	Count	Sign	Count	Sign	Count	Sign
1	Lena	Cold	1	+	36	+	113/225	+	25	+
2	Yeni	Threshold	12	-	37	+	146/207	+	37	+
3	Ob	Warm	0	NA	10	+	7/216	+	0	NA
4	Lena1	Cold	2	+	50	+	55/156	+	NA	NA
5	Lena2	Threshold	0	NA	50	+	8/207	?	NA	NA
6	Lena3	Threshold	1	-	47	+	22/207	+	NA	NA
7	Yeni1	Threshold	0	NA	49	+	50/198	+	NA	NA
8	Yeni2	Threshold	47	-	21	+	10/216	?	NA	NA
9	Ob1	Warm	0	NA	10	+	13/216	?	NA	NA
10	Ob2	Warm	0	NA	24	+	19/216	+	6	?
11	SDvina	Warm	0	NA	0	NA	14/216	+	NA	NA

the MK statistic does not because it is sensitive to seasonal differences in trend. This explains why Adam et al. (2007) detected no significant trends in observed annual Ob' discharge, whereas several positive trends were detected here using the SMK statistic. These positive trends may reflect the large increase in winter discharge that occurred after the construction of reservoirs in 1956 and 1986 (Adam et al. 2007).

Figures 4.8a and 4.8b show the results of the trend analysis for UDeI temperature and UW precipitation, respectively. The figures show that there has been a general long-term warming over the region, with exception of the Severnaya Dvina basin. Furthermore, warming appears to have accelerated with the largest warming occurring since the 1970s,

although a few of the basins show a period of cooling between around 1980 and 2000. The few significant long-term precipitation increases are in the Lena and Lena1 basins prior to the 1980s. Because most of the literature suggests that precipitation must be α , if

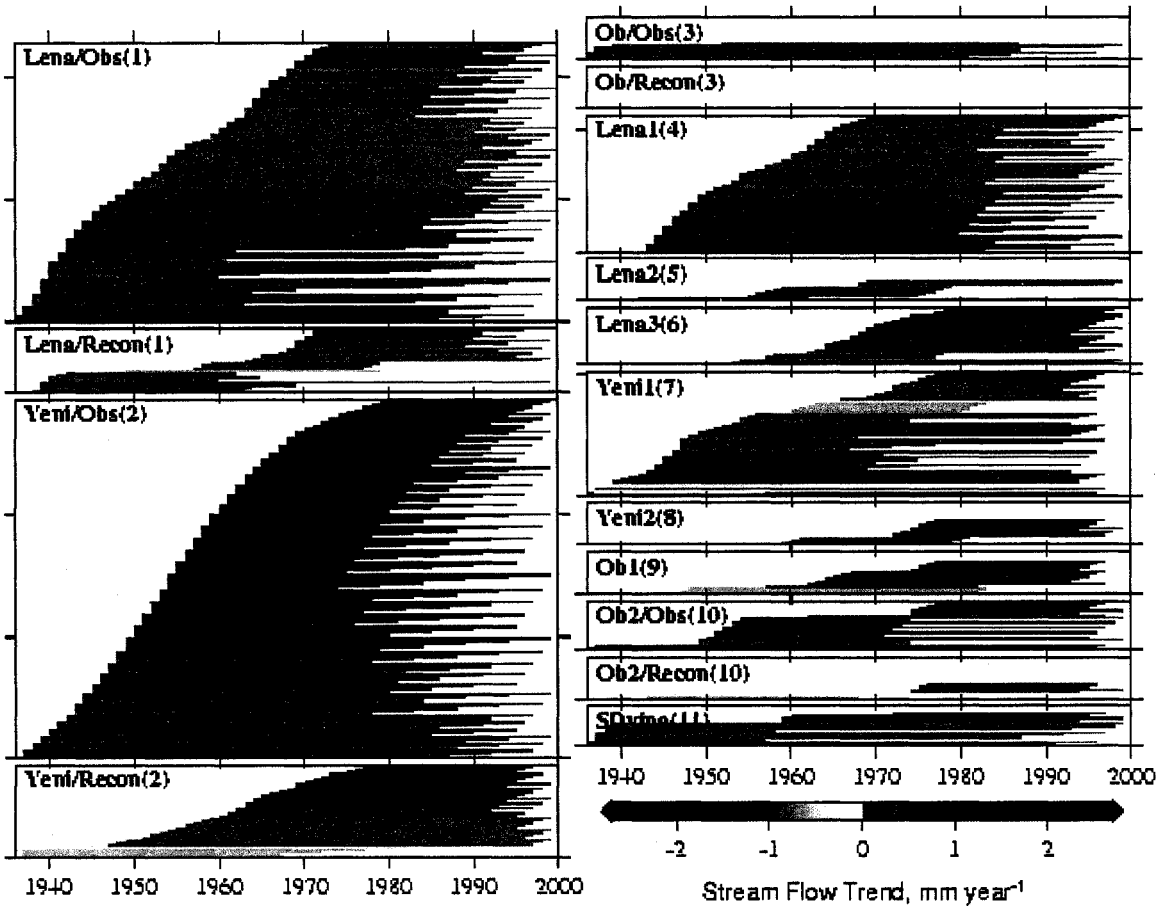


Figure 4.7 Streamflow trend plots for all periods with trends significant at 99% using SMK. Each line represents a period for which the trend slope is given by the color of the line and the period length is given by the length of the line (starting and ending at the start and end of the period, respectively). Each panel is labeled according to basin reference name and ID (see Table 3.1) and whether the streamflow product is observed (“Obs”) or reconstructed (“Recon”).

not *the*, major factor leading to streamflow increases (see Section 4.1.1.2), the lack of observed significant precipitation increases has made streamflow trend attribution difficult in these regions. An explanation for some of the study basins is that, other than

the snowmelt period, there is considerably more variability in precipitation than there is in streamflow (e.g. for the winter months, the standard deviation in the Ob2 monthly streamflow time-series is approximately 20% that of precipitation). Therefore, increases in precipitation may be occurring that can more than account for some of the observed changes in streamflow but because of the large variance, they are not statistically significant. This issue is examined in Section 4.4.3.

4.4.3. Comparison of Precipitation and Streamflow Trends

In Section 4.4.2, we examined precipitation trends for periods in which they are statistically significant. Here, we examine the precipitation trends for the periods in which the streamflow trends were statistically significant (Figure 4.9). Comparing and contrasting the line colors in Figures 4.7 and 4.9 gives an indication of the importance of precipitation to streamflow change for each basin and for each period. To ease the comparison, we created scatter-plots of streamflow trends versus precipitation trends (Figure 4.10). The black circles represent the periods with statistically significant changes at 99% (e.g. the same periods as in Figures 4.7 and 4.9), while the gray circles are for changes significant at 90% but not at 99%. These scatter-plots can be interpreted as follows: points along the one-to-one line indicate that precipitation may be contributing directly (without changes to ET or dS/dt , unless they are competing effects) to streamflow change (e.g. Lena2); a series of points that form a line that is rotated clockwise away from the one-to-one line indicate that precipitation is contributing to streamflow change, but that ET may also be changing either through changes in precipitation and/or temperature (e.g. Ob1); groups of points that are scattered in the upper halves of the plots, where streamflow trends are positive regardless of the sign of precipitation trends, indicate that there may be a release of moisture from storage, likely through warming-induced permafrost degradation (e.g. Lena1). Several of the plots show a combination of effects; for example, the Lena reconstructed streamflow trends appear to be caused by precipitation changes, increasing ET , as well as storage release effects.

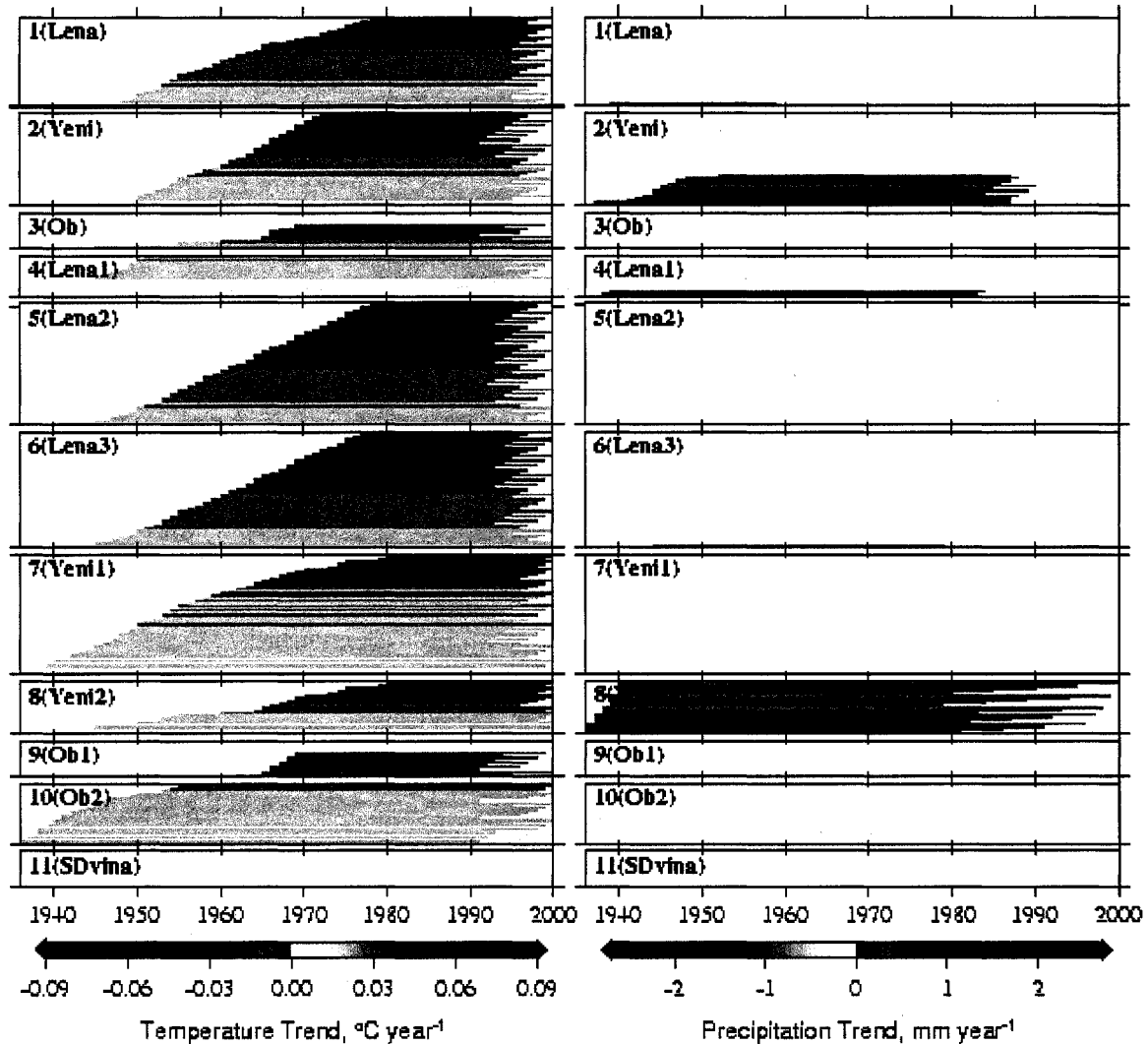


Figure 4.8 Trend plots for (a) UDel temperature and (b) UW precipitation (see Figure 4.7 caption for explanation).

Table 4.4 summarizes the most probable controls on long-term streamflow changes for each of the study basins. The table was based on information gathered from Figures 4.7, 10, and 11, and the hypothesis formulated in Section 4.4.1. In the following paragraphs, each set of basins (cold, threshold, and warm) are discussed. Because we focus the remaining discussion on climate-induced changes, hereafter we will discuss only the

reconstructed streamflow results for the regulated basins (Lena, Yenisei, Ob', and Ob2), as well as the observed streamflow results for the unregulated basins.

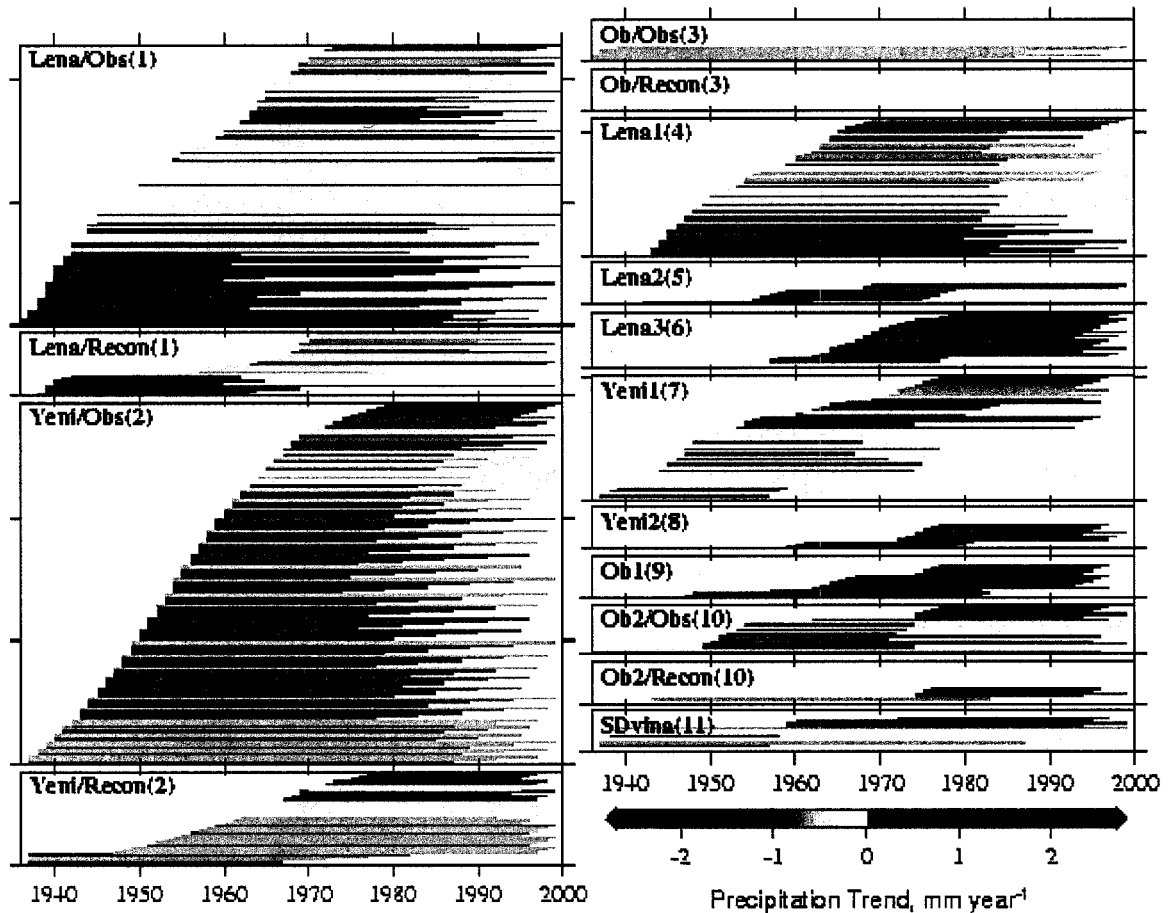


Figure 4.9 UW precipitation trend plots for all periods in which streamflow trends are significant at 99% using SMK. (See Figure 4.7 caption for further explanation).

Many of the periods for the cold basins (Lena and Lena1) are scattered above the one-to-one line in Figure 4.10, indicating that positive streamflow trends exceeded precipitation trends. This suggests another source of water, most likely release from storage due to permafrost degradation. Comparison of Figures 4.7 and 4.9 gives us an indication of the year that permafrost influences may have started. For the Lena basin, the positive streamflow trends beginning in the 1960s cannot be explained by the negative or slightly

positive precipitation trends during those periods. For the Lena1 sub-basin, the mismatch between streamflow and precipitation trend signs began in the mid-1940s but became

Table 4.4 Summary of Section 4.4 results and hypothesized primary controls for each of the study basins. The columns are derived from the following sources: column 3 from Figure 4.5, columns 4 and 5 from Table 3.2, and columns 6 and 7 from Figure 4.10. "NA" indicates lack of reconstructed data for these basins (which do not contain large reservoirs, see Table 3.1).

ID	Basin Reference Name	Regime	Cont. Permafrost	Discont. Permafrost	Q/P Trend R ²		Suggested Controls
					Obs	Recon	
1	Lena	Cold	80%	11%	0%	3%	precipitation/ <i>ET</i> through 1960s, permafrost effects starting 1960s
2	Yeni	Threshold	33%	12%	4%	49%	precipitation entire record, permafrost effects starting ~1950
3	Ob	Warm	2%	4%	24%	-	insignificant change
4	Lena1	Cold	89%	10%	4%	NA	precipitation through ~1980, permafrost effects starting ~1950, mainly permafrost after ~1980
5	Lena2	Threshold	55%	23%	89%	NA	precipitation
6	Lena3	Threshold	45%	15%	87%	NA	precipitation, permafrost effects (perhaps starting 1960s)
7	Yeni1	Threshold	30%	10%	31%	NA	combination of precipitation, <i>ET</i> , and permafrost effects entire record
8	Yeni2	Threshold	32%	55%	93%	NA	precipitation, permafrost effects (perhaps starting 1970s)
9	Ob1	Warm	0%	0%	96%	NA	precipitation/ <i>ET</i>
10	Ob2	Warm	0%	0%	47%	77%	precipitation/ <i>ET</i>
11	SDvina	Warm	0%	0%	96%	NA	precipitation/ <i>ET</i>

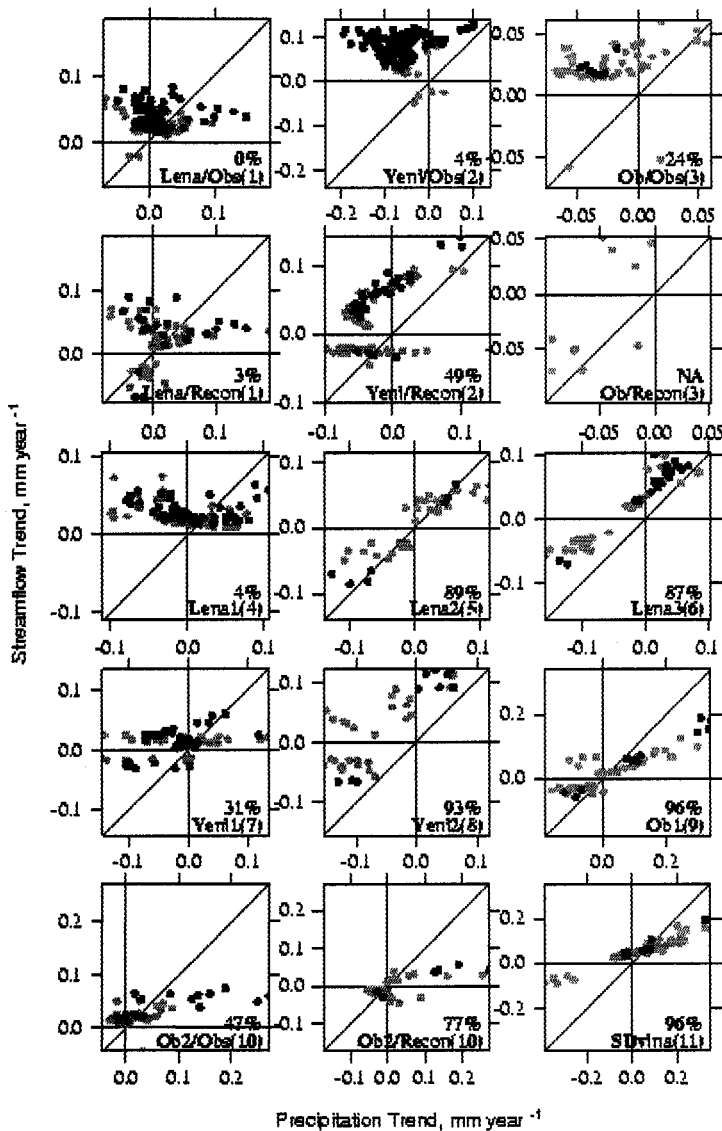


Figure 4.10 Scatter-plots of trend slopes between streamflow and UW precipitation for all periods in which streamflow trends are significant at 90% (gray circles) and 99% (black circles) using SMK. Each panel is labeled according to basin reference name and ID (see Table 3.1) and whether the streamflow product is observed (“Obs”) or reconstructed (“Recon”). The R^2 value for each set of pairs (for 99% significance) is shown in the lower right corner.

most apparent in the mid-1950s and increasingly so up until 2000. Therefore, permafrost degradation effects may have begun in the 1960s for the Lena and in the 1950s for the

Lena1. The Lena1 is a sub-basin to the Lena, so it may have taken an additional ten years for the permafrost signature apparent in the Lena1 to be the dominant effect for the entire basin. There are also a number of points scattered along or to the right of the one-to-one line in Figure 4.10, suggesting that precipitation combined with *ET* effects was the dominant control for these periods. Figures 4.7 and 4.9 suggest that, for the Lena, the positive streamflow trends between the 1940s and 1960s and the negative streamflow trends between the 1950s and 1970s are likely precipitation/*ET* induced. For the Lena1, positive streamflow trends starting in the 1940s may have been precipitation/*ET* induced, but for periods starting in the 1950s to mid-1960s, streamflow trends were likely a combination of precipitation and permafrost effects, and permafrost effects became dominant for periods starting in the late-1960s. These results are in agreement with Frauenfeld et al. (2004) who show that the positive trend in active layer thickness (averaged over Russian permafrost regions) has a greater slope for the 1956 to 1990 period as compared to the 1930 to 1990 period, indicating an increased thawing rate since the mid-1950s. This observed increase in permafrost thaw rate may explain the divergence of streamflow and precipitation trends beginning in the mid-1950s to 1960s in the Lena and Lena1 basins, as well as some of the threshold permafrost basins (e.g. Yenisei and Lena3, see below).

Figures 4.7, 4.9, and 4.10 indicate that precipitation, *ET*, and dS/dt changes have all, in varying degrees, influenced streamflow changes in the threshold basins (the Yenisei and its sub-basins and two of the Lena's sub-basins: Lena2 and Lena3). For example, Yenisei streamflow trends were consistently more positive than precipitation trends (Figure 4.10). This is in agreement with Serreze et al. (2002) who showed divergent trends in streamflow and $P-ET$ for the Yenisei. They suspected that permafrost thaw was the primary cause. Unlike the cold basins, there is no general picture of key mechanisms of change. For example, precipitation changes in the Lena2 sub-basin appear to be the primary control for the entire period of record (i.e. the points in Figure 4.10 are scattered along the one-to-one line), whereas permafrost effects may have also played a role for

changes in Lena3 streamflow (i.e. the points in Figure 4.10 are shifted upwards from the one-to-one line). Recall that the Lena3 is a sub-basin of Lena2, occupying approximately 50% of the Lena2 area. Compared to the Lena2 as a whole, the Lena3 is slightly warmer and is underlain by larger percentages of sporadic and isolated permafrost types, which may be more sensitive to warming. The Yenisei and its sub-basins all appear to have been influenced by both precipitation and permafrost effects, with the largest discrepancies between streamflow and precipitation trends in the Yenisei and Yeni2 basins (Figure 4.10). Compared to the Yeni1, the Yeni2 is colder and is underlain by larger percentages of continuous and discontinuous permafrost types. This is the opposite relationship as observed between the Lena2 and Lena3 sub-basins, which indicates that permafrost type, according to the definition given in Figure 3.1, is not the sole permafrost characteristic needed to understand streamflow changes in permafrost basins. For example, it is possible that the Yeni2 basin is underlain with permafrost that has a greater volumetric fraction of ice as compared to the Yeni1, which may explain the greater permafrost role in observed streamflow changes in that basin.

Figure 4.10 suggests that the streamflow changes in the warm basins (the Ob' sub-basins and the Severnaya Dvina) were due to changes in precipitation and *ET*, i.e. the points are scattered along a straight line that is rotated to the right from the one-to-one line. Therefore, although not significant, precipitation trends in each of these basins can more than account for the majority of the significant streamflow trends, especially for the positive trends. The remainder of the additional precipitation likely contributed towards increased basin *ET*. Of the three basin types (cold, threshold, and warm), the clearest consistent relationship between streamflow and precipitation trends is for the warm or non-permafrost basins. This suggests that the presence of permafrost in a basin is likely the most important complicating factor in understanding the primary controls on observed streamflow changes for that basin.

4.5. Conclusions

Observed streamflow changes in the northward-flowing Eurasian rivers may be due to climatic influences, mainly through changing precipitation and temperature, or to human influences, mainly through reservoir construction and operation. We explored the degree to which precipitation may explain observed streamflow changes and how temperature changes may account for discrepancies between precipitation and streamflow trends using trend analysis of precipitation, temperature, and streamflow time-series. Before exploring the role of climate in observed trends, the role of the reservoirs was identified. As shown by Adam et al. (2007) (Chapter 5), reservoirs had the greatest effect on streamflow seasonality, by increasing winter streamflow and decreasing summer streamflow. Because the SMK test is sensitive to seasonal changes, there were large differences between the observed and reconstructed streamflow trend results for the regulated basins. For the Lena, Yenisei, and Ob2 basins, significant observed streamflow trends were positive for all periods, whereas significant reconstructed streamflow trends were a mix of negative and positive trends, in which periods with negative trends ended prior to the mid-1980s. This is consistent with the trend plots for most of the unregulated basins (Figure 4.7). There were no periods with significant trends for Ob' reconstructed streamflow, indicating that the significant trends for observed streamflow were likely a result of reservoir effects on streamflow seasonality.

The attribution of observed streamflow changes to climatic influences is complicated by the lack of significant precipitation trends in northern Eurasia. As discussed in Section 4.1.1.2, much of the literature suggests that changes in precipitation should be a primary contributor to the observed streamflow increases, but there is an inconsistency between precipitation and streamflow changes for many of the basins. Our analysis has identified when and where precipitation and streamflow trends are divergent in sign and/or magnitude, and how these divergences may be attributed to changes in temperature. By correlating annual time-series of temperature to streamflow (reconstructed data for regulated basins and observed data for unregulated basins), we advanced the hypothesis

that warming could lead to differing agents of change for streamflow variability depending on the mean climate and permafrost state of the basin: melt of ground ice for basins in north-eastern Siberia (leading to streamflow increases exceeding precipitation increases), *ET* effects for basins in European Russia and western Siberia (leading to precipitation changes exceeding streamflow changes), and competing effects for basins in the central threshold regions. Our trend analysis results indicated that the most likely controls on streamflow changes are generally in agreement with this hypothesis. For the “cold” Lena and Lena1 basins in north-eastern Siberia, inconsistencies between streamflow and precipitation trends began in the 1950s and 1960s, and permafrost melt is the most probable explanation for this additional streamflow. The divergence between precipitation and streamflow trends accelerated up until the end of the last century. For the “warm” basins largely outside of the permafrost region (the Ob’ sub-basins and the Severnaya Dvina basin in western Siberia), there is a clear and consistent conclusion that precipitation changes coupled to *ET* changes are the likely explanation for the observed streamflow trends, i.e. precipitation trends nearly always exceeded streamflow trends in absolute magnitude. For the “threshold” basins in central Siberia (the Lena2 and Lena3 sub-basins, and the Yenisei and its sub-basins), there is less agreement in the most likely controls on streamflow changes, suggesting that permafrost and *ET* effects were competing in causing streamflow trends to be inconsistent with precipitation trends. For example, streamflow trends exceeded precipitation trends for nearly all of the periods for the Yenisei, Lena3, and Yeni2 basins, suggesting that permafrost degradation played a primary role. Alternatively, for the Lena2 and Yeni1 sub-basins, some of the streamflow trends were less than that of precipitation, suggesting that *ET* played a primary role. For the periods when streamflow trends matched that of precipitation trends, it is possible that *ET* effects canceled-out the effects of permafrost degradation or that neither made a significant contribution. One conclusion of this study is that the presence of permafrost is a complicating factor in understanding long-term streamflow changes for river basins in the Eurasian Arctic. The degree to which warming-induced permafrost degradation played a role in observed streamflow changes depends not only on the extent of

permafrost in the basin, but also the temperature and ice-richness of the permafrost, and likely other factors.

5. Simulation of Reservoir Influences on Annual and Seasonal Changes

This chapter summarizes and excerpts research submitted to Journal of Geophysical Research as:

Adam, J.C., I. Haddeland, F. Su, and D. P. Lettenmaier, 2007: Simulation of reservoir influences on annual and seasonal streamflow changes for the Lena, Yenisei and Ob' Rivers, *J. of Geophysical Research* (accepted).

5.1. Background and Chapter Goals

White et al. (2007) summarize changes that have been documented across the pan-Arctic basin. In the Eurasian portion of this domain, increasing annual streamflow volumes and a shift in streamflow seasonality have occurred over the last seventy years (Berezovskaya et al. 2005; Georgievsky et al. 1996; Lammers et al. 2001; Peterson et al. 2002; Savelieva et al. 2000; Shiklomanov et al. 2006; Shiklomanov et al. 2000; Yang et al. 2004a; Yang et al. 2004b; Yang et al. 2002; Ye et al. 2003; Ye et al. 2004). The forces driving these changes are unclear, although numerous factors have been examined, including changes in precipitation, permafrost degradation, changes in snowmelt volume and timing, and enhanced fire frequency (Adam and Lettenmaier 2007b; Berezovskaya et al. 2004; Berezovskaya et al. 2005; McClelland et al. 2004; Nijssen et al. 2001; Pavelsky and Smith 2006; Rawlins et al. 2006; Smith et al. 2007; Wu et al. 2005; Yang et al. 2003; Ye et al. 2004). A complication is that direct human alterations have also affected streamflow of the major Siberian rivers over the same period (Berezovskaya et al. 2005; Dynesius and Nilsson 1994; Haddeland et al. 2007; McClelland et al. 2004; Plishkin 1979; Shiklomanov 1978; Shiklomanov and Veretennikova 1978; Shiklomanov et al. 2000; Yang et al. 2004a; Yang et al. 2004b; Ye et al. 2003). For example, the

construction and operation of large reservoirs result in a shift in streamflow seasonality which reduces spring and summer peak flows and increases fall and winter low flows. These reservoir-related changes and shifts in streamflow seasonality resulting from climate change can be confounded, as their effects on streamflow magnitude and timing can be similar in these northern Eurasian rivers (Georgievsky et al. 1996).

Humans can directly affect land surface hydrology by redistributing runoff over space and time, such as by storing water in reservoirs or constructing runoff diversions; and by disturbing the natural partitioning of precipitation between runoff, evapotranspiration, and storage changes, such as via reservoir construction, irrigation, or land cover changes (Shiklomanov 1978; Vörösmarty and Sahagian 2000). Over the Lena, Yenisei, and Ob' River basins, humans have most significantly altered the natural hydrologic regime by the construction and operation of large reservoirs, which have substantially changed streamflow seasonality. For example, Yang et al. (2004b) report that two large reservoirs in the upper Yenisei basin have increased winter low flows by 45% to 85% and decreased summer flows by 10% to 50% between 1935 and 1999. Effects on annual streamflow volumes are less significant. Annual consumptive use of water (essentially diversions of water from the river that are not returned) is less than 0.5% (Berezovskaya et al. 2005), between 0.8% and 1.4% (Shiklomanov et al. 2000), and less than 1% (Dynesius and Nilsson 1994) of the mean annual flow at the outlets of the Lena, Yenisei, and Ob' River basins, respectively. Increases in annual evaporation due to reservoir construction are of similar magnitude: up to 0.1%, 0.1% to 0.5%, and 0.6% to 1.0% of the mean annual flow for the Lena, Yenisei, and Ob' River basins, respectively (Berezovskaya et al. 2007). Two other effects on annual streamflow volume occur after reservoir construction. Filling of the reservoir and increase in groundwater storage due to the raising of the water table in the areas surrounding the reservoir can take up to eight years of transition after reservoir construction (Berezovskaya et al. 2007). Inter-basin water diversions are another means by which the seasonality and annual volumes of streamflow can be altered, but in the three Siberian rivers in question, these effects are small; diversions into

the Ob' River basin amount to 0.5% of its mean annual flow (Dynesius and Nilsson 1994), and are negligible in the other two basins.

The goal of this study is to isolate the effects of the reservoirs on long-term (≥ 30 years) annual and seasonal streamflow trends between 1937 and 1999 from other causes. We apply a coupled hydrology-routing-reservoir model to simulate the effects of reservoirs on streamflow. As a result of these analyses, we produce reconstructed streamflow time series, in which the effects of reservoirs have been removed from streamflow at the outlets of the Lena, Yenisei, and Ob' River basins. Our analyses account for the shift in streamflow seasonality due to reservoir operations, and the effects of reservoir evaporation and filling on annual streamflow volume. We do not account for the other effects on annual streamflow volume, although these effects, with exception of the small diversion of water into the Ob' River basin, result in a decrease in volume, and therefore cannot explain observed streamflow increases. We compare our reconstructed product to those developed using only streamflow observations (McClelland et al. 2004; Yang et al. 2004b; Ye et al. 2003). The unique contribution of this work is that it provides estimates of the reservoir signature on Eurasian Arctic streamflow using a physically-based representation of reservoir operations.

5.2. Methods

5.2.1. Selection of Reservoirs for Analysis

Eleven large reservoirs were constructed in the Lena, Yenisei, and Ob' River basins between 1950 and 1990. Some of these reservoirs are exceptionally large; four are among the ten largest hydroelectric facilities in the world (ICOLD 2003). The locations and some characteristics of these reservoirs are given in Figure 5.1 and Table 3.1, respectively. Other reservoirs were not included in this analysis for various reasons. The Boguchansky reservoir (on the Angara River) was not considered because it is not yet operational. Furthermore, "small" reservoirs (storage capacity less than 1 km³) were

excluded. For example, we did not analyze the Ust'-Kamengorsky reservoir on the Irtysh River because it has a reservoir capacity of only 0.6 km^3 , and effects of this reservoir are not detected in downstream discharge by Yang et al. (2004a). A small reservoir on the

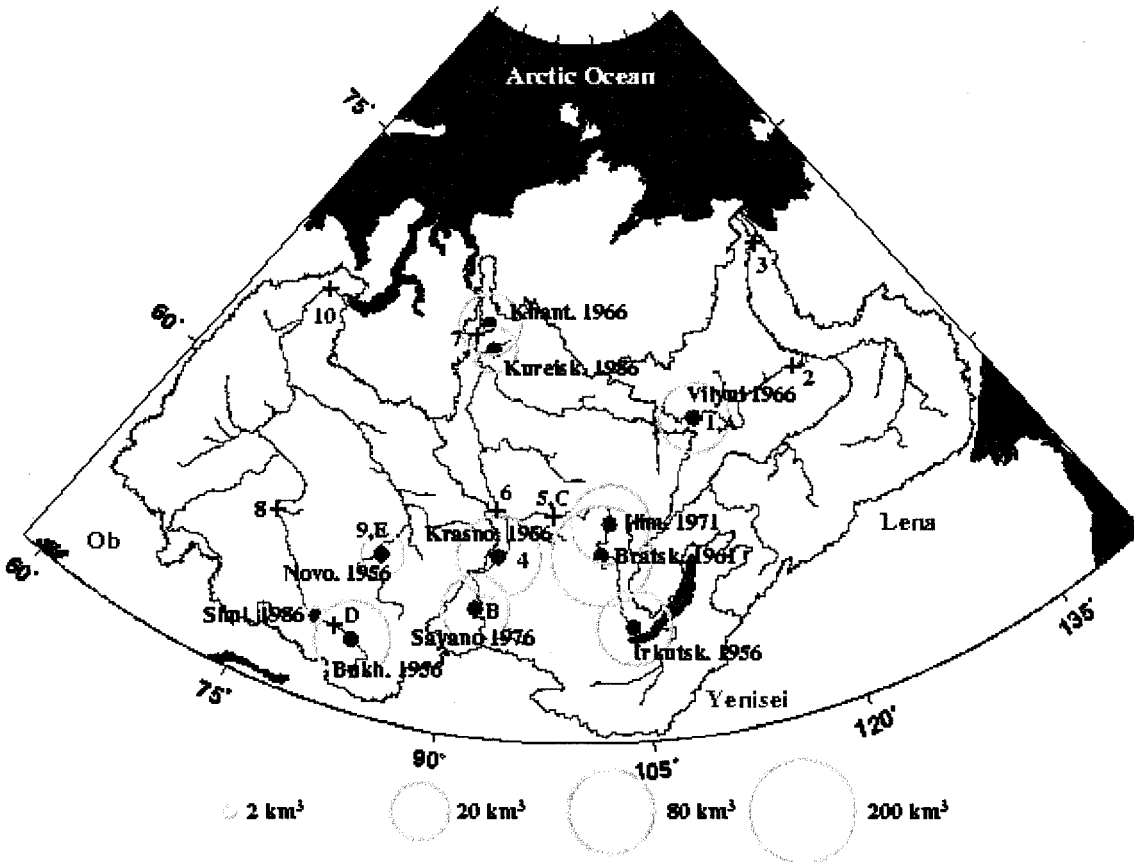


Figure 5.1 Locations of operational reservoirs for which the storage capacities exceed 1 km^3 (shown as solid red circles) for the Lena, Yenisei, and Ob' River basins (see Tables 5.1 and 5.2 for reservoir characteristics). The storage capacities of the reservoirs are given on a log ten scale by the diameters of the yellow circles. The green pluses indicate the locations of the streamflow gauging stations used either for bias correction of inflow into the farthest upstream reservoir on each tributary (letters A:E, see Table 5.3 for station information) or for reservoir model evaluation (numerals 1:10, see Table 5.6 for station information). Some stations are used for both purposes. If a green plus is located directly over a reservoir station, this indicates that the gauging station is just downstream of the reservoir outlet. Note: Boguchanskoe reservoir on the Angara tributary (located at gauging station #5) is not shown because it is not yet operational.

Vitim River in the Lena River basin was not included for the same reason (Berezovskaya et al. 2005).

Table 5.1 Characteristics of the large (> 1 km³) operational reservoirs in the Lena, Yenisei, and Ob' River basins. Information is obtained from ICOLD (2003), Malik et al. (2000), and McLelland et al. (2004). Fraction of annual inflow is calculated by dividing the reservoir storage capacity by the average annual flow of the nearest gauging station using the R-ArcticNET dataset (Lammers and Shiklomanov 2000). Fraction of annual flow is calculated by dividing the reservoir storage capacity by the average annual flow at the most downstream station in each of the Lena, Yenisei, and Ob' River basins (stations 3, 7, and 10, respectively, in Table 5.6).

Reservoir	Tributary	Basin	First Year of Filling	Cap., km ³	Fraction of Annual Inflow	Fraction of Annual Flow at Basin Outlet	Surface Area, km ²	Dam Height, m
Vilyuiskoe	Vilyui	Lena	1966	35.9	1.77	0.07	2170	64
Sayano-Shushenskoe	Yenisei	Yenisei	1976	31.3	0.65	0.05	621	245
Krasnoyarskoe	Yenisei	Yenisei	1966	73.3	0.81	0.13	2000	124
Irkutskoe*	Angara	Yenisei	1956	46 / 23680	0.78 / 402.71	0.08 / 40.79	3300 / 34794	44
Bratskoe	Angara	Yenisei	1961	169	1.90	0.29	5470	125
Ust'-Ilimskoe	Angara	Yenisei	1971	59.3	0.54	0.10	1890	102
Kureiskoe	Kureika	Yenisei	1986	9.9	Not Gauged	0.02	500	81
Ust'-Khantaiskoe	Khantaika	Yenisei	1966	23.5	2.66	0.04**	2120	65
Bukhtarminskoe	Irtish	Ob'	1956	49.8	5.28	0.13	5490	90
Shul'binskoe	Irtish	Ob'	1986	2.4	0.08	0.01	255	36
Novosibirskoe	Ob'	Ob'	1956	8.8	0.15	0.02	1070	27

**The Irkutskoe reservoir is conjoined to Lake Baikal, a natural lake (Vyruchalkina 2004). The values before the slashes in this row describe the Irkutskoe reservoir were it separate from Lake Baikal, whereas the values after the slash describe the combined Irkutskoe/Baikal system. The smaller volume, 46 km³, is the regulated capacity of the system (see Section 5.2.2.3(4)), whereas the combine dimensions are used to describe the shape of the system (see Section 5.2.2.3(3)). **The confluence of the Khantaika tributary and the Yenisei River is downstream of the Igarka gauging station (station 7 in Table 5.5), therefore the effects of this reservoir are not seen in the Yenisei basin outlet analyses. Note: the Boguchanskoe reservoir on the Angara tributary is not included because it is not yet operational.*

Table 5.2 The ratio of the characteristic length to the depth of the reservoir, f , is calculated according to Equation 5.2. The alternate value is f' and is calculated using Equation 5.4.

Reservoir	Tributary	Basin	f	f'
Vilyuiskoe	Vilyui	Lena	1327	906
Sayano-Shushenskoe	Yenisei	Yenisei	233	113
Krasnoyarskoe	Yenisei	Yenisei	575	480
Irkutskoe*	Angara	Yenisei	1943 / 129	1800 / 164
Bratskoe	Angara	Yenisei	1128	721
Ust'-Ilimskoe	Angara	Yenisei	653	579
Kureiskoe	Kureika	Yenisei	532	334
Ust'-Khantaiskoe	Khantaika	Yenisei	1958	717
Bukhtarminskoe	Irtish	Ob'	3851	640
Shul'binskoe	Irtish	Ob'	800	556
Novosibirskoe	Ob'	Ob'	1875	1638

5.2.2. Modeling Framework

We used a hydrology/routing/reservoir coupled model system, as shown in Figure 5.2.

The steps involved in the process are as follows:

- (1) Run the grid-based hydrology model (driven with observed precipitation, temperature, and other surface meteorological variables; see Section 5.2.2.1 and Nijssen et al. (1997) for details) for each grid cell and combine the simulated runoff and baseflow as input to the routing model.
- (2) For all grid cells upstream of the reservoir, route the runoff to the reservoir (red cell in Figure 5.2) and bias correct the simulated streamflow using pre-reservoir observed streamflow data. The bias correction procedure is described in Section 5.2.2.2.
- (3) Run the reservoir model for each operational year by maximizing revenue from hydropower production. The reservoir model is described in Section 5.2.2.3.
- (4) Route reservoir releases and all other basin contributions to the basin outlet.

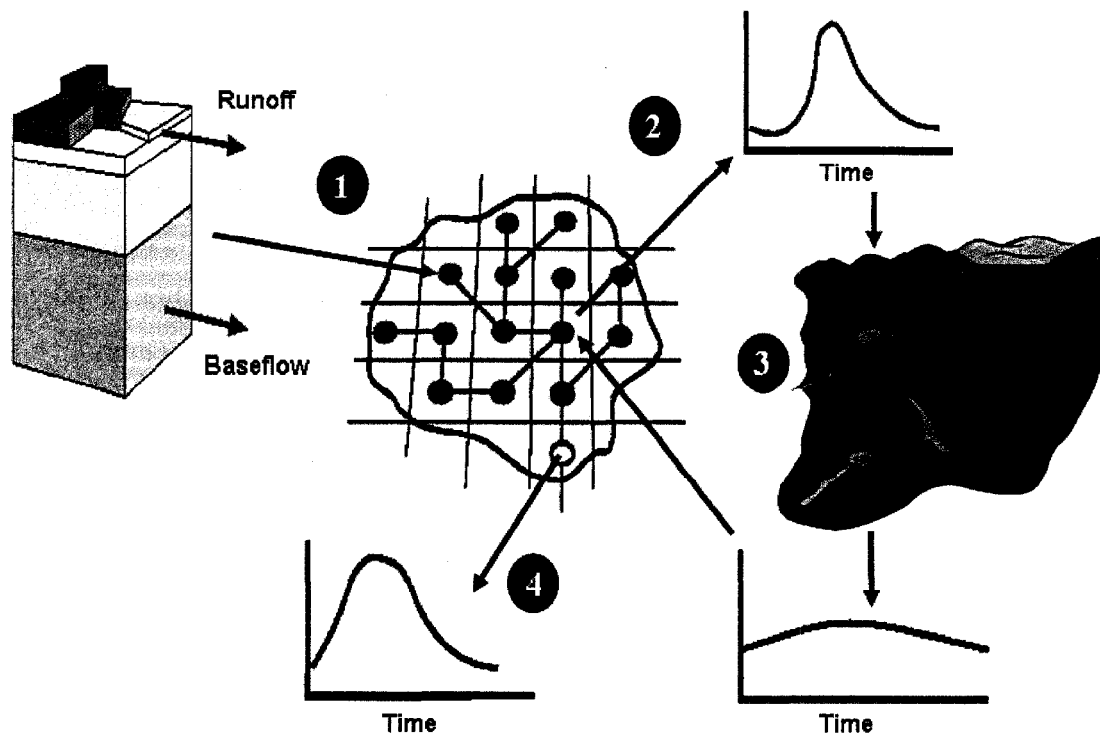


Figure 5.2 Coupling schematic for 1) hydrology (Adam and Lettenmaier 2007a; Cherkauer and Lettenmaier 1999; Liang et al. 1994; Su et al. 2005), 2) routing (Lohmann et al. 1996; Lohmann et al. 1998), and 3) reservoir (Haddeland et al. 2006a; Haddeland et al. 2006b; Haddeland et al. 2007) models.

5.2.2.1. Hydrology and Routing Models

We used the Variable Infiltration Capacity (VIC) large-scale hydrology model (Liang et al. 1994; Nijssen et al. 1997). The version we used includes algorithms that are important for processes occurring in northern Eurasia (Cherkauer et al. 2003): a lakes and wetlands model (Bowling 2002), an algorithm for the sublimation and redistribution of blowing snow (Bowling et al. 2004), a finite-difference frozen soils algorithm (Cherkauer and Lettenmaier 1999) with sub-grid frost variability (Cherkauer and Lettenmaier 2003), and a two-layer energy balance snow model (Storck and Lettenmaier 1999) that allows for sub-grid variability in snow cover (Cherkauer and Lettenmaier 2003). We used the Su et al. (2005) pan-Arctic implementation of VIC at an Equal-Area Scalable Earth Grid (EASE-Grid) (Brodzik 1997) spatial resolution of 100 km. Su et al. (2005) describe the

data involved in creating this setup, the calibration of soil depths and infiltration characteristics using observed streamflow data for a constrained period (1979 to 1999), and the evaluation of the simulations using observed snow cover extent, lake freeze-up and break-up dates, and permafrost active layer thickness. We ran the model in full energy mode (in which the model iteratively solves the effective surface temperature by resolving the energy and water balances) at a 3-hourly time step from 1930 to 2000. There are three differences between the Su et al. (2005) implementation and this implementation: (1) a longer simulation period (Su et al. (2005) used the period from 1979 to 1999), (2) forcing data, and (3) modifications to the frozen soils algorithm, of which the latter two are discussed briefly below.

The VIC model is forced with daily gridded precipitation, maximum and minimum temperature, and wind speed; which are downscaled to the model time-step of three hours using methods described by Maurer et al. (2002). From these data, vapor pressure, incoming shortwave radiation, and net long-wave radiation are calculated using algorithms described in Maurer et al (2002). Monthly time-series of gridded precipitation and temperature are based on meteorological station observations and, for this, we used the products of Willmott and Matsuura (2005) and Mitchell and Jones (2005), respectively. To improve the monthly precipitation estimates, we applied the Adam and Lettenmaier (2003) corrections for the under-catch of solid and liquid precipitation in manual gauges and the Adam et al. (2006) corrections for orographic effects on the interpolation of precipitation point measurements. Furthermore, we made adjustments for spurious trends in the monthly precipitation and temperature products using the method of Hamlet and Lettenmaier (2005). For this, we used a set of high-quality meteorological stations with long-term records (from Groisman (2005)) to constrain the low-frequency variability of the original gridded products (Mitchell and Jones 2005; Willmott and Matsuura 2005), which were derived from much denser networks of stations. These adjustments are intended to avoid trends that are artifacts of changing networks; instead, decadal (and longer) variability in the gridded precipitation and

temperature reflect observed changes in a set of high-quality stations. This procedure is described in detail by Adam and Lettenmaier (2007b) (Chapter 4). Daily disaggregation was achieved by rescaling daily NCEP/NCAR reanalysis data (Kalnay et al. 1996) to match the observation-based monthly time series of precipitation and temperature. For this we used the product of Sheffield et al. (2004) that includes rain day bias corrections. For wind speed, daily NCEP/NCAR reanalysis (Kalnay et al. 1996) was used without rescaling. Prior to 1948, daily disaggregation was performed using a method described by Wood et al. (2004) in which month-long daily patterns of precipitation, temperature, and wind speed were sampled at random from the 1948 to 2000 period of existing daily reanalysis data.

We made three major modifications to the VIC algorithms for simulation of frozen soils in northern Eurasia used in Su et al. (2005). These modifications are described in detail by Adam et al. (2007a) (Chapter 6). (1) Su et al. (2005) experienced problems with the parameterization of frozen soils in Arctic regions, particularly with respect to the soil column bottom boundary. As suggested by Cherkauer et al. (2003), rather than treating the lower boundary as constant-temperature, we treat it as zero-flux. This allows for a dynamic bottom boundary temperature which can be predicted as a function of climatic, soil, and ground cover (including vegetation and snow) conditions. This change necessitates increasing the lower boundary depth to at least three times the annual temperature damping depth (Sun and Zhang 2004), in our case from 4 to 15 m. Temperature at the bottom boundary was initialized using gridded observed soil temperature data (Frauenfeld et al. 2004), and we spun up soil column temperature and moisture by running the model for 60 years using forcing data constrained to the climate of the 1930s. (2) Rather than solve the heat equation explicitly for each node, we solved for all the soil temperatures and ice contents simultaneously using the implicit Newton-Raphson method (Press et al. 1992). This method is unconditionally stable and, therefore, the model can be run at time-steps longer than 1 hour. (3) Because the greatest variability in temperature occurs at the near surface thermal nodes, we distributed the

nodes exponentially with depth. We used 18 thermal nodes in a soil column of 15 m which results in node spacings of 20 cm near the surface and 5 m near the bottom boundary. We performed a grid transformation in which the physical system exists in exponential space, while the heat equations are solved in linear space.

The Lohmann et al. (1996; 1998) routing model is coupled off-line to the VIC hydrology model. The routing model transports the combined surface runoff and baseflow to the outlet of any grid cell of interest in the basin. The Unit Hydrograph approach is used for within-cell routing, and the linearized Saint-Venant equations are used for channel routing. The model assumes that all runoff exits a cell in a single flow direction (of which there are eight possible directions) and uses the convolution integral to calculate accumulated flux.

5.2.2.2. *Bias Correction*

Despite the improvements in simulated soil temperatures that resulted from model changes summarized in Section 5.2.2.1, the VIC model under-simulates winter baseflow, especially in permafrost regions (Adam and Lettenmaier 2007a) (Chapter 6). Because the seasonality of inflow to the reservoir strongly affects the storage and release of water from the reservoir, we corrected the streamflow bias at the inlet of the farthest upstream reservoir for each tributary. We applied the probability-mapping technique of Snover et al. (2003) in which percentile maps are generated for each calendar month for both observed and simulated streamflow populations for the period of overlap. For each month in the simulated time series, the percentile for the simulated value was identified relative to the empirical probability distribution of observed flows for that month. The bias corrected value is then equal to the observed discharge corresponding to this percentile. (For additional information, see www.hydro.washington.edu/Lettenmaier/permanent_archive/hamleaf/bams_paper/technical_documentation.pdf.) To preserve the effects of reservoirs that operate in series along a single tributary, we did not bias correct streamflow at the inlets of reservoirs that

are downstream of other reservoirs. Therefore, the runoff contributions that enter the river network between reservoirs are not bias-corrected although, in each case, these contributions to downstream discharge are less than the headwater contributions. The streamflow gauging stations nearest to each of the farthest upstream reservoirs were selected for bias correction. If the gauging station was downstream of the reservoir, the period of observation record before dam construction was used for bias correction training. Table 5.3 lists the selected stations for five of the regulated tributaries, which are indicated as letters A through E in Figure 5.1.

Table 5.3 Streamflow gauging stations (from the R-ArcticNET dataset; Lammers and Shiklomanov (2000)) used for bias correction of inflow to the farthest upstream reservoir in each tributary. Bias correction was not performed for the Kureiskoe reservoir because of the lack of observed streamflow data for this tributary, or the Ust'-Khantaiskoe reservoir because the Khantaika tributary discharges to the Yenisei River downstream of the Igarka gauging station. The location of each station is shown in Figure 5.1 according to the station ID (A through E).

Reservoir	Tributary	Basin	Streamflow Gauging Station	ID	Period
Vilyuiskoe	Vilyui	Lena	Vilyui At Chernyshevskiy	A	1959-1965
Sayano-Shushenskoe	Yenisei	Yenisei	Yenisei At Nikitino	B	1931-1975
Irkutskoe	Angara	Yenisei	Angara At Boguchany	C	1936-1955
Bukhtarminskoe	Irtish	Ob'	Irtish At Shul'ba	D	1937-1955
Novosibirskoe	Ob'	Ob'	Ob At Novosibirsk	E	1936-1955

5.2.2.3. Reservoir Model

We applied the Haddeland et al. (2006a; 2006b; 2007) reservoir model which is intended to be used for large-scale modeling in regions where reservoir management details (i.e. operating policies) are not available. For hydroelectric dams, the reservoir model operates by maximizing hydropower production for each operational year using an optimization scheme based on the SCEM-UA algorithm (Vrugt et al. 2003). While this approach of maximizing hydropower for a single operational year is not completely applicable to reservoirs that are regulated on a multi-annual basis such as the Bratskoe

reservoir (Korobova 1968), this relatively simple reservoir operations model nonetheless should give us an understanding of the effects of the reservoirs on long-term trends (≥ 30 years), over which time-period the differences between single-year and multi-annual operations are somewhat muted. The operational year is identified for each reservoir and begins in the month when mean monthly simulated naturalized streamflow shifts to being less than mean annual streamflow (following Hanasaki et al. (2006)). The reservoir model is operated at a daily time-step and determines reservoir releases, storage, and evaporation. Reservoir evaporation is calculated using the Penman equation for potential evaporation, which is subtracted from reservoir storage each day. To maintain a reservoir water balance, daily precipitation is added to the reservoir surface. To improve parameterization of the model in the Siberian basins, we made several modifications to the Haddeland et al. (2006a; 2006b; 2007) set-up as follows.

(1) *Estimation of minimum allowable reservoir outflow.* To estimate the minimum release from each reservoir, Haddeland et al. (2006a; 2006b; 2007) use $7Q10$, the seven-day ten-year recurrence interval low flow, which is calculated from naturalized simulated streamflow at each reservoir location. Because long-term observations records exist downstream of most of the reservoirs in these basins, we instead set the minimum flow to the mean of winter (DJF) observed streamflow after reservoir construction (Table 5.4). For reservoirs with insufficient nearby streamflow data, we apply $7Q10$.

(2) *Reservoir filling.* Because we use the reservoir simulation results for long-term trend studies, we needed to allow for reservoirs to come online at the end of the construction period. This is followed by a period of reservoir filling. The years filling began are shown in Table 5.1. During the filling period, reservoir discharge is maintained at minimum flow (Table 5.4) and the remainder of the inflow to the reservoir is used for reservoir filling until the reservoir reaches capacity. This results in a filling period of two to five years.

Table 5.4 Minimum flow released from each reservoir calculated as the mean of winter (DJF) flow for the record period after reservoir construction. The nearest downstream streamflow gauging station (from the R-ArcticNET dataset; Lammers and Shiklomanov (2000)) to each reservoir was selected for the calculation. For reservoirs with no nearby downstream gauging station, the seven-day consecutive low flow with a ten-year recurrence period (7Q10) was calculated from the naturalized simulated streamflow at the reservoir location (following Haddeland et al. (2006a; 2006b; 2007)). Note: for gauging stations identified with names other than that of the upstream reservoir, the station ID (corresponding to the locations shown in Figure 5.1) are given.

Reservoir	Streamflow Gauging Station	Minimum Qr, m ³ s ⁻¹
Vilyuiskoe	Vilyui At Chernyshevskiy (ID=1)	738
Sayano-Shushenskoe	Yenisei At Nikitino (ID=B)	986
Krasnoyarskoe	Yenisei At Krasnoyarskaya GES	2819
Irkutskoe	Angara At Irkutskaya GES	1868
Bratskoe	Angara At Bratskaya GES	3074
Ust'-Ilimskoe	Angara At Boguchany (ID=5)	3282
Kureiskoe	7Q10 of Naturalized Flow	232
Ust'-Khantaiskoe	7Q10 of Naturalized Flow	26
Bukhtarminskoe	Irtish At Shul'ba	468
Shul'binskoe	Irtish At Omsk (ID=8)	523
Novosibirskoe	Ob' At HPS Novosibirskaya	612

(3) *Reservoir storage-area-depth relationships.* Whereas the original Haddeland et al. (2006a; 2006b; 2007) system uses a rectangular reservoir shape (vertical walls), we apply the Liebe et al. (2005) formulation. This shape is described by a top-down square-based pyramid that has been cut in half (Figure 5.3). The volume of this shape is given by

$$V = \frac{1}{3} \cdot A \cdot d, \quad (5.1)$$

where the area of the base of the half pyramid, A , is given by $\frac{1}{2} \cdot l^2$, and the height of the pyramid, d , is given by l/f , in which l is the characteristic length of the reservoir, and f is

equivalent to the inverse of the reservoir bed slope. Using these relationships, the dimensionless constant, f , can be determined as

$$f = \frac{\sqrt{2}}{3} \cdot \frac{A_{\max}^{3/2}}{V_{\max}}. \quad (5.2)$$

We estimate f for each reservoir from maximum storage and surface area information (Table 5.2). This allows us to calculate both surface area and depth as a function of storage according to Equations 5.3 and 5.4.

$$A = \left(\frac{3 \cdot f \cdot V}{\sqrt{2}} \right)^{2/3} \quad (5.3)$$

$$d = \left(\frac{6 \cdot V}{f^2} \right)^{1/3} \quad (5.4)$$

Allowing surface area to vary with volume improves the estimation of reservoir evaporation. We use reservoir depth as a proxy for hydrostatic head, h . This formulation provides an improvement to the optimization process because it more realistically simulates the slow change in head with storage when the reservoir is full, and a faster change in head with storage when the reservoir is less full. Note that an alternate value of f , which we denote as f' , can be calculated by rearranging Equation 5.4 (i.e. $f' = \sqrt[3]{6 \cdot V_{\max} / d_{\max}^3}$), where d_{\max} is the dam height), assuming that the dam height is representative of the reservoir depth near the dam. Comparing f to f' (see Table 5.2) gives a rough indication as to how well this theoretical shape describes the relationships between V , A , and d . With the exception of the Bukhtarminskoe reservoir, which has a relatively large surface area with respect to its storage capacity, and to a lesser extent the

Sayano-Shushenskoe and Ust'-Khantaiskoe reservoirs, f and f' are of comparable magnitude.

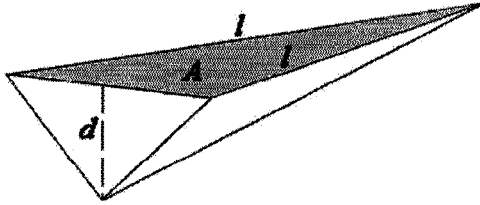


Figure 5.3 Theoretical shape used for the reservoir storage-area-depth relationships. Figure taken with permission from Liebe et al. (2005).

(4) *Minimum storage.* When values of active or regulated storage could be found in the literature, we added an additional constraint on minimum storage, which was calculated as storage capacity minus active storage. Active storage values were found for the Irkutskoe/Baikal system (46 km³, Vyruchalkina (2004)), the Bratskoe reservoir (48.2 km³, Nazarov (1985)), and the Ust'-Ilmskoe reservoir (2.8 km³, Vyruchalkina (2004)). For the Sayano-Shushenskoe reservoir, active storage was calculated using Equation 5.4 and f' , given that the top of dead storage is 42 m below the top of the dam (Stafievskii et al. (2003)). This resulted in a value of 13.5 km³.

(5) *Maximization of hydropower revenue.* Haddeland et al. (2007) suggest that the reservoir simulations may be improved in Arctic regions if the seasonal variability of the economic value of hydropower is considered. Doing so results in the inclusion of the variable P (the monthly price of hydropower) in the following objective function:

$$\min \sum_{i=1}^{365} \frac{1}{P_i \cdot Q_i \cdot \eta \cdot \rho \cdot g \cdot h_i}, \quad (5.5)$$

where i is day of year, Q is reservoir release, ρ is the density of water, η is the efficiency of the power generating system, h is the hydrostatic head, and g is the acceleration due to

gravity. Note that this objective function produces identical results to the original Haddeland et al. (2006a; 2006b; 2007) formulation if P is constant, i.e. the monthly pricing coefficient of variation is zero. Because historical hydropower demands are unknown, we use the monthly pricing curve as a means to calibrate the monthly signature of each reservoir on streamflow. This method is therefore a surrogate to reproduce historical reservoir operations given the different purposes for the hydropower produced at each reservoir. We perform the following steps:

1. *Monthly pricing distribution:* We use a sine curve for the pricing distribution because both the amplitude and the phase of the curve can be determined via calibration. The formulation is as follows:

$$P_i = P_{mean} \cdot \left\{ \frac{Cv}{0.71} \left[\sin \left(\frac{\Pi}{6} (i + Ns) \right) \right] + 1 \right\}$$

and $P_i \geq 0.05 \cdot P_{mean}$, for $i = 1:12$ (5.6)

in which P_i is the price of hydropower for month i , P_{mean} is the mean annual or base hydropower price, Cv is the coefficient of variation of the distribution, and Ns is the phase shift of the function. Cv and Ns are the two calibration parameters. Note that the value 0.71 is the coefficient of variation of the function $\sin(\Pi/6(i+Ns))$.

2. *Base price, P_{mean} .* In 1990, the average cost of hydropower in the Soviet Union was 0.15 kopecks per kWh (Platov 1995), and we use this value as our mean annual price in hydropower. Because P_{mean} scales the weighting factor, the effect of P_{mean} is felt only if P_i is less than 5% of P_{mean} , in which case P_i is set equal to 5% of P_{mean} (see Equation 5.6).
3. *Calibration Parameters:* We calibrated for the values of Cv and Ns by minimizing the difference between the simulated and observed “reservoir signatures” at gauging stations downstream of the reservoirs. Reservoir signature is defined as the net change in the mean monthly hydrograph as a result of reservoir operations.

The assumption here is that these net changes are entirely due to reservoir operations, although in reality some of these changes may be attributable to other effects (e.g., climate change). The key difference between reservoir and climate influences is that the reservoirs should cause an abrupt change in streamflow during the reservoir filling period and immediately thereafter, whereas climate influences should result in more gradual changes. Therefore, the gradual effects of climate will still be apparent in the trend results shown in Section 5.3.3. C_v was constrained to values between 0 and 0.7 (because values greater than 0.7 caused the prices to become negative in some months) and N_s was constrained to values between 1 and 12. The values are given in Table 5.5. As the use of a calibrated pricing curve is a surrogate to reproduce historical reservoir operations given the different purposes for the hydropower produced at each reservoir, different values for N_s may indicate different hydropower uses, as reflected in varying seasons of greatest power needs. See Section 5.3.1 for results.

5.2.3. Development of the Reconstructed Product

We created a reconstructed streamflow product which accounts for the effects of reservoirs as follows. The coupled modeling system was run with and without the reservoir model. At each of the downstream-most gauging stations in the three basins (stations 3, 7, and 10 in Figure 5.1 and Table 5.6) we subtracted the naturalized routed streamflow from the routed streamflow with reservoir effects. These values were then subtracted from observed streamflow. This procedure effectively cancels out the seasonal biases that exist in simulated streamflow. Also, before the reservoirs come online, the reconstructed product is identical to observed streamflow. Comparisons of this product to other reconstructed products are shown in Section 5.3.2.

5.2.4. Trend Analysis

We used the non-parametric Mann-Kendall (Mann 1945) test for trend significance ($p=0.02$, two-tailed), and the Hirsch et al. (1982) method to estimate trend slope.

Because the controls on streamflow variability operate at varying time-scale and in different periods, we apply the trend test to a large number of periods with varying lengths and start years between 1937 and 1998. This is defensible because our objective is to determine the causes of observed streamflow changes for different historical periods,

Table 5.5 The calibration parameters, Cv and Ns, for the monthly pricing distribution were determined by minimizing the differences between observed and simulated reservoir signatures at the locations of the gauging stations listed in column 2. Reservoirs sharing the same gauging station were calibrated simultaneously and therefore have the same calibrated values. Note: the station IDs (corresponding to the locations shown in Figure 5.1) are given in parentheses.

Reservoir	Streamflow Gauging Station	Cv	Ns
Vilyuiskoe	Vilyui At Chernyshevskiy (ID=1)	0.7	5
Sayano-Shushenskoe	Yenisei At Bazaikha (ID=4)	0.36	3
Krasnoyarskoe	Yenisei At Bazaikha (ID=4)	0.36	3
Irkutskoe	Angara At Boguchany (ID=5)	0.46	12
Bratskoe	Angara At Boguchany (ID=5)	0.46	12
Ust'-Ilimskoe	Angara At Boguchany (ID=5)	0.46	12
Kureiskoe	Angara At Boguchany (ID=5)*	0.46	12
Ust'-Khantaiskoe	Angara At Boguchany (ID=5)*	0.46	12
Bukhtarminskoe	Irtish at Omsk (ID=8)	0.44	5
Shul'binskoe	Irtish at Omsk (ID=8)	0.44	5
Novosibirskoe	Ob At Novosibirsk (ID=9)	0.1	3

**Streamflow observations were not available downstream of the Kureiskoe and Ust'-Khantaiskoe reservoirs, therefore they were given the same values as the Angara reservoirs.*

rather than to detect change. We examined periods that have a minimum length of 30 years, increasing in length by increments of 5 years. This was done for every start year beginning with 1937. Therefore, trends were tested for the following periods: 1937-

1967, 1937-1972, 1937-1977, ..., 1938-1968, 1938-1973, 1938-1978, etc... This results in a total of 112 analyzed periods. Trends were calculated using annual, seasonal, and monthly streamflow rates for both observed and reconstructed products. The trend analysis results are reported in Section 5.3.3.

Table 5.6 Streamflow gauging stations (from the R-ArcticNET dataset; Lammers and Shiklomanov (2000)) used for evaluation of the simulated reservoir signature on streamflow seasonality. The location of each station is shown in Figure 5.1 according to the station ID (1 through 10).

ID	Streamflow Gauging Station	Basin	Period of Record	Contributing Area, km ²	Upstream Large Reservoirs	Pre-Res. Period	Post-Res. Period
1	Vilyui at Chernyshevskiy	Lena	1959-1994	140000	1	1959-1966	1970-1994
2	Vilyui at Khatyrik-Khomo	Lena	1936-1998	450000	1	1936-1966	1970-1998
3	Lena at Kusr	Lena	1934-2000	2430000	1	1936-1966	1970-1999
4	Yenisei at Bazaikha	Yenisei	1902-1999	300000	2	1936-1966	1980-1999
5	Angara at Boguchany	Yenisei	1936-1999	870000	3	1936-1956	1975-1999
6	Yenisei at Yeniseisk	Yenisei	1936-1999	1400000	5	1936-1956	1980-1999
7	Yenisei at Igarka	Yenisei	1936-1999	2440000	6	1936-1956	1980-1999
8	Irtish at Omsk	Ob'	1936-1999	770000	2	1936-1956	1990-1999
9a	Ob at Novosibirsk	Ob'	1936-1962	250000	1	1936-1956	NA
9b	Ob at HPS Novosibirskaya	Ob'	1958-2000	230000	1	NA	1960-1999
10	Ob' at Salekhard	Ob'	1930-1999	2950000	3	1936-1956	1990-1999

5.2.5. Reservoir Model Error Propagation

We used satellite-derived reservoir stage estimates for two reservoirs (Lakes Baikal and Bratskoe) to obtain independent estimates of the uncertainty in seasonally-averaged reservoir outflow. By making the assumption that the mean uncertainty in stage height

for these two reservoirs is representative of the uncertainty for other reservoirs, we estimated the total error in the seasonal reconstructed flows at the basin outlets due to the reservoir simulations (via Equations 5.9 through 5.11 below). Finally, we compared these errors to the magnitudes of observed changes and trends occurring in the seasonal flows at the basin outlets.

Stage estimates for Lake Baikal (Irkutskoe reservoir) and the Bratskoe reservoir were obtained from the Surface Water Monitoring by Satellite Altimetry (SWMSA; available at <http://www.legos.obs-mip.fr/soa/hydrologie/hydroweb/>) for the period 1992 to 1999 (the years of overlap with our reservoir operations). The simulated and SWMSA stage heights were set to the same reference height by subtracting their respective mean annual values from each monthly data point. From these, the root mean square errors (RMSE) were calculated on a monthly basis and then averaged for each season.

The water balance in a reservoir (assuming no groundwater exchange) between times t_1 and t_2 is given by

$$Q_{out} = Q_{in} + A \cdot (P - E) - \frac{V_2 - V_1}{t_2 - t_1} \quad (5.7)$$

in which Q_{out} and Q_{in} are the reservoir outflow and inflow, respectively, A is the reservoir surface area, P and E are the precipitation and evaporation depths, respectively, over the reservoir, and V_1 and V_2 are the volumes of the reservoir at times t_1 and t_2 , respectively. We want to express the error in Q_{out} as a function of the errors in the other variables. For a generic function $q = g(x, \dots, z)$, the error in q is related to the errors in x, \dots, z as

$$\Delta q \begin{cases} = \sqrt{\left(\frac{\partial q}{\partial x} \Delta x\right)^2 + \dots + \left(\frac{\partial q}{\partial z} \Delta z\right)^2} & \text{for independent and random errors} \\ \leq \frac{\partial q}{\partial x} \Delta x + \dots + \frac{\partial q}{\partial z} \Delta z & \text{always} \end{cases} \quad (5.8a,b)$$

in which Equation 5.8a holds true if Δx , ..., Δz are independent and random, and Equation 5.8b gives the upper limit of Δq and holds true for all cases (Taylor 1997). Therefore, the error in Q_{out} can be expressed as

$$\Delta Q_{out} \begin{cases} = \sqrt{(\Delta Q_{in})^2 + A^2 \cdot [(\Delta P)^2 + (\Delta ET)^2] + \frac{(\Delta V_2)^2 + (\Delta V_1)^2}{(t_2 - t_1)^2}} & \text{for independent and} \\ & \text{random errors} \\ \leq \Delta Q_{in} + A \cdot (\Delta P + \Delta ET) + \frac{\Delta V_2 + \Delta V_1}{t_2 - t_1} & \text{always} \end{cases} \quad (5.9a,b)$$

where the error in V can be determined using Equation 5.4 as

$$\Delta V = \frac{\partial V}{\partial d} \cdot \Delta d = \frac{1}{2} f^2 \cdot d^2 \cdot \Delta d \quad (5.10)$$

where d is the mean depth of the reservoir at the dam between the times of t_1 and t_2 , and Δd is the RMSE between simulated and SWMSA stage height. Because the method we used to develop reconstructed streamflow is dependent on the differences between regulated and naturalized simulated streamflow (see Section 5.2.3), the error associated with runoff contributions that enter the stream network downstream of the farthest downstream reservoir on each tributary does not need to be accounted for. Therefore, the error in the reconstructed flow at the basin outlet, due only to the reservoir simulations, is a function of the error in Q_{out} for each of the n farthest downstream reservoirs on each of the contributing tributaries and is given by Equation 5.11.

$$\Delta Q_{outlet} \begin{cases} = \sqrt{\sum_{i=1}^n (\Delta Q_{out,i})^2} & \text{for independent and random errors} \\ \leq \sum_{i=1}^n \Delta Q_{out,i} & \text{always} \end{cases} \quad (5.11a,b)$$

This analysis gives us only a very rough approximation of the uncertainty in the reconstructed flows for several reasons: (1) ΔV , as estimated according to Equation 5.10, is a function not only of Δd but also of the error in Equation 5.4, i.e. even if we were able to simulate V with zero error, our estimate of ΔV may be nonzero due to the structural error in Equation 5.4; (2) the satellite-derived stage heights are themselves subject to error; and (3) the stage height errors for Lake Baikal and Bratskoe reservoir are only an approximation for the stage height errors of other reservoirs. The net result may be either an overestimation or underestimation of errors. The results of this analysis are shown and discussed in context of observed changes and trends in Section 5.3.4.

5.3. Results and Discussion

5.3.1. Comparison of Simulated and Observed Reservoir Signatures

The green “plusses” associated with the numerals one through ten in Figure 5.1 are the locations of the gauging stations used to compare our simulated reservoir signature to that inferred from observed streamflow. To calculate the reservoir signature, we compared the mean monthly hydrographs for the period before all upstream reservoirs came online to the mean monthly hydrographs for the period after all upstream reservoirs came online and were filled (given in Table 5.6). Detailed information for each of these gauging stations is given in Table 5.6. For evaluation at station 9 (Ob’ at Novosibirsk), we used separate observed streamflow records for pre and post-reservoir construction monthly hydrographs because neither of the stations have lengthy observations for years both before and after reservoir construction. Because station 9a is downstream of station 9b, and therefore has a larger drainage area, we used the period of overlap (1958 to 1962) as a training period to apply a monthly correction to station 9a streamflow.

The effects of reservoir operations on simulated and observed streamflow seasonality are shown in Figure 5.4. The primary effects are an increase in winter low flow and a decrease in summer peak flow, thereby diminishing streamflow seasonality. The pre and post-reservoir construction differences in monthly streamflow (column 2) demonstrate that the reservoir model captures the major features of the effects of reservoir operations on streamflow seasonality. The largest discrepancies between simulated and observed reservoir influences occur during the summer. If the differences are normalized by mean monthly streamflow (column 3), these discrepancies are distributed more uniformly throughout the year. Note that the Ob' simulations do not capture observed seasonality shifts as well as the Lena and Yenisei simulations. This is probably because we do not take into account irrigation demands. Indeed, the only significant irrigation that occurs over the three basins is in the Ob', of which the basin area is 37% cropland, 2% of which is irrigated (Revenga et al. 1998).

We also examined the effects of reservoir operations on annual streamflow. Table 5.7 shows the pre and post-reservoir construction streamflow rates for both observed and simulated data (for the same periods as above, see Table 5.6). The table also shows the differences and percent differences (with respect to mean annual flow) in streamflow between the two periods. The simulated and observed changes are generally in the same direction, but the model consistently (with the exceptions of stations 1, 4, and 9) simulates a change that is less than (or more negative) than what was observed. It would seem that the model over-simulates the effects of reservoir evaporation on annual flow, especially for the reservoirs on the Angara (Yenisei) and Irtish (Ob') tributaries. This is expected because reservoir evaporation, although calculated using VIC model simulations of available energy, is subtracted from the energy balance offline, replacing the land surface evaporation that would have occurred had the land not been flooded. Therefore, the additional energy required to evaporate at the potential rate is not subtracted from the energy balance. Furthermore, reservoir evaporation was calculated

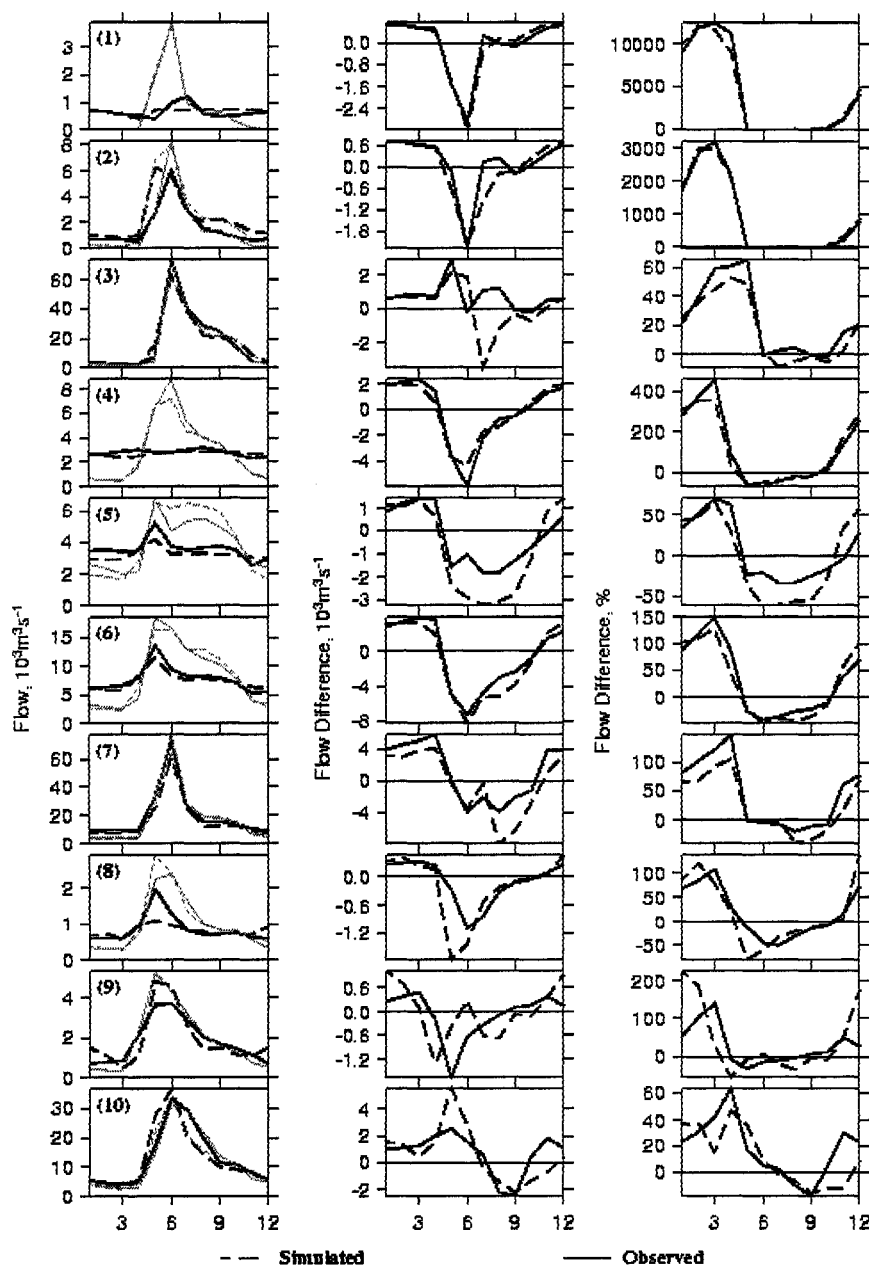


Figure 5.4 Comparison of observed and simulated monthly reservoir signatures at each of the evaluation gauging stations. The station IDs correspond to those in Figure 5.1 and Table 5.6. First column: pre-reservoir (thin lines) and post-reservoir (bold lines) streamflow at reservoir outlet. Second column: difference between post and pre-reservoir mean monthly streamflow. Third column: percent difference (with respect to observed pre-reservoir mean monthly flow) between post and pre-reservoir mean monthly streamflow.

without considering the effects of ice cover on the reservoir. Although evaporation during the freeze season is small in comparison to the thaw season, this assumption does contribute to slight overestimation of reservoir evaporation. The simulated effects of reservoir evaporation on annual flow should be thought of as an upper bound on the actual effects of reservoir evaporation. Finally, it is important to note that changes that occur between the two periods are not due to reservoir influences only. For example, it is unlikely that the observed increases in annual flow at the outlets of the Lena and Yenisei basins are due to direct human influences. Adam et al. (2007a) (Chapter 6) demonstrate that the VIC model does not capture this volume increase and document possible reasons, such as an under-simulation of ground ice melt, which may have contributed to observed

Table 5.7 Comparison of observed and simulated mean annual streamflow at each of the evaluation gauging stations. The station IDs correspond to those in Figure 5.1 and Table 5.6. Columns 2 and 3: pre-reservoir streamflow at reservoir outlet. Columns 4 and 5: post-reservoir streamflow at reservoir outlet. Columns 6 and 7: difference between post and pre-reservoir mean annual streamflow. Columns 8 and 9: percent difference (with respect to observed pre-reservoir mean annual flow) between post and pre-reservoir mean annual streamflow.

ID	Before, $10^3 \text{ m}^3 \text{ s}^{-1}$		After, $10^3 \text{ m}^3 \text{ s}^{-1}$		Diff., $10^3 \text{ m}^3 \text{ s}^{-1}$		% Diff.	
	Obs.	Sim.	Obs.	Sim.	Obs.	Sim.	Obs.	Sim.
1	0.70	0.73	0.65	0.69	-0.05	-0.04	-6.94	-6.38
2	1.48	2.26	1.62	2.28	0.13	0.02	9.01	1.37
3	16.27	16.21	17.04	16.39	0.77	0.18	4.76	1.10
4	2.93	2.78	2.78	2.70	-0.15	-0.08	-5.28	-2.64
5	3.80	4.02	3.57	3.26	-0.23	-0.76	-6.02	-19.93
6	8.12	8.25	7.65	7.30	-0.47	-0.95	-5.82	-11.72
7	18.29	16.61	19.49	16.44	1.19	-0.17	6.52	-0.91
8	0.95	1.01	0.83	0.80	-0.11	-0.21	-11.79	-22.41
9	1.88	1.87	1.80	1.89	-0.08	0.02	-4.49	0.91
10	12.15	11.84	12.86	12.46	0.71	0.62	5.87	5.10

streamflow changes. Therefore, it is possible that the reservoir model adequately captures the effects of reservoirs on annual flow but that the effects of ground ice melt

augmenting annual flow are not captured. The most likely case is that both explanations pertain in varying degrees for each basin.

5.3.2. Comparison to Other Reconstructed Streamflow Products

5.3.2.1. Descriptions of Other Products

In Section 5.2.3 we describe the development of our reconstructed streamflow product, for which the simulated effects of reservoirs were removed from the observed streamflow. Other reconstructed products exist for these basins which were derived from observational data only. The McClelland et al. (2004) product is for the outlets of all three basins (as well as the Kolyma basin which is also regulated), while the Ye et al. (2003) and Yang et al. (2004b) products are for the Lena and Yenisei basins, respectively.

The McClelland et al (2004) product was created by comparing the gauged discharge data before and after dam construction (for stations at or near the reservoirs) and applying the (monthly) differences to the downstream discharge. For the periods during reservoir filling, data were reconstructed on a year-by-year basis relative to the pre-dam average to allow for large inter-annual changes in discharge due to the filling process. Differences were subtracted from downstream values in months showing excess discharge after reservoir filling and were added to the downstream values in months showing deficits in discharge after reservoir filling. The authors note two possible limitations to the data. First, they assumed that all changes in average streamflow (upstream of the stations) are attributed only to reservoirs, although they argue that the long-term effects of climate on streamflow are negligible compared to the effects of the reservoirs. Furthermore, the fraction of watershed area upstream of the stations used for analysis is small compared to the downstream fraction (especially for the Lena and Ob'), and climate change effects on streamflow generated in the downstream fraction are represented (McClelland et al. 2004). Second, there were no corrections for time lags, i.e. the travel time of streamflow

between the dam and the gauging station near basin outlet, which can be up to two months. From here on, we will refer to this product as “McClelland”.

Ye et al. (2003) and Yang et al. (2004b) use a paired-basin method to create reconstructed streamflow for the Lena and Yenisei basins, respectively. This method consists of three steps. (1) Use of stepwise regression to select input streamflow variables. For lags of zero to two months (to reflect the time of flow routing within the basin), the authors calculated correlations between streamflow from basins that are unregulated and streamflow at the basin outlet for the pre-reservoir period. The lag-times that produced the highest correlations were selected. (2) A multiple least-squares regression approach was applied to obtain the best relationship for each month. Results were reasonable for all months except for May for the Lena basin, for which an exponential model was applied. (3) Monthly flow records from the unregulated basins were input into the regression relationships to obtain a reconstructed monthly discharge time series at the basin outlet for the full study period (1942 to 1999 for the Lena, and 1936 to 1999 for the Yenisei). Reconstructed streamflow was not produced for the Ob’ River basin because of complications due to irrigation and other water uses and diversions (D. Yang, personal communication). From here on, we will refer to these products as “Ye/Yang”.

5.3.2.2. Comparison of Reservoir Effects on Flow Seasonality

Figure 5.5 shows the seasonal reservoir signatures inferred from each of the three reconstructed streamflow products. These signatures were calculated by subtracting the observed mean monthly hydrograph from the reconstructed mean monthly hydrograph for the post-reservoir period (column 1). Whereas the signatures from our product and that of McClelland have very similar shapes for the Lena and Yenisei basins, the Ye/Yang signature is much different in the summer. The winter low flow comparison is more easily seen by examining the percent changes in seasonal streamflow, which we calculate by normalizing the absolute differences by mean monthly observed streamflow

(column 2). Although the three products were constructed using completely different methodologies, they imply very similar effects on winter low flows for the Lena and Yenisei basins. This is an indication that the primary human influence in these basins is through reservoir construction for hydropower production. For the Ob' basin, the signatures from our product and that of McClelland, although sharing general features such as an increase in winter streamflow and a decrease in summer streamflow, have some significant discrepancies. For example, our product suggests a much larger effect on winter flows. As mentioned earlier, these discrepancies are likely due to more complicated water uses in this basin, which affect our ability to accurately simulate human effects on streamflow while only considering hydropower production.

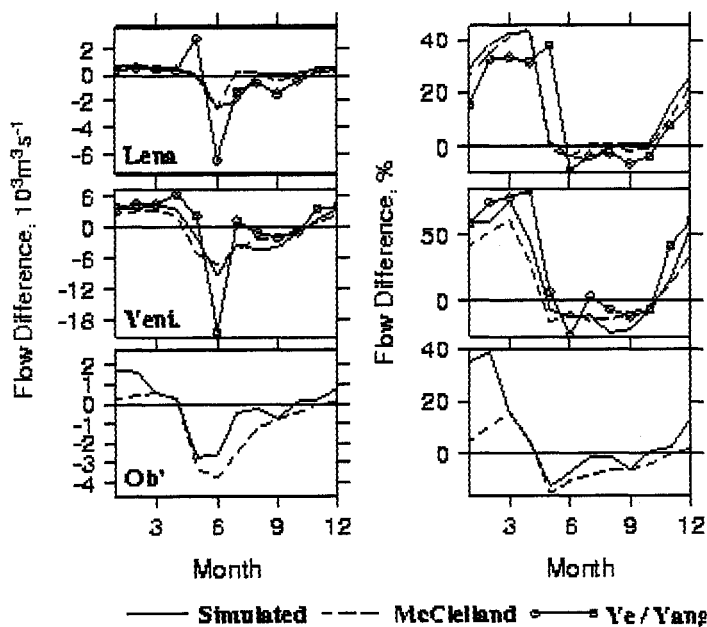


Figure 5.5 Comparison of simulated monthly reservoir signatures to the reservoir signatures inferred from three reconstructed streamflow products (McClelland et al. (2004); for the Lena, Ye et al. (2003); and for the Yenisei, Yang et al. (2004b)) at the outlets of the Lena, Yenisei, and Ob' River basins (gauging stations 3, 7, and 10, respectively; see Figure 5.1 and Table 5.6).

Seasonal streamflow time-series for each of the reconstructed products and the observed data are shown in Figure 5.6. The year that reservoirs for each basin came online and

began to fill are shown by grey vertical lines in each of the figures. By construct, our product and the McClelland product are identical to observed streamflow before reservoir filling. Because the Ye/Yang products for the complete period (pre and post-reservoir) were created by paired-basin analysis, these products do not necessarily match observed streamflow before reservoir implementation. All products show that the most significant changes occur during the winter season. Although these products show similar winter changes in the long-term for the Lena and Yenisei basins, the timing during the filling period is slightly different. In both cases, our product shows a more abrupt decrease in winter streamflow after the construction of each additional reservoir, which may indicate that we constrain the reservoir minimum outflow to be too large during the filling period, thus precluding winter flow to contribute to reservoir filling. The behavior of the three reconstructed products during the spring, summer, and fall for the Lena and Yenisei basins are fairly similar, with the exception that the Ye/Yang products tend to have a greater inter-annual variability for all seasons except for winter, as was noted earlier. This may be an artifact of the paired-basin analyses, i.e. fall Ye/Yang flows for the Lena in particular show “peakier” variations than observed for the pre-reservoir period. As discussed earlier, larger discrepancies between the two reconstructed products exist for the Ob’ basin, particularly for winter and summer, the seasons most influenced by reservoirs.

5.3.2.3. Comparison of Reservoir Effects on Annual Flows

Annual time-series for each of the reconstructed products and the observed data are shown in Figure 5.7. As discussed earlier, Ye/Yang used paired-basin analysis to produce a reconstructed product. This makes it difficult to ascertain what divergences between the reconstructed and observed data after reservoir construction are due to reservoir effects as opposed to variability inherent in the paired-basin analyses. Therefore, we focus in this section on the McClelland and our reconstructed products. Figure 5.7 suggests that the primary effects of the Lena reservoir on annual flow in the Lena basin occurred immediately after filling. Our product diverges significantly from

observations for five years after reservoir construction, whereas the McClelland product diverges from observed for about ten years. In the Yenisei, the inter-annual effects of reservoirs are more complex due to numerous reservoirs coming online over a thirty-year period. For the Ob' and the Yenisei basins, our product and that of McClelland both show significant reservoir evaporation influences in that the reconstructed products maintain a higher annual streamflow after filling completion.

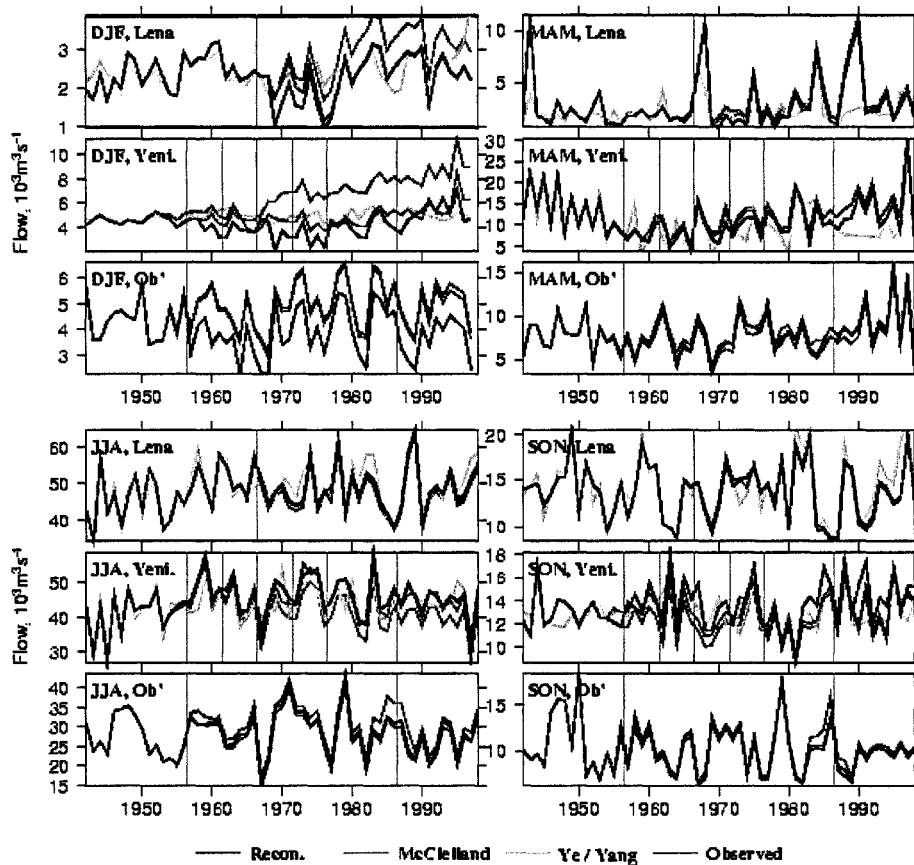


Figure 5.6 Comparison of seasonal flows for four reconstructed streamflow products (ours; McClelland et al. (2004); for the Lena, Ye et al. (2003); and for the Yenisei, Yang et al. (2004b)) to observed streamflow at the outlets of the Lena, Yenisei, and Ob' River basins. Note: DJF is winter, MAM is spring, JJA is summer, and SON is fall. Vertical gray lines indicate the year when filling began for each reservoir in the basin.

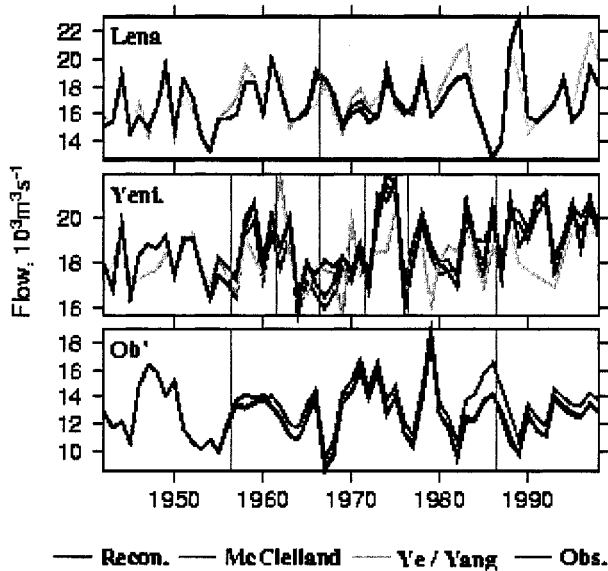


Figure 5.7 Comparison of annual flows for four reconstructed streamflow products (ours; McClelland et al. (2004); for the Lena, Ye et al. (2003); and for the Yenisei, Yang et al. (2004b)) to observed streamflow at the outlets of the Lena, Yenisei, and Ob' River basins. Vertical gray lines indicate the year when filling began for each reservoir in the basin.

To better interpret the effects of reservoir evaporation, we plot the differences between observed and reconstructed flow for our product and the McClelland product (Figure 5.8). Also included in this plot are our simulated reservoir evaporation estimates summed over each basin. For McClelland, inferred reservoir evaporation can be estimated as the long-term difference between reconstructed and observed annual streamflow by assuming that all changes to the annual flow regime for areas upstream of the reservoirs (after filling) are due only to reservoir evaporation. This is not a robust assumption as can be seen in Figure 5.8; the McClelland product infers a negative evaporation over the Lena basin, indicating that other factors are indeed likely occurring in the basin headwaters to change the annual flow regime. These annual losses of reservoir storage to evaporation are given in Table 5.8 along with the year 2000 estimates of Berezovskaya et al. (2007). Berezovskaya et al. based their estimates on those of Shiklomanov and Veretennikova (1978) (which were derived from mean evaporation maps), but reduced the values to account for the over-estimation of predicted reservoir

storage by the end of the last century. Our estimates are greater than those of Berezovskaya et al. As mentioned in Section 5.3.1, we are likely over-simulating reservoir evaporation, which would suggest that the Berezovskaya et al. estimates may provide a realistic range of values. The McClelland flows for the Ob' basin show considerably higher evaporation effects than our reconstructed product, which may be an indication that evaporation rates have increased over the land surface in the Ob' headwaters, i.e. not all of the increased evaporation inferred by the McClelland product is due to reservoir construction. To a lesser degree, this may be true for the Yenisei basin as well.

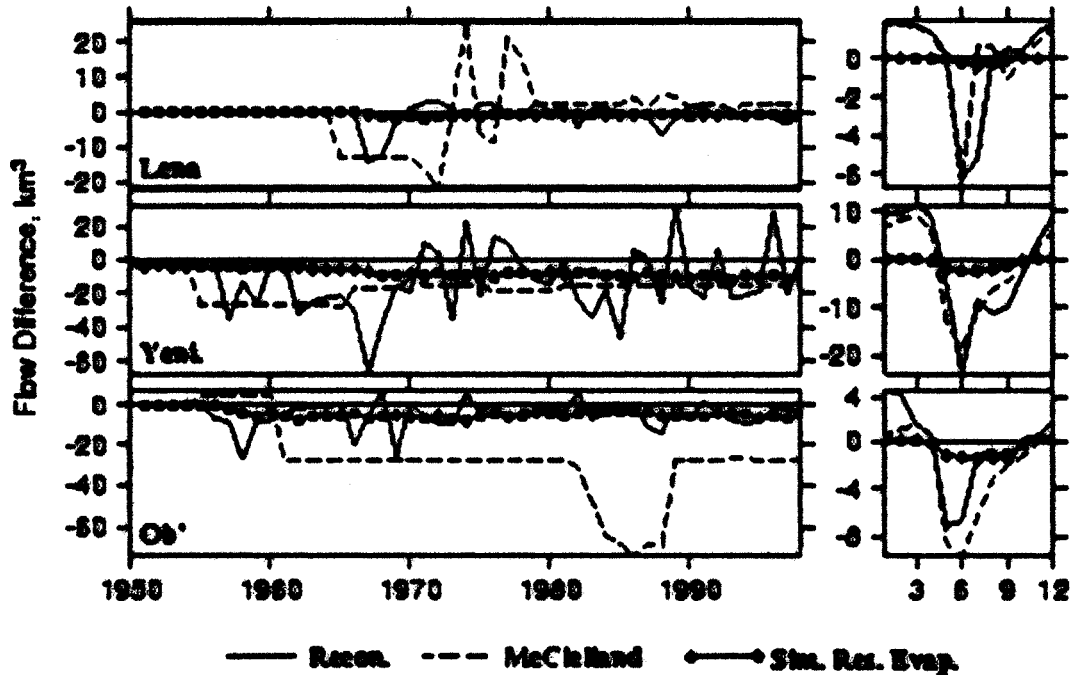


Figure 5.8 Annual and mean monthly potential reservoir evaporation in the Lena, Yenisei, and Ob' River basins. The negative of the evaporation value is plotted to demonstrate the effects of reservoir evaporation on annual flow. Also plotted are the annual and mean monthly differences between our reconstructed streamflow and observed streamflow, and the McClelland et al. (2004) streamflow and observed streamflow. Units are $\text{km}^3 \text{ y}^{-1}$ for annual values and $\text{km}^3 \text{ month}^{-1}$ for mean monthly values.

Table 5.8 Annual reservoir evaporation estimates from three sources: Berezovskaya et al. (2007), our reconstructed product, and as inferred from McClelland et al. (2004). The Berezovskaya data are estimates for the year 2000, while the other estimates are for the period of 1990 to 1998.

Basin	Reservoir Evaporation, km ³ yr ⁻¹			Percent of Mean Annual Flow		
	Berezovskaya	Reconstructed	McClelland	Berezovskaya	Reconstructed	McClelland
Lena	0.1-0.7	0.8	-2.0	0.02 to 0.12%	0.15%	-0.36%
Yenisei	0.9-3.3	10.1	15.6	0.14 to 0.52%	1.57%	2.43%
Ob'	2.6-4.3	5.3	27.3	0.62 to 1.02%	1.27%	6.47%

5.3.3. Effect of Reservoirs on Streamflow Trends

As described in Section 5.2.4, annual and seasonal flows for observed and two reconstructed products (ours and that of McClelland) were trend tested (using the Mann-Kendall test) for periods with varying lengths and start years between 1937 and 1998. The results for sign of the trends for annual and seasonal flows are given in Table 5.9. Generally, annual flows are increasing, primarily for the Lena and Yenisei basins. Winter and spring are the seasons with significant observed streamflow increases, although in many cases these trends are likely due to reservoir effects, i.e. trends for the reconstructed products are both positive and negative. We explored these results in depth by plotting the magnitude for each of the trends (that passed 99% significance) for each basin. The annual trends are shown in Figure 5.9. Positive flow trends at the Lena outlet between the mid 1930s and the mid 1980s are persistent for both the observed and reconstructed products, indicating that this increase is not associated with reservoirs. Furthermore, long-term flow trends at the Yenisei outlet between the 1940s/1950s and the end of last century are also persistent for all products, but larger trends in the later years for the observed product could be a result of reservoir filling effects on inter-annual variability (e.g. the flow will increase once reservoir filling is complete for each of the reservoirs). This cannot be stated conclusively, however, because our reconstructed streamflows do not exhibit these short but large trends, suggesting that they may be a

result of reservoir filling. On the other hand, the McClelland product does, suggesting that the trends are natural. We did not detect any long-term annual trends over the Ob' for either the observed data or for our product. The McClelland product exhibits positive trends in the middle of the period, which are consistent with the product having larger annual flows than the other products after the 1950s and 1980s, and we suspect may be a result of inclusion of upstream effects in the McClelland algorithm that are not entirely reservoir-induced (see Section 5.3.2.3).

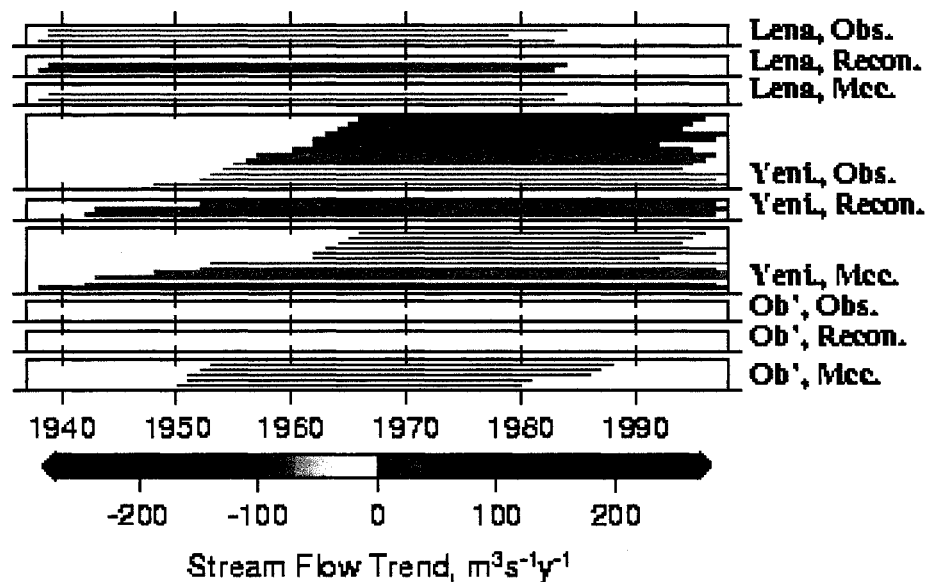


Figure 5.9 Trends in annual basin-outlet streamflow for significance level 99%. Each line represents a period for which the trend slope is given by the color of the line and the period length is given by the length of the line (starting and ending at the start and end of the period, respectively). Each panel is labeled according to basin and whether the streamflow product is observed, our reconstructed streamflow product, or the McClelland et al. (2004) reconstructed streamflow product.

We show trend plots for the two more interesting seasons: winter and spring (Figures 5.10 and 5.11, respectively). Both our product and the McClelland product indicate that the persistent positive trends for periods starting earlier than the 1960s in Lena and Yenisei winter flow are primarily due to reservoirs. Positive winter trends beginning in the 1960s for the Lena and the Yenisei basins may only be partially due to reservoirs, e.g.

a decrease in the ratio of solid to liquid precipitation and an increase in permafrost active layer depth are both hypotheses to explain the remainder of the winter changes. The reconstructed data suggest that Lena and Yenisei winter flows were naturally decreasing in the early part of the record, but increasing between the 1950s/1960s and the end of the last century. Results for Ob' winter flow trends are less conclusive. Whereas our product suggests that long-term trends were entirely due to reservoir operations, the McClelland data suggest that long-term trends starting in the 1930s may be natural. These results are similar to those for spring flow trends (Figure 5.11). Both products suggest that the persistent positive trends in the Lena spring flow are due to reservoirs.

Table 5.9 The number of periods (of the 112 periods analyzed, see Section 5.2.4 for details) for which trends are significant at 99% for both positive and negative trends. Trend analysis results are shown for annual and seasonal flows, and for each of the following products: observed (R-ArcticNET; Lammers and Shiklomanov (2000)), our reconstructed product, and McClelland et al. (2004).

Interval	Basin	Observed		Reconstructed		McClelland	
		Increase	Decrease	Increase	Decrease	Increase	Decrease
Annual	Lena	4	0	2	0	2	0
	Yenisei	14	0	4	0	12	0
	Ob'	0	0	0	0	5	0
DJF	Lena	65	0	3	2	0	1
	Yenisei	111	0	14	47	6	3
	Ob'	19	0	0	1	4	0
MAM	Lena	52	0	1	0	2	0
	Yenisei	41	2	19	11	33	6
	Ob'	0	0	0	0	2	0
JJA	Lena	0	0	0	0	1	0
	Yenisei	0	0	16	0	3	0
	Ob'	0	0	0	0	4	0
SON	Lena	0	0	0	0	0	0
	Yenisei	0	2	0	0	0	0
	Ob'	0	0	0	0	0	0

Alternatively, both reconstructed products exhibit very similar patterns of change to that of the observed product for the Yenisei basin, with negative trends in the early period of the record and persistent positive trends starting around 1950, suggesting that these changes are not reservoir-induced. Once again, the Ob' results are less conclusive with only the McClelland product exhibiting long-term positive trends. We do not show results for summer and fall because there are fewer significant changes during these seasons. The only noteworthy features are persistent positive trends in Yenisei summer flow between the 1940s and the 1970s for both reconstructed products, whereas there are no significant trends for the observed product, suggesting that reservoir effects countered these changes. Also negative trends in Yenisei fall flow between the 1940s and the 1980s are apparent in the observed product but not in the reconstructed products, indicating that these trends are reservoir-induced.

Using the McClelland product and our reconstructed product and at the outlet of each basin, we estimated the fraction of the statistically significant trend magnitude in the observed data that may be due to reservoir effects. The longest period over which the observed trend was significant (99%) was selected for the analysis. Analysis periods were selected separately for each time aggregation interval (i.e. annual, seasonal, and monthly) and for each basin. The reconstructed products were then tested for trend for this same period. If there were no significant long-term (≥ 30 years) observed trends, results for this time interval are not shown (e.g. for the Ob', annual, spring, summer, fall, etc...). The streamflow trend magnitudes from the observed data and two of the reconstructed products are given in Tables 5.10, 5.11, and 5.12 for the Lena, Yenisei, and Ob' basins, respectively. The difference between the observed trend magnitude and either of the reconstructed trend magnitudes provides an estimate of the fraction of the observed trend that was reservoir-induced.

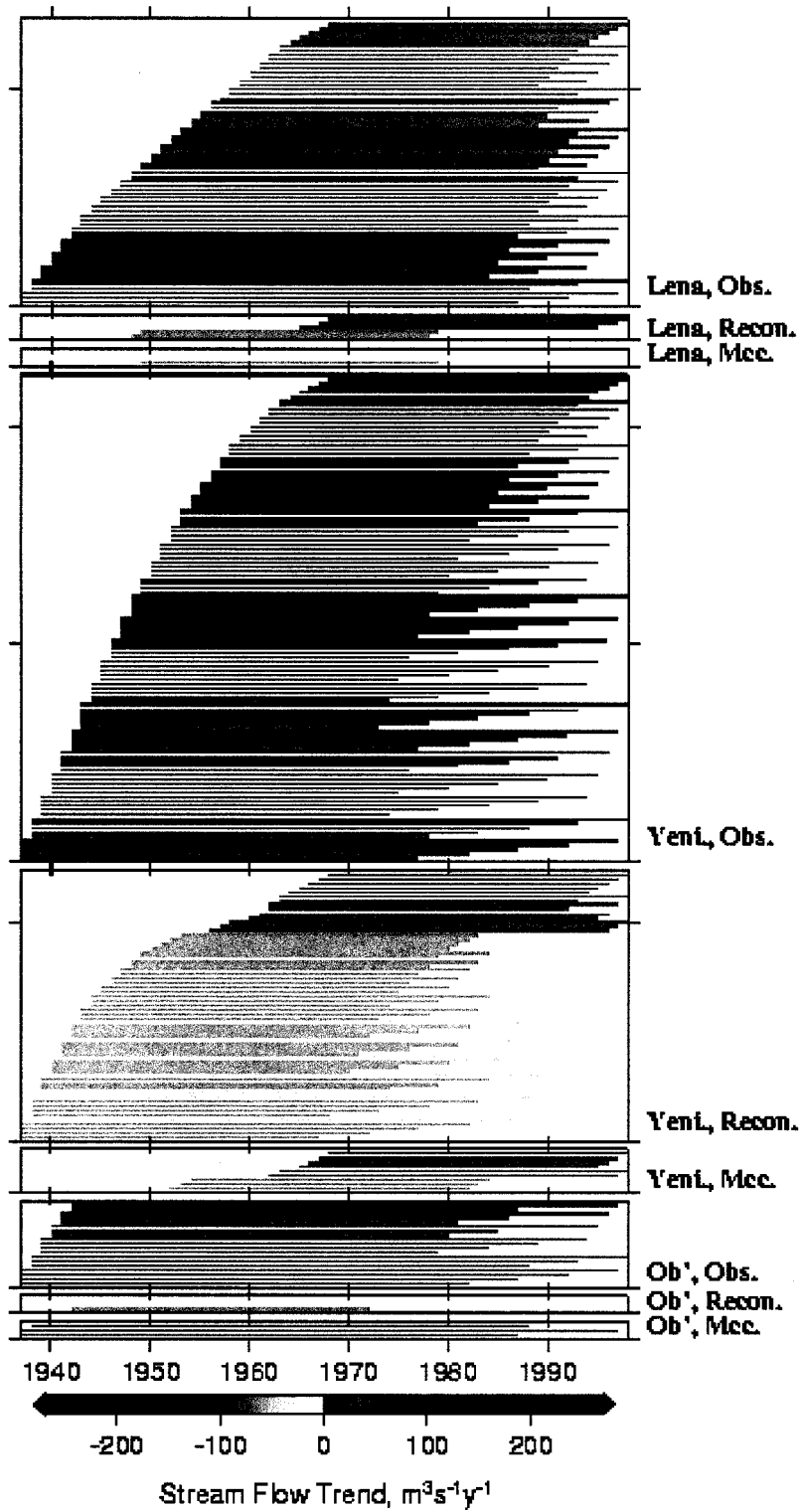


Figure 5.10 Trends in winter (DJF) basin-outlet streamflow (see Figure 5.9 caption for explanation).

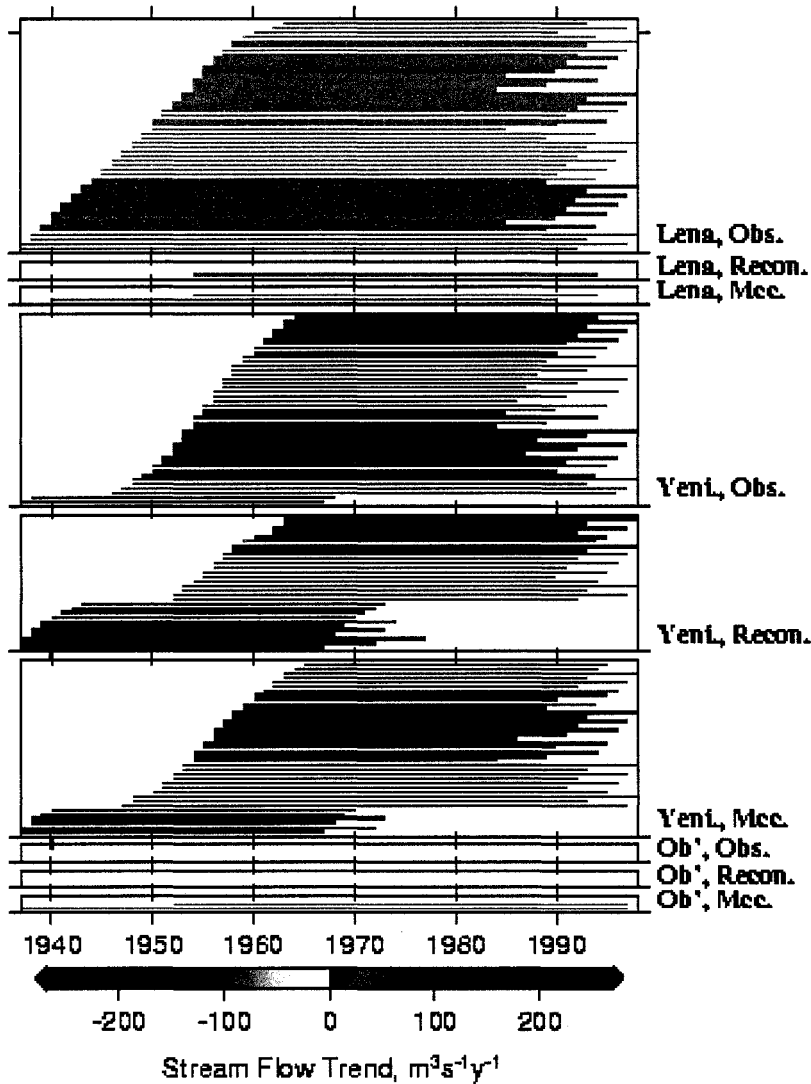


Figure 5.11 Trends in spring (MAM) basin-outlet streamflow (see Figure 5.9 caption for explanation).

The two reconstructed products produce similar results for the Lena basin, accounting for 77% of the observed winter trend and 33% of the observed spring trend (primarily for March and April), but little of the observed annual trend. The two products are in less, but still similar, agreement for the Yenisei basin. Both products indicate that reservoirs are mostly (>88%) responsible for the observed winter trend. Furthermore, they may account for between 44% and 90% of early spring (March and April) trends, and

potentially 26% to over 100% of late summer and fall trends. Like the Lena, the reservoirs appear to account for none of the Yenisei observed annual trend; in fact the reservoirs reduced the annual trend by 15% to 21%, likely due to increased evaporation. The two reconstructed products are in much less agreement for the Ob', with our product suggesting that most or all of the change in January through March are due to reservoirs, whereas the McClelland product indicates that between 21% and 48% of these changes are due to reservoirs. They both produce greater June trends than observed, indicating that reservoirs acted to decrease the natural June flow increases.

Table 5.10 Analysis details for the longest period with a trend significant at 99% for annual, seasonal, and monthly observed streamflows at the outlet of the Lena basin (gauging station 3 in Figure 5.1 and Table 5.6). Seasons or months for which none of the analyzed 112 periods had a significant trend are not included in the table. Column 4: trend magnitude for observed streamflow (R-ArcticNET; Lammers and Shiklomanov (2000)) Columns 5 through 7: for our reconstructed product, trend magnitude, most strict significance level passed, and the difference between the reconstructed and observed trends expressed as a fraction of the observed trend. Columns 8 through 10: for the McClelland et al. (2004) reconstructed product, trend magnitude, most strict significance level passed, and the difference between the reconstructed and observed trends expressed as a fraction of the observed trend. Significance levels tested are 0.99, 0.98, 0.95, 0.90, 0.80, and 0.60. Trends not passing 0.60 significance are indicated by "-". Fractional differences are shown in bold if they exceed 0.5.

Interval	Start Year	End Year	Obs.	Reconstructed			McClelland		
			Trend, $m^3s^{-1}y^{-1}$	Trend, $m^3s^{-1}y^{-1}$	Sig. Passed	Fraction Diff.	Trend, $m^3s^{-1}y^{-1}$	Sig. Passed	Fraction Diff.
Annual	1939	1989	45.9	46.2	0.98	-0.01	46.2	0.98	-0.01
DJF	1938	1998	21.3	4.8	0.80	0.77	4.9	0.80	0.77
MAM	1938	1998	25.8	17.3	0.95	0.33	17.3	0.98	0.33
Jan.	1938	1998	19.8	3.9	-	0.80	3.7	0.60	0.81
Feb.	1938	1998	24.9	8.8	0.95	0.65	7.9	0.98	0.68
Mar.	1938	1998	25.1	11.3	0.99	0.55	9.0	0.99	0.64
Apr.	1938	1998	21.0	9.4	0.99	0.55	6.8	0.99	0.68
May	1954	1994	98.5	95.4	0.99	0.03	111.3	0.99	-0.13
Nov.	1938	1998	20.3	6.6	0.60	0.67	10.0	0.90	0.51
Dec.	1938	1998	17.9	2.0	-	0.89	2.5	-	0.86

Table 5.11 Analysis details for the longest period with a trend significant at 99% for annual, seasonal, and monthly observed streamflows at the outlet of the Yenisei basin (gauging station 7 in Figure 5.1 and Table 5.6). See Table 5.10 caption for further information.

Interval	Start Year	End Year	Obs.	Reconstructed			McClelland		
			Trend, $m^3s^{-1}y^{-1}$	Trend, $m^3s^{-1}y^{-1}$	Sig. Passed	Fraction Diff.	Trend, $m^3s^{-1}y^{-1}$	Sig. Passed	Fraction Diff.
Annual	1948	1998	30.0	34.5	0.98	-0.15	36.4	0.99	-0.21
DJF	1938	1998	79.6	-2.5	-	1.03	9.9	0.90	0.88
MAM	1948	1998	135.5	77.9	0.95	0.42	122.4	0.99	0.10
SON	1937	1982	-36.1	-5.9	-	0.84	-20.4	0.80	0.44
Jan.	1938	1998	79.4	-4.7	-	1.06	9.4	0.90	0.88
Feb.	1938	1998	96.4	12.6	0.90	0.87	16.3	0.99	0.83
Mar.	1938	1998	106.2	11.0	0.60	0.90	21.0	0.99	0.80
Apr.	1938	1998	122.0	42.8	0.99	0.65	68.9	0.99	0.44
May	1938	1978	-431.0	-430.0	0.98	0.00	-380.9	0.95	0.12
Jul.	1946	1986	-190.9	-77.3	0.60	0.59	-39.6	-	0.79
Aug.	1938	1998	-57.6	32.7	0.80	1.57	-9.9	-	0.83
Sep.	1944	1994	-75.0	12.9	-	1.17	-38.7	0.80	0.48
Oct.	1937	1992	-50.0	-3.9	-	0.92	-37.0	0.90	0.26
Nov.	1938	1998	55.1	20.1	0.90	0.63	26.4	0.99	0.52
Dec.	1938	1998	64.6	-13.5	0.90	1.21	10.4	0.80	0.84

5.3.4. Reservoir Model Error Propagation

In Section 5.2.5 we describe the equations used to propagate error in our reservoir simulations to the basin outlet. The errors in simulated reservoir stage height as well as the mean stage heights for the two reservoirs are given in Table 5.13. The results of the error propagation are given in Tables 5.14-5.16 for the Yenisei, Ob', and Lena River basins, respectively. Each table is composed of two to four sub-tables, which are separated by gray space. There is a sub-table for each of the basin's tributaries that is

Table 5.12 Analysis details for the longest period with a trend significant at 99% for annual, seasonal, and monthly observed streamflows at the outlet of the Ob' basin (gauging station 10 in Figure 5.1 and Table 5.6). See Table 5.10 caption for further information.

Interval	Start Year	End Year	Obs.	Reconstructed			McClelland		
			Trend, $\text{m}^3\text{s}^{-1}\text{y}^{-1}$	Trend, $\text{m}^3\text{s}^{-1}\text{y}^{-1}$	Sig. Passed	Fraction Diff.	Trend, $\text{m}^3\text{s}^{-1}\text{y}^{-1}$	Sig. Passed	Fraction Diff.
DJF	1938	1998	20.8	-5.6	0.60	1.27	16.3	0.98	0.22
Jan.	1938	1998	20.0	-13.6	0.80	1.68	15.8	0.98	0.21
Feb.	1938	1998	22.0	-9.1	0.60	1.42	14.0	0.99	0.36
Mar.	1938	1998	22.8	7.3	0.90	0.68	11.9	0.99	0.48
Apr.	1938	1998	21.1	15.8	0.99	0.25	13.8	0.99	0.34
Jun.	1951	1981	185.7	219.3	0.90	-0.18	360.0	0.99	-0.94
Nov.	1963	1998	89.1	82.3	0.98	0.08	85.2	0.98	0.04

regulated by one or more large dams (with the exception of the Khantaika tributary because it enters the Yenisei River downstream of the gauging station we used for analysis). In each of these sub-tables there are four columns for each reservoir on that tributary, one for each of the terms in Equation 5.9a. ΔQ_{in} for the farthest upstream reservoir on each tributary was approximated using the best available information for streamflow measurement errors in these basins. Shiklomanov et al. (2006) estimated the measurement error on a monthly basis at the outlets of the Lena, Yenisei, and Ob' River basins (among others). Averaging over each of the four seasons (DJF, MAM, JJA, and SON) results in the following errors: 17.0%, 15.6%, 4.3%, and 11.2% for the Lena; 17.9%, 15.9%, 3.3%, and 12.0% for the Yenisei; and 16.0%, 15.1%, 4.6%, and 8.9% for the Ob', expressed as the percent of flow. Although these values do not necessarily apply to streamflow measurements other than at the basin outlets, we used them as the best estimates of error for streamflow at the upstream gauging stations in each basin. For the remaining reservoirs, ΔQ_{in} was set equal to ΔQ_{out} of the upstream reservoir. The inter-reservoir contributions of runoff are generally small in comparison to Q_{out} , therefore we neglect the error associated with these contributions. Other than for Lake Baikal (Irkutskoe reservoir) which has a very large surface area, ΔP and ΔE are negligible.

Therefore, the errors we attribute to P and E contributions to/from the water balance have little effect on the final error estimates. We apply a rough error estimate of 20% of mean seasonal P for both terms (recall that precipitation has already been adjusted for systematic bias).

Table 5.13 RMSE values (in m) between simulated and SWMSA stage height, averaged for each season.

Season	Lake Baikal	Bratskoe Reservoir	Mean
DJF	0.07	1.83	0.95
MAM	0.24	1.63	0.94
JJA	0.22	1.87	1.05
SON	0.20	1.73	0.97

An addition, there is a final sub-table at the bottom of each table that provides estimates of the error at the gauging station nearest to the basin outlet. This table is divided into three groups: errors in seasonal flows, seasonal differences in flow as a result of reservoirs, and trends in seasonal flows. The first group gives ΔQ_{outlet} as calculated via Equation 5.11a (ΔQ_{outlet}^I) and Equation 5.11b (ΔQ_{outlet}^M), where I indicates the case of independent and random errors while M indicates maximum error. These values were calculated using the ΔQ_{out} estimates for the farthest downstream reservoir on each tributary (i.e. the last column for each of the tributary sub-tables). In the second group are simulated flows for the period of 1931 to 1955 (before all reservoirs were constructed) subtracted from simulated flows for the period of 1988 to 1999 (after all reservoirs were filled) in the first column (i.e. reservoir signature), and these absolute differences divided by the two estimates of ΔQ_{outlet} in the second and third columns. In the third group are the numbers of periods for which observed streamflow trends are significant at 99% (also see Table 5.9) in the first column, and in the second and third columns are the percentages of these trends for which the trend magnitudes exceed ΔQ_{outlet} in absolute value, for both estimates of ΔQ_{outlet} . The purpose of this final sub-table is to show, at the outlet of each basin, (a) the relative value of seasonal flow

Table 5.14 Analysis of the error in reconstructed Yenisei River streamflow due to uncertainties in the reservoir simulations. Unless marked with an asterisk, all units are in $10^3 m^3 s^{-1}$. See text for details. Note: " $\Delta P, \Delta E$ " = $A \cdot (\Delta P^2 + \Delta E^2)^{1/2}$ where A is obtained from Table 5.1, and " $\Delta dV/dt$ " = $(\Delta V_2^2 + \Delta V_1^2)^{1/2} / (t_2 - t_1)$, where "2" refers to the current season and "1" refers to the previous season.

Tributary:		Angara							
Reservoir:		Irkutsk.				Bratsk.			
Season	ΔQ_{in}	$\Delta P, \Delta E$	$\Delta dV/dt$	ΔQ_{out}	ΔQ_{in}	$\Delta P, \Delta E$	$\Delta dV/dt$	ΔQ_{out}	
DJF	0.30	0.11	0.44	0.54	0.54	0.02	1.61	1.70	
MAM	0.44	0.15	1.48	1.55	1.55	0.02	1.40	2.09	
JJA	0.14	0.17	1.36	1.37	1.37	0.03	1.62	2.12	
SON	0.34	0.15	1.25	1.30	1.30	0.02	1.51	1.99	
Reservoir:		Ilims.							
Season	ΔQ_{in}	$\Delta P, \Delta E$	$\Delta dV/dt$	ΔQ_{out}					
DJF	1.70	0.01	0.70	1.84					
MAM	2.09	0.01	0.69	2.20					
JJA	2.12	0.01	0.69	2.23					
SON	1.99	0.01	0.70	2.11					
Tributary:		Yenisei (above Angara confluence)							
Reservoir:		Sayano.				Krasno.			
Season	ΔQ_{in}	$\Delta P, \Delta E$	$\Delta dV/dt$	ΔQ_{out}	ΔQ_{in}	$\Delta P, \Delta E$	$\Delta dV/dt$	ΔQ_{out}	
DJF	0.06	0.00	0.25	0.25	0.25	0.01	0.20	0.32	
MAM	0.19	0.00	0.22	0.29	0.29	0.01	0.09	0.30	
JJA	0.11	0.00	0.23	0.26	0.26	0.01	0.18	0.31	
SON	0.14	0.00	0.25	0.29	0.29	0.01	0.25	0.38	
Tributary:		Kureika							
Reservoir:		Kureisk.							
Season	ΔQ_{in}	$\Delta P, \Delta E$	$\Delta dV/dt$	ΔQ_{out}					
DJF	0.05	0.00	0.08	0.09					
MAM	0.04	0.00	0.05	0.07					
JJA	0.14	0.00	0.04	0.14					
SON	0.10	0.00	0.07	0.12					
River:		Yenisei							
Station:		Yenisei at Igarka							
Season	Errors		Flow Differences			Seasonal Trends (sig. 99%)			
	Ind. Error	Max Error	Flow Diff	Diff/ I.Error*	Diff/ M.Error*	Total No. *	No. \geq I.Error*	No. \geq M.Error*	
DJF	1.87	4.34	2.98	1.60	0.69	111	93%	20%	
MAM	2.22	5.70	3.19	1.43	0.56	43	100%	95%	
JJA	2.26	5.69	-3.80	1.69	0.67	0	-	-	
SON	2.15	5.62	-2.65	1.23	0.47	2	0%	0%	

*These values are unitless.

differences due to reservoir regulation compared to the error due to reservoir modeling, and (b) the relative values of seasonal flow trends compared to the error due to reservoir modeling.

For the Yenisei basin (Table 5.14), ΔQ_{outlet}^I is less than the simulated reservoir signature on seasonal streamflow for all seasons, although ΔQ_{outlet}^M exceeds the reservoir signature for all seasons. Therefore, in the more likely case that the errors in each of the terms in equations 5.9 and 5.11 are independent and random, the signal exceeds the noise. In the

Table 5.15 Analysis of the error in reconstructed Ob' River streamflow due to uncertainties in the reservoir simulations. See text and Table 5.14 caption for details.

Tributary:	Ob' (above Irtish confluence)								
Reservoir:	Novos.								
Season	ΔQ_{in}	$\Delta P, \Delta E$	$\Delta dV/dt$	ΔQ_{out}					
DJF	0.07	0.00	0.12	0.14					
MAM	0.37	0.00	0.03	0.37					
JJA	0.14	0.01	0.13	0.19					
SON	0.10	0.00	0.17	0.20					
Tributary:	Irtish								
Reservoir:	Bukh.				Shul.				
Season	ΔQ_{in}	$\Delta P, \Delta E$	$\Delta dV/dt$	ΔQ_{out}	ΔQ_{in}	$\Delta P, \Delta E$	$\Delta dV/dt$	ΔQ_{out}	
DJF	0.04	0.02	0.50	0.50	0.50	0.00	0.02	0.50	
MAM	0.16	0.02	0.47	0.50	0.50	0.00	0.01	0.50	
JJA	0.04	0.03	0.56	0.56	0.56	0.00	0.03	0.56	
SON	0.04	0.02	0.53	0.53	0.53	0.00	0.04	0.53	
River:	Ob'								
Station:	Ob' at Salekhard (outlet)								
Season	Errors		Flow Differences			Seasonal Trends (sig. 99%)			
	ΔQ_{outlet}^I	ΔQ_{outlet}^M	Flow Diff	* Diff / ΔQ_{outlet}^I	* Diff / ΔQ_{outlet}^M	*Total No.	*No. \geq ΔQ_{outlet}^I	*No. \geq ΔQ_{outlet}^M	
DJF	0.52	1.02	0.85	1.61	0.83	19	100%	100%	
MAM	0.62	1.29	2.19	3.51	1.70	0	-	-	
JJA	0.59	1.20	-0.06	0.10	0.05	0	-	-	
SON	0.57	1.24	-1.83	3.20	1.48	0	-	-	

Table 5.16 Analysis of the error in reconstructed Lena River streamflow due to uncertainties in the reservoir simulations. See text and Table 5.14 caption for details.

Tributary:	Vilyui								
Reservoir:	Vilyui.								
Season	ΔQ_{in}	$\Delta P, \Delta E$	$\Delta dV/dt$	ΔQ_{out}					
DJF	0.00	0.01	0.14	0.14					
MAM	0.12	0.01	0.08	0.15					
JJA	0.07	0.01	0.14	0.15					
SON	0.04	0.01	0.18	0.18					
River:	Lena								
Station:	Lena at Kusur (outlet)								
Season	Errors		Flow Differences			Seasonal Trends (sig. 99%)			
	ΔQ_{outlet}^I	ΔQ_{outlet}^M	Flow Diff	* Diff / ΔQ_{outlet}^I	* Diff / ΔQ_{outlet}^M	*Total No.	*No. \geq ΔQ_{outlet}^I	*No. \geq ΔQ_{outlet}^M	
DJF	0.14	0.21	0.78	5.49	3.75	65	100%	100%	
MAM	0.15	0.23	1.21	8.27	5.19	52	100%	100%	
JJA	0.15	0.24	1.18	7.64	4.87	0	-	-	
SON	0.18	0.30	-0.41	2.30	1.37	0	-	-	

worst-case scenario in which the errors are dependant or systematically biased, the noise may exceed the signal. Regarding trends, ΔQ_{outlet}^I is less than most to all of the significant winter and spring trends, and greater than both of the fall trends, while ΔQ_{outlet}^M is less than most of the spring trends and less than only 20% of the winter trends. Therefore, comparisons between observed and reconstructed streamflow trends for the Yenisei basin may be robust for spring, unreliable for fall, and should be interpreted with caution for winter. Similarly, for the Ob' basin (Table 5.15), ΔQ_{outlet}^I is less than the reservoir signature for all seasons but summer, and ΔQ_{outlet}^M is less than the reservoir signature for all seasons except winter and summer. Regarding trends, ΔQ_{outlet}^M , and thus ΔQ_{outlet}^I , were less than all of the significant winter trends. There were no significant trends for the other seasons. As mentioned in Section 5.2.5, these error estimates are particularly unreliable for the Ob' basin because the error estimates in stage height, which were derived from two of the Yenisei reservoirs, may not be applicable to the Ob' reservoirs which are partially operated for irrigation purposes. For the Lena basin (Table 5.16), both estimates of ΔQ_{outlet} are less than the reservoir signature for all

seasons. Similarly, both estimates of ΔQ_{outlet} are less than all significant winter and spring trends, while no significant trends were detected for the other seasons. Of the three basins, comparisons between observed and reconstructed streamflow trends for the Lena basin may be the most robust.

5.4. Conclusions

We have estimated the influence of reservoirs on long-term annual, seasonal, and monthly trends at the outlets of the Lena, Yenisei and Ob' River basins. Although reservoirs appear to have had little effect on annual trends, we conclude that they are responsible for much of the seasonal changes that have been observed, especially during the winter and early spring. Results for the three basins are as follows:

- *Lena:* We conclude that the positive long-term (1938-1998) trend in the observed Lena winter flow at basin outlet is primarily due to the construction and operation of the reservoir at the headwaters of the Vilyui tributary, accounting for approximately 80% of the observed trend. This reservoir accounts for approximately 30% of the observed spring positive trend (primarily because of reservoir-induced increases in March and April).
- *Yenisei:* Whereas the positive observed winter trend at the basin outlet persists for the entire observational record, our analyses suggest that winter flows were naturally decreasing in the early part of the record, and increasing between the 1960s and the end of the last century. Analysis over the long term (1938-1998) shows that the positive observed winter trend for this period is due to reservoir influences. Both observed and reconstructed spring trends are negative in the earliest part of the record, followed by a positive trend beginning around 1950. For the period of 1948 to 1998, reservoir influences may account for approximately 40% of the observed spring positive trend (primarily during March

and April, i.e. reservoir influences on May trends are small to negligible). Observed negative trends occurring in July to October are also primarily due to reservoir influences, by as much as 60% to over 100%, depending on the month. Also, August and September trends would have been positive (yet insignificant) over the long-term, were it not for reservoir influences.

- *Ob'*: Our analyses suggest that most or all (>70%) of the changes in the winter and early spring (i.e. March) are due to reservoirs. Our reconstructed product exhibits a greater June trend than observed, indicating that reservoirs acted to decrease natural June flow increases (by approximately 20% of the reconstructed flow trend).

6. Application of a Macroscale Hydrologic Model to Streamflow Trend Attribution

This chapter excerpts and summarizes research to be submitted to *Journal of Climate* as:

Adam, J.C., and D.P. Lettenmaier, 2007: Application of a macroscale hydrologic model to streamflow trend attribution in northern Eurasia, *J. of Climate* (to be submitted).

6.1. Background and Chapter Goals

The hydrological processes of high-latitude regions differ markedly from those at lower latitudes largely because of the predominance of frozen water during much of the year, and because of the large release and uptake of latent heat during the transitional seasons when temperatures are within a few degrees of freezing – conditions which cause the surface water and energy budgets to be closely linked. For these reasons, Arctic hydrology is particularly sensitive to climate and significant changes can occur even from small changes in temperature. These changes are generally largest when and where temperatures are near the 0 °C threshold. Terrestrial frozen water can be found in snow, as ice on the land surface (glaciers, frozen lakes, streams, aufeis), and in the ground (permafrost and seasonally frozen soil). Snow and frozen groundwater particularly have the potential to influence terrestrial hydrological processes, such as streamflow generation, and they play important roles in the climatic influence on these processes. Furthermore, climate-induced changes to snow and frozen soils and the relationships of these changes to the hydrological cycle have the potential to strengthen global climate system feedbacks. These feedbacks involve the world ocean's thermohaline circulation (Broecker 1997), land surface albedo (Groisman et al. 1994a; Groisman et al. 1994b), and the global carbon cycle (Walter et al. 2006).

6.1.1. Observed Changes to Snow and Frozen Soils in the Eurasian Arctic

Snow-cover extent over Eurasia (as well as North America) has declined in recent decades, most dramatically during the spring (April, in particular), while little long-term change has been observed during the fall to mid-winter (Brown 2000; Groisman et al. 1994a; Groisman et al. 1994b; Gutzler and Rosen 1992; Robinson and Dewey 1990; Robinson and Frei 2000). The length of the snow-free season has generally lengthened over Northern Hemisphere land areas, mainly due to earlier snowmelt, and in some cases partially due to a later snow accumulation start (Dye 2002; Foster et al. 1992). Changes in snow depth over Northern Eurasia have been more variable and depend on a combination of temperature and precipitation changes, the season in which the changes take place, as well as the mean climate of the region and various other factors. Some general changes include increased snow accumulation during cold months and reduced snow accumulations during spring, net snow accumulation increases in northern regions and net snow accumulation decreases in southern regions (Brown 2000; Fallot et al. 1997; Ye et al. 1998).

Soil temperature observations indicate that permafrost active layer depth has deepened by approximately 20 cm on average throughout Russian permafrost regions, and freezing depth has decreased by approximately 34 cm on average throughout Russian seasonally frozen soil regions between 1956 and 1990 (Frauenfeld et al. 2004). Increasing soil temperatures may be due to increasing air temperature as well as increasing snow cover or snow depth, particularly in areas of seasonally frozen ground. For example, Pavlov (1994) suggests that 1970 to 1990 warming in the shallow permafrost layers of northern Russia is likely due to global warming, but that increasing soil temperatures of 0.6 to 0.7 °C in the European northeast is likely due to an increase in snow cover. Permafrost thaw can also result in a change of permafrost extent (Nelson et al. 2001), and a northward

shift in permafrost distribution has been observed in parts of North America (Beilman et al. 2001; Kwong and Gan 1994; Thie 1974).

6.1.2. The Importance of Snow and Frozen Soils to Hydrology

The presence of snow plays an important role in both the radiation balance and water cycle of mid to high-latitude regions because of its high albedo (in contrast to the much lower albedo of snow-free vegetation and bare soil), low thermal conductivity, and high spatial and temporal variability. Seasonally, the northern hemisphere's terrestrial snow cover fraction ranges from 7 to 40% (Hall 1988; Liston 1999; Ye et al. 1998; Ye et al. 2004). Furthermore, the snowpack is a dynamic freshwater reservoir that stores solid precipitation and delays runoff generation. For this reason, snowmelt runoff is the major source of streamflow and groundwater recharge over most of the middle and high latitudes. Also in part for this reason, high-latitude streamflow has a large seasonal component, with its peak during the spring snowmelt period.

The presence of frozen water in the ground either perennially (permafrost) or ephemerally (seasonally frozen soil) also plays an important role in the hydrologic processes of much of the high latitude land area. Fall freeze-up of the surface layers limits infiltration and restricts subsurface flow, consequences of which include small cold-season groundwater contributions to streamflow and accentuated spring peak flows (Williams and Smith 1989). These effects are greatest for continuous permafrost for which there are essentially no hydraulic connections between the surface thawed layer (termed the "active layer") and subsurface unfrozen groundwater (below the permafrost), although connections can exist in discontinuous and other "threshold" permafrost types (Kane and Stein 1983).

6.1.3. Snow and Permafrost as Linkages between Climate and Hydrology

Due to its high albedo, climate-induced decreases in snow cover extent may provide the necessary albedo change to accelerate regional and/or global climate change (Brown 2000; Groisman et al. 1994a; Groisman et al. 1994b). Changes to snow can influence further changes to the hydrologic cycle in other ways as well. These interactions are largest during transient seasons and for transient regions (i.e. when and where the temperature is within a few degrees of freezing) because small changes in temperature invoke a change of phase. In particular, spring has been found to be the period with the most dramatic cryosphere-climate interactions (Liston 1999), which is also partly because the greatest warming over the last half-century has occurred during the winter. Because the snow pack integrates the effects of climate (and hence climate change) over the entire period of snow accumulation, very large runoff changes occur during snow melt, affecting the seasonality of streamflow (Nijssen et al. 2001; Yang et al. 2003). Effects on annual (as well as seasonal) streamflow changes can also be due to changes in sublimation. Warming temperatures may lead to enhanced sublimation (via an increase in the vapor pressure deficit), but climate-induced changes to tundra vegetation have the potential to reduce sublimation. For example, climate-induced changes to tundra vegetation have the potential to reduce sublimation, i.e. shrubs that are denser and bushier trap greater amounts of drifting snow, leaving less snow available to sublimate during blowing snow events (Sturm et al. 2001). Evapotranspiration may be enhanced by a longer snow-free season, affecting both warm season runoff generation and the annual water balance (Woo et al. 1992).

Permafrost warming results in a deepening of the active layer, an extended thaw season, and a longer period of infiltration (Hinzman and Kane 1992; Kane et al. 1992), all of which may lead to increased subsurface contributions to winter streamflow (Serreze et al. 2002; Yang et al. 2002; Ye et al. 2004; Zhang et al. 2003). Annual streamflow is augmented by the thawing and release of excess ground ice (Frauenfeld et al. 2004; Zhang et al. 2003). Permafrost degradation may also influence surface water storage, and

hence evaporation, through effects on lakes and wetlands. Patchy wetlands that are supported by warm season overland flow may disappear (Rouse et al. 1997), whereas small lakes may drain in discontinuous permafrost regions as subsurface connections are formed (Smith et al. 2005; Yoshikawa and Hinzman 2003). Alternately, small lakes may grow in regions of continuous permafrost as the excess ground ice melts and before subsurface connections are formed to cause drainage (Smith et al. 2005).

6.1.4. Chapter Goal

The purpose of this research is to explore the ways that precipitation and temperature changes have affected streamflow generation in the Eurasian Arctic, and to identify the roles of land surface modulators in influencing how seasonal and annual streamflow have been affected by climatic change. As described in Chapter 2, the modulators considered are evapotranspiration, snowpack storage, and subsurface soil moisture storage (liquid and frozen).

6.2. Data and Model

6.2.1. Data Sources

All atmospheric variables needed to force the VIC model, such as vapor pressure, incoming shortwave radiation, and net long-wave radiation, are derived from precipitation, daily maximum and minimum temperatures, and wind speed (see Maurer et al (2002) for a description of the algorithms used). Adam et al. (2007) (Chapter 5) outline in detail the methods and data used to prepare the meteorological data used as model input. For temperature, we applied the monthly gridded time-series of Mitchell and Jones (2005). For precipitation, we used the Adam and Lettenmaier (2007b) (Chapter 4) monthly gridded product, which is derived from the Willmott and Matsuura (2005) product by applying the Adam and Lettenmaier (2003) corrections for the under-catch of solid and liquid precipitation in manual gauges and the Adam et al. (2006)

corrections for orographic effects on the interpolation of precipitation point measurements. We also made adjustments for spurious trends using the method of Hamlet and Lettenmaier (2005). This procedure is described by Adam and Lettenmaier (2007b) (Chapter 4).

We evaluate the ability of the model to reproduce streamflow trends by comparing them to trends calculated using either observed or reconstructed streamflow. The R-ArcticNET v3.0 data set (Lammers and Shiklomanov 2000) was used for observed streamflow, whereas the Adam et al. (2007) (Chapter 5) data set was used for reconstructed streamflow for the regulated basins (basins 1, 2, 3, and 10 in Table 3.1). This product was created by running the VIC model coupled to a routing model with and without a coupled reservoir model (2006a; Haddeland et al. 2006b; 2007) which operates by maximizing annual hydropower production. At the outlet of each of the regulated basins, simulated streamflow without the reservoir model was subtracted from simulated streamflow with the reservoir model, producing a time-series of reservoir influences that were then subtracted from the observed basin-outlet discharge. This constrained the reconstructed flow to be identical to the observed before reservoir construction. (See Adam et al. (2007) (Chapter 5) for details). Because Adam et al. (2007) found that the effects of reservoirs on long-term trends in annual streamflow were minimal, we used the observed streamflow for all annual trend calculations. The reconstructed streamflow was only applied when calculating monthly trends for regulated basins (see Section 6.4.4).

6.2.2. Modeling Framework

The version of the VIC model that we applied for this study (v. 4.1.0) includes algorithms that are important for processes occurring in Arctic regions (Cherkauer et al. 2003), including a lakes and wetlands model (Bowling 2002), an algorithm for the sublimation and redistribution of blowing snow (Bowling et al. 2004), a finite-difference frozen soils algorithm (Cherkauer and Lettenmaier 1999) with sub-grid frost variability (Cherkauer and Lettenmaier 2003), and a two-layer energy balance snow model (Andreadis et al.

2007; Storck and Lettenmaier 1999) that allows for sub-grid variability in snow cover (Cherkauer and Lettenmaier 2003). To simulate streamflow, the VIC model is coupled off-line to the Lohmann et al. (1996; 1998) routing model, as described by Adam et al. (2007) (Chapter 5). Su et al. (2005) applied the VIC model to the pan-Arctic land domain using the 100 km by 100 km Equal-Area Scalable Earth (EASE) grid projection of Brodzik (1997), calibrated according to the monthly streamflow hydrograph, and tested the results against satellite-derived snow cover extent, lake freeze-up and break-up date observations, and summer active layer depth observations. They found that the model performed satisfactorily in reproducing various mean hydrological quantities with the exceptions of winter base-flow and active layer depth. Because both of these are related to permafrost processes, we present the following description of the frozen soils algorithm.

Cherkauer and Lettenmaier (1999) introduced the predecessor to the finite difference frozen soil algorithm used in version 4.1.0 of the VIC model. In this algorithm, frost penetration is determined by solving the thermal fluxes through the soil column, and the infiltration and runoff response parameterizations are adjusted to account for the effects of soil ice content. In this early version, frozen soils were simulated uniformly across each grid cell, but in reality meltwater will pond or flow across the surface until it finds an area with less soil ice that has a higher infiltration capacity. As a result, the early model tended to over-predict spring floods (Cherkauer and Lettenmaier 2003). To improve spring peak flow predictions, a parameterization of the spatial distribution of soil frost was added to the model (Cherkauer and Lettenmaier 2003). Furthermore, Cherkauer et al. (2003) describe the improvements made to the frozen soils algorithm to simulate permafrost, including representation of multiple freeze/thaw fronts, an option for a zero flux bottom boundary rather than the commonly applied constant temperature bottom boundary, and a more efficient soil heat flux solution. The Su et al. (2005) implementation used a constant temperature bottom boundary set at the depth of 4 m (approximately the annual thermal damping depth for most areas of the Arctic) for which

the temperature at the damping depth was constrained to be the long-term annual average air temperature. They used 15 finite difference thermal nodes linearly distributed through the soil column, and utilized the spatial soil freezing algorithm of Cherkauer and Lettenmaier (2003). As also described by Adam et al. (2007) (Chapter 5), there are three differences between the implementation used here and that used in Su et al. (2005): (1) a longer simulation period (1930-2000 for this study), (2) differences in the model forcing data, and (3) modifications to the frozen soils algorithm. The modifications include the following:

(1) *Bottom Boundary Specification.* To increase computational efficiency, we applied a constant temperature bottom boundary at a depth of 4 m, in which we defined the temperature at the bottom boundary using the observed soil temperature datasets of Zhang et al. (2001).

(2) *Thermal Node Distribution.* For maximum computational efficiency, the spacing of computational thermal nodes should reflect the variability in soil temperature. Because the greatest variability in soil temperature occurs near the surface, it is preferable to have tighter node spacings near the surface and wider node spacings near the bottom boundary where temperature variability is reduced. Therefore, we distributed the thermal nodes exponentially with depth and performed a coordinate transformation exponential space to linear space. We used 10 thermal nodes, which resulted in spacings of 20 cm near the surface and 80 cm near the bottom boundary.

(3) *Implicit Solver.* We solve the system implicitly using the Newton-Raphson method. Previous implementations of the VIC frozen soils algorithm used an explicit method to solve the temperature at each thermal node independently and, therefore, were required to satisfy the Courant-Friedrichs-Lewy condition for numerical stability. The implicit solver ensures unconditional numerical stability, therefore, we were able to perform the simulations at a three-hour time-step and improve computational efficiency and stability.

(4) *Excess Ground Ice and Ground Subsidence.* We include an excess ground ice and ground subsidence algorithm in the VIC model. Each layer of the soil column must be initialized with an ice fraction, n' . If n' exceeds the soil porosity, n , then the soil layer contains excess ice, which is defined as $n' - n$. As excess ice melts in response to climatic warming, the ground collapses and the excess meltwater is expelled to the surface. Because of ground subsidence, the water-holding capacity of the soil column is diminished.

6.3. Analytical Methods

6.3.1. Water Balance Approach

The hydrologic water balance equation, given by

$$P = Q + ET + \frac{dS}{dt}, \quad (6.1)$$

is valid over all time and space-scales, where P , ET , and Q are spatially-averaged precipitation, evapotranspiration, and runoff, respectively, and dS is the increase of water stored in the system over the time increment, dt . We examined changes in each of the water balance components (via trend analysis), to identify mechanisms that may have caused the observed changes in streamflow. The discretized first derivative of Equation 6.1 is

$$\frac{\Delta P}{\Delta t} = \frac{\Delta Q}{\Delta t} + \frac{\Delta ET}{\Delta t} + \frac{\Delta(dS/dt)}{\Delta t}. \quad (6.2)$$

Therefore, an increase in Q may be caused by an increase in P , a decrease in ET , or a decrease in dS/dt (signifying a net release of water from storage). Most realistically, all components are changing over time to some extent, and changes in two or more

components may have competing effects on streamflow. For example, warming air temperatures may cause ET to increase, thereby reducing the response of Q to increases in P . Adam and Lettenmaier (2007b) (Chapter 4) discuss the mechanisms that may have contributed to increases in annual Q , including reservoir construction and operation, increases in P due to intensification of the hydrologic cycle, permafrost degradation and other subsurface water storage dynamics, and changes in ET in response to climatic change. In this study, we expanded the analysis by exploring the roles of the various water balance components in causing both annual and monthly Q changes, as well as examining the spatial distribution of annual changes in each water balance component. For the monthly change analysis, we partitioned the storage term dS/dt into the individual storage terms that we hypothesize to have had the largest effects on streamflow generation, the snowpack and near surface soil moisture (liquid and frozen). Our objectives (as related to the purpose mentioned in Section 6.1.4) are to identify when and where Q trends diverge from P trends, to distinguish the roles of the “modulators” (see Figure 2.1) in causing the divergences, and to comment on how increasing surface temperatures may have invoked changes in the modulators.

6.3.2. Trend Analysis

We used the non-parametric Mann-Kendall (Mann 1945) test for trend significance and the Hirsch et al. (1982) method to estimate trend slope. The Mann-Kendall test is a non-parametric test for trend with no linearity assumption (see Section 4.3.3.1). Trend significance was tested for significance levels of 99% and 90% (e.g. using a two-sided test, $P = 0.02$ and 0.20 , respectively). Because we are interested in understanding how controls on streamflow changes have varied in time, we follow Adam et al. (2007) (Chapter 5) and Adam and Lettenmaier (2007b) (Chapter 4) in applying the trend test to a large number of periods with varying lengths and start years between 1936 and 1999. We examined periods that have a minimum length of 20 years, increasing in length by increments of 5 years. This was done for every start year beginning with 1936. Therefore, annual and monthly trends were calculated for the following periods: 1936-

1956, 1936-1961, 1936-1966, ..., 1937-1957, 1937-1962, 1937-1967, etc... Annual trend tests were performed for the hydrological water year, October through September. To be consistent with the literature, we use the short-hand unit of mm year^{-1} for both monthly and annual trend slopes (i.e. this should be interpreted as $\text{mm month}^{-1} \text{ year}^{-1}$ for monthly data and mm year^{-2} for annual data). For the spatial trend analysis, spatially-distributed trend slopes were calculated for the following periods: 1936-1999, 1949-1999, and 1979-1999.

6.3.3. Description of Tasks Performed

(1) *Initialization of Ground Ice Concentrations.* To test the sensitivity of simulated streamflow trends to varying amounts of initial excess ground ice, we multiplied ground ice contents derived from the Brown et al. (1998) data by various scale factors. The derived ground ice content for each 100 km grid cell was calculated by multiplying the coverage by area of permafrost (Table 6.1a) by the ground ice volumetric fraction (Table 6.1b). For both of these values we used maximum estimates (see column 3 of Table 6.1). We performed three experiments by using the following scale factors: 2.5, 3.5, and 4.5 (run #'s 2, 3, and 4, respectively – run #1 was a baseline zero excess ice simulation). The excess ground ice concentration was then calculated as the difference between the volumetric ice fraction and the soil porosity of the soil layer. (Note the lowest scale factor was chosen because it is the lowest value, in increments of 0.5, that causes excess ice to exist in the system.) For each scale factor, we applied an initial background or minimum concentration of excess ice, which we chose to be 0.05, 0.1, and 0.2, respectively. Excess ground ice was initialized only over permafrost regions and for the bottom of three soil layers in the VIC model, which we defined to have a thickness of 3.6 m. The top and middle soil layers were assigned thicknesses of 0.1 and 0.3 m, respectively. For the non-permafrost regions (grid cells with no coverage of any of the permafrost types), we used the calibrated soil thickness values of Su et al. (2005). For each experiment, we ran the VIC model for a spin-up period of ten years, in which the climate of the ten-year period was constrained to match that of the 1930s. The final state

of the spin-up run was used to initialize the full 1930-2000 run. The experimental run used for streamflow trend attribution was the run that produced the closest match between simulated (routed) and observed streamflow trends. To further evaluate the chosen run, we calculated error statistics for annual and monthly streamflow for each basin. Results are shown in Section 6.4.1.

Table 6.1 Brown et al. (1998) permafrost classifications by (a) permafrost classification and (b) ground ice content. For the range of values given by Brown et al. (1998) (column 2), we use the upper value for excess ice initialization. In the case of "high" ground ice content, we use twice the lower limit. Brown et al. (1998) defines the "f" landforms as "lowlands, highlands, and intra- and intermontane depressions characterized by thick overburden cover", and the "r" landforms as "mountains, highlands ridges, and plateaus characterized by thin overburden cover and exposed bedrock".

(a) Permafrost Extent	Fraction of Area	Upper Value
Continuous	90-100%	100%
Discontinuous	50-90%	90%
Sporadic	10-50%	50%
Isolated	0-10%	10%
<hr/>		
(b) Ground Ice Content	Volumetric Ice Fraction	Upper Value
High, "f" landforms	>20%	40%
High, "r" landforms	>10%	20%
Medium, all landforms	10-20%	20%
Low, all landforms	0-10%	10%

(2) *Selection of Periods and Basins for Trend Analysis.* Because we expect that the model may not capture all of the observed streamflow trends found to be significant (see Section 6.3.2 for a list of periods tested), we limited our discussion of trend attribution only to those basins and periods for which the model was able to reproduce the significant observed trends in streamflow. By comparing the trend slopes between observed and simulated (routed) streamflow for each of the periods for which the streamflow trend was significant at 90%, we identified a "period of captured trends" for

each of the basins. The entire study period (1936-2000) was captured for four of the eleven study basins; significant trends in the years following 1975 were captured for all the study basins. Results are shown in Section 6.4.2.

(3) *Spatial Distributions of Annual Trends in Each Water Balance Component.* To investigate how changes in the water balance varied spatially, we calculated trend slopes for each 100 km grid cell for each of the major water balance components given by Equation 6.1. Because 20th century warming accelerated up through the end of the century, we calculated the spatially-distributed trend slopes for three periods: 1936-1999, 1949-1999, and 1979-1999. For each of these periods, discussion of the trend slopes as they relate to runoff trend attribution is constrained to those basins for which the “period of captured trends” overlaps with the period of analysis. Results are shown in Section 6.4.3.

(4) *Monthly Trends in Each Water Balance Component.* The goal for this task was to identify the roles of the modulators (see Figure 2.1) in affecting the way annual and monthly runoff generation responded to changes in precipitation and temperature. Eight basins were chosen for this analysis, two “cold” basins, three “threshold” basins, and three “warm” basins. A separate period of analysis was selected for each basin that included the years of greatest change. Results are shown in Section 6.4.4.

6.4. Results and Discussion

6.4.1. Initialization of Ground Ice Concentrations

Figure 6.1 shows the concentrations of excess ground ice before model spin-up, after the ten-year model spin-up, and after the full 1930-2000 simulation, for three of the four simulations (the first simulation was a baseline simulation with zero excess ground ice). In each case, most of the excess ice disappeared after the spin-up period, leaving excess ice in the coldest regions of Siberia, the northern Yenisei basin, the mountainous regions

in the southern Yenisei basin, and much of the Lena basin, particularly the areas of yedoma permafrost, where excess ground ice concentrations are highest (cf. Figure 3a of Walter et al. (2006)). Excess ice is further diminished at the end of the 1930-2000 simulation, with the least amounts for run #2 (Figure 6.1a) (mainly occurring in the Aldan River basin, i.e. Lena1), and the greatest melt for run #4 (Figure 6.1c).

Table 6.2 gives the error statistics between trends in observed and simulated (routed) streamflow for each simulation and for each of the study basins. Included is a “baseline” simulation (run #1), in which excess ground ice was initialized with a value of zero. Recall that observed streamflow was tested for trend for a large number of periods between 1936 and 1999 (see Section 6.3.2). The total number of periods tested for each basin is dependent on the length of the observational record and is given as the second value in column 3 of Table 6.3. For each study basin, trend slopes were compared between simulated and observed streamflow for all periods over which the observed streamflow trend was significant at the 90% level; the number of periods with significant observed streamflow trends is given as the first value in column 3 of Table 6.3. To identify the run that best reproduced trends in observed streamflow, we considered three statistics relating simulated and observed trend slopes, the square of the Pearson product-moment correlation coefficient (R^2), relative bias (Bias), and root-mean-square-error (RMSE), all of which are listed in Table 6.2 for each run and basin. For each basin, we shaded the run with the most favorable statistic in gray, allowing us to identify the run to be used for all further analysis. Although runs #1 and #2 both performed significantly better than runs #3 and #4, run #2 marginally outperformed run #1. Therefore, we used run #2 (which had a ground ice scale factor of 2.5 and an excess ice background fraction of 0.05, see Section 6.3.3(1)) for the streamflow trend attribution study, and all remaining results are for this simulation.

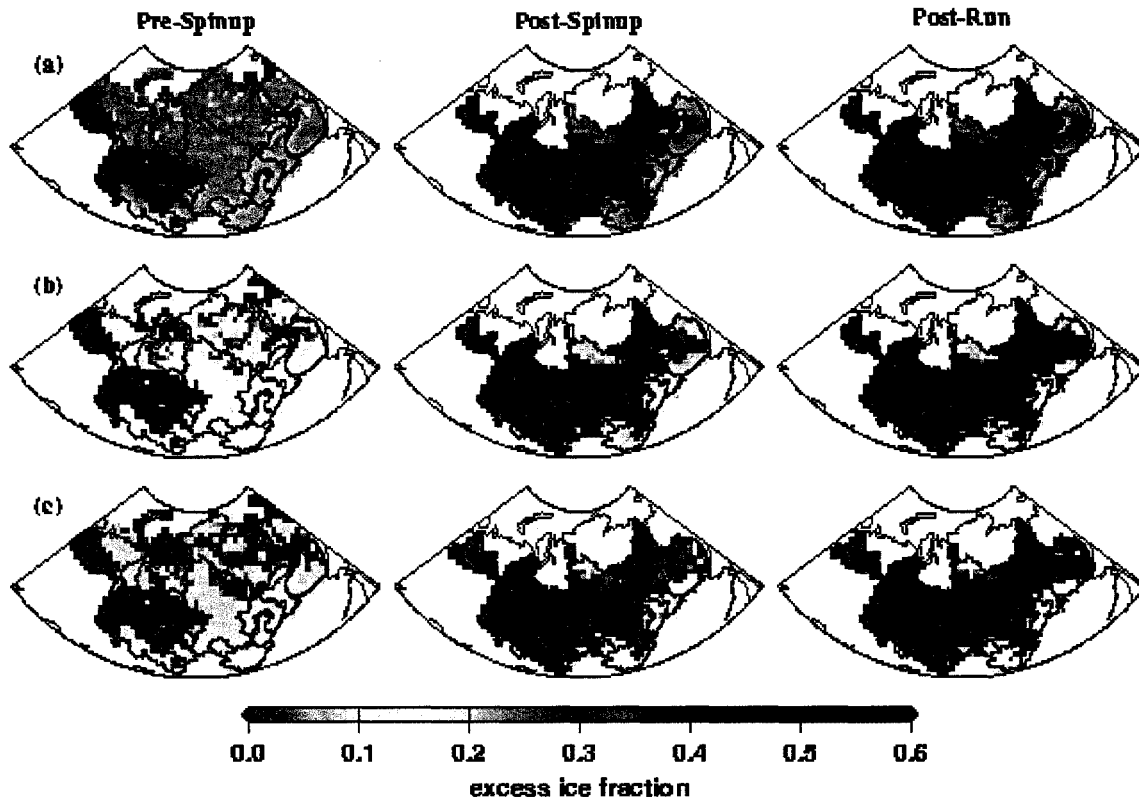


Figure 6.1 Excess ground ice concentrations, defined as the difference between effective porosity and soil porosity ($n' - n$), before model spin-up (left column), after ten years of model spin-up (middle column), and after the 1930-2000 simulations (right column). Results are shown for runs two, three, and four (a, b, and c, respectively). See Table 6.2 for details of each run.

As a further evaluation of the simulation, we sorted the observed and simulated trends by sign (Table 6.3). The model captured all the correct trend signs for the warm basins, as well as for Lena1 (a cold basin) and Yeni2 (a threshold basin). Therefore, only in permafrost basins, particularly some of the threshold basins, was the model not able to capture all the correct trend signs. For these basins, the model is biased towards too many negative trends. As a further comparison, we created scatter-plots of simulated versus observed streamflow trends (Figure 6.2). The black circles represent the periods with statistically significant changes at the 99% level, while the gray circles are for changes significant at 90% but not at 99%. For many of the permafrost basins, clustered points above the one-to-one line indicate positive observed trends that are not captured or

are only partially captured by the model. Possible explanations for this are given in Section 6.4.2.

Table 6.2 Multi-period trend-slope error statistics for each simulation and basin (see text for further details). The “base-line” simulation is without excess ground ice, whereas runs two through four were initialized with varying excess ice concentrations (see Figure 6.1). Initial excess ice concentrations were calculated by multiplying the upper bound of the Brown et al. (1998) ground ice estimates by the factor “F” and by constraining the excess ice concentration to have a minimum of “B” (see column 1), where excess ice concentration is defined as the difference between effective porosity and soil porosity ($n' - n$). Shaded cells indicate runs that have the best statistic (highest value for R^2 , value closest to zero for Bias, lowest value for RMSE). In situations where a statistic is nearly identical for all runs, no cell was shaded for that particular basin and statistic. If two runs tied for first place for a particular statistic, they were both shaded.

	Basin:	Lena	Yeni	Ob	Lena1	Lena2	Lena3	Yeni1	Yeni2	Ob1	Ob2	SDvina
Run #1 Base-line	R^2	55%	40%	94%	79%	68%	61%	72%	96%	85%	86%	80%
	Bias	-34%	-146%	-18%	-26%	-95%	-64%	-18%	72%	-14%	-9%	-33%
	RMSE	76%	217%	79%	77%	159%	118%	334%	109%	367%	515%	50%
Run #2 F=2.5 B=0.05	R^2	41%	39%	94%	84%	67%	63%	71%	97%	88%	86%	80%
	Bias	-48%	-151%	-19%	-29%	-91%	-63%	-2%	88%	-11%	-9%	-33%
	RMSE	92%	221%	81%	67%	156%	115%	407%	114%	351%	516%	50%
Run #3 F=3.5 B=0.1	R^2	33%	45%	94%	43%	67%	59%	64%	96%	88%	86%	80%
	Bias	-76%	-156%	-19%	-88%	-93%	-71%	-7%	83%	-11%	-9%	-33%
	RMSE	118%	219%	79%	167%	159%	128%	385%	119%	351%	514%	50%
Run #4 F=4.5 B=0.2	R^2	6%	56%	94%	32%	66%	21%	63%	96%	85%	86%	80%
	Bias	-153%	-180%	-19%	-121%	-112%	-88%	-15%	78%	-13%	-8%	-33%
	RMSE	218%	228%	77%	228%	174%	152%	382%	109%	368%	510%	50%

*Note: $Bias = \left[\frac{(\bar{T}_s - \bar{T}_o)}{\bar{T}_o} \right] \times 100\%$ where T_o is the trend slope for observed streamflow and T_s is the trend slope for simulated (routed) streamflow.

$RMSE = \left[\sqrt{1/n \sum_i (T_{s,i} - T_{o,i})^2} / \bar{T}_o \right] \times 100\%$ where i represents one period in which observed streamflow is significant and n is the number of periods with significant observed streamflow trends (given by the first value in Table 6.3, column 3).

Table 6.3 The number of periods for which annual trends are significant at 90% for observed streamflow for each of the study basins (column 3, first value). The total number of tested periods depends on the period of record for each basin and is given as the second value in column 3. Columns 4 and 5: the number of positive (≥ 0) and negative (< 0) trends for observed streamflow. Columns 6 and 7: the number of positive and negative trends for simulated (routed) streamflow for the periods in which observed streamflow trends are significant. See Figures 6.4 and 6.5 for visualizations of these trends.

ID	Basin Reference Name	No. Significant	Observed Streamflow		Simulated Streamflow		Regime
			No. Positive	No. Negative	No. Positive	No. Negative	
1	Lena	66/330	66	0	60	6	Cold
2	Yeni	100/308	80	20	19	81	Threshold
3	Ob	29/319	9	20	9	20	Warm
4	Lena1	68/245	62	6	62	6	Cold
5	Lena2	82/308	68	14	32	50	Threshold
6	Lena3	48/308	46	2	38	10	Threshold
7	Yeni1	67/297	48	19	28	39	Threshold
8	Yeni2	8/319	1	7	1	7	Threshold
9	Ob1	17/319	7	10	7	10	Warm
10	Ob2	31/319	16	15	16	15	Warm
11	SDvina	42/319	40	2	40	2	Warm

The model was also evaluated for its ability to reproduce observed annual and monthly streamflow at each of the basin outlets. Simulated, observed, and (for regulated basins) reconstructed streamflow annual anomalies are shown in Figure 6.3, along with the mean monthly hydrographs. Error statistics (RMSE and relative bias) for annual and monthly simulated streamflow are given in Table 6.4. The largest discrepancies between observed and simulated flows occur for basins that were not explicitly calibrated by Su et al. (2005) (basins 6 through 9), i.e. calibration parameters for these basins were determined by calibrating streamflow at the outlet of each of their respective primary basins (the Lena, Yenisei, or Ob'). Biases and RMSEs are also largest for the permafrost basins, i.e. averaged over each temperature regime, RMSEs are between 8% and 85% for the cold basins, between 17% and 75% for the threshold basins, and between 15% and 50% for the warm basins. For all basins, RMSEs are highest during the snowmelt season, between April and June. Biases are also highest during the snowmelt season, and for

most basins are positive. For many of the basins, the lowest biases occur during the summer (post-snowmelt) season, whereas for the non-permafrost basins, low biases also occur during the winter season.

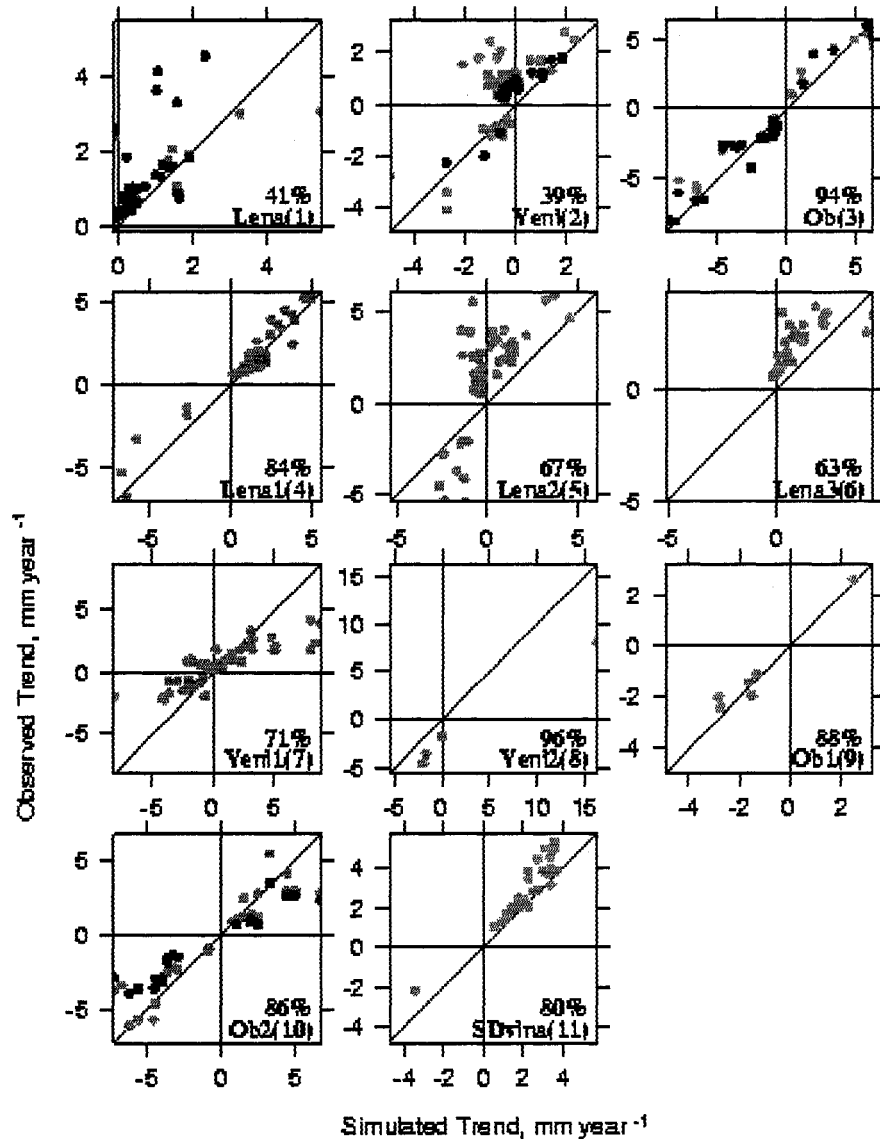


Figure 6.2 Scatter-plots of trend slopes between observed and simulated (routed) annual streamflow for all periods in which observed streamflow trends are significant at 90% (gray circles) and 99% (black circles) using the Mann-Kendall (Mann 1945) non-parametric test. Each panel is labeled according to basin reference name and ID (see Table 3.1). The R^2 value for each set of pairs (for 90% significance) is shown in the lower right corner.

Table 6.4 Error statistics for annual and monthly simulated (routed) streamflow. See Figure 6.3 for visualizations of the annual anomalies in streamflow for each basin.

	Basin:	Lena	Yeni	Ob	Lena1	Lena2	Lena3	Yeni1	Yeni2	Ob1	Ob2	SDvina
Ann.	RMSE	9%	8%	9%	8%	14%	10%	39%	13%	18%	24%	8%
	Bias	6%	4%	12%	13%	-47%	69%	198%	19%	-39%	56%	-13%
Jan	RMSE	32%	29%	21%	41%	19%	32%	37%	18%	25%	53%	29%
	Bias	188%	-51%	-14%	222%	7%	258%	203%	-53%	-71%	53%	-42%
Feb	RMSE	42%	33%	20%	52%	22%	37%	52%	19%	22%	45%	27%
	Bias	220%	-54%	-27%	264%	26%	286%	291%	-47%	-78%	32%	-46%
Mar	RMSE	53%	37%	22%	55%	23%	39%	153%	21%	21%	37%	22%
	Bias	252%	-55%	-41%	253%	39%	277%	495%	-40%	-82%	9%	-50%
Apr	RMSE	58%	44%	40%	96%	63%	54%	111%	101%	82%	35%	45%
	Bias	278%	-33%	-13%	272%	106%	264%	433%	133%	76%	51%	31%
May	RMSE	89%	31%	38%	29%	30%	18%	79%	43%	21%	30%	15%
	Bias	112%	-3%	73%	-15%	-41%	34%	257%	183%	-34%	41%	2%
Jun	RMSE	12%	15%	32%	15%	20%	19%	114%	23%	31%	32%	18%
	Bias	-40%	7%	52%	11%	-77%	-5%	235%	-34%	-45%	73%	9%
Jul	RMSE	15%	20%	15%	29%	27%	25%	63%	26%	23%	30%	21%
	Bias	-20%	11%	-2%	-3%	-65%	5%	166%	-3%	-30%	86%	-25%
Aug	RMSE	15%	19%	28%	23%	26%	25%	69%	29%	27%	38%	28%
	Bias	-13%	23%	-20%	-4%	-42%	63%	198%	12%	-44%	72%	-57%
Sep	RMSE	16%	17%	27%	26%	28%	23%	54%	25%	24%	39%	30%
	Bias	6%	34%	-16%	7%	-39%	102%	164%	-7%	-56%	36%	-60%
Oct	RMSE	14%	19%	14%	24%	21%	30%	43%	24%	28%	32%	25%
	Bias	60%	28%	-12%	39%	-27%	212%	103%	-15%	-57%	18%	-49%
Nov	RMSE	36%	27%	27%	134%	23%	39%	40%	21%	26%	54%	35%
	Bias	276%	19%	27%	110%	56%	376%	94%	-53%	-59%	59%	-34%
Dec	RMSE	30%	28%	27%	31%	18%	30%	56%	20%	25%	59%	39%
	Bias	226%	-38%	9%	156%	14%	252%	106%	-54%	-68%	61%	-34%

*Note: Bias = $\left[\frac{(\bar{Q}_s - \bar{Q}_o)}{\bar{Q}_o} \right] \times 100\%$ where Q_o is observed streamflow and Q_s is simulated (routed) streamflow.

$$RMSE = \left[\sqrt{\frac{1}{n} \sum_i^n \left((Q_{s,i} - \bar{Q}_s) - (Q_{o,i} - \bar{Q}_o) \right)^2} / \bar{Q}_o} \right] \times 100\% \text{ where } i \text{ represents one month}$$

or year of the time-series and n is the number of months or years in the time-series (given by the period of overlap between the period of record (see Table 3.1) and the period of analysis (1936-1999)).

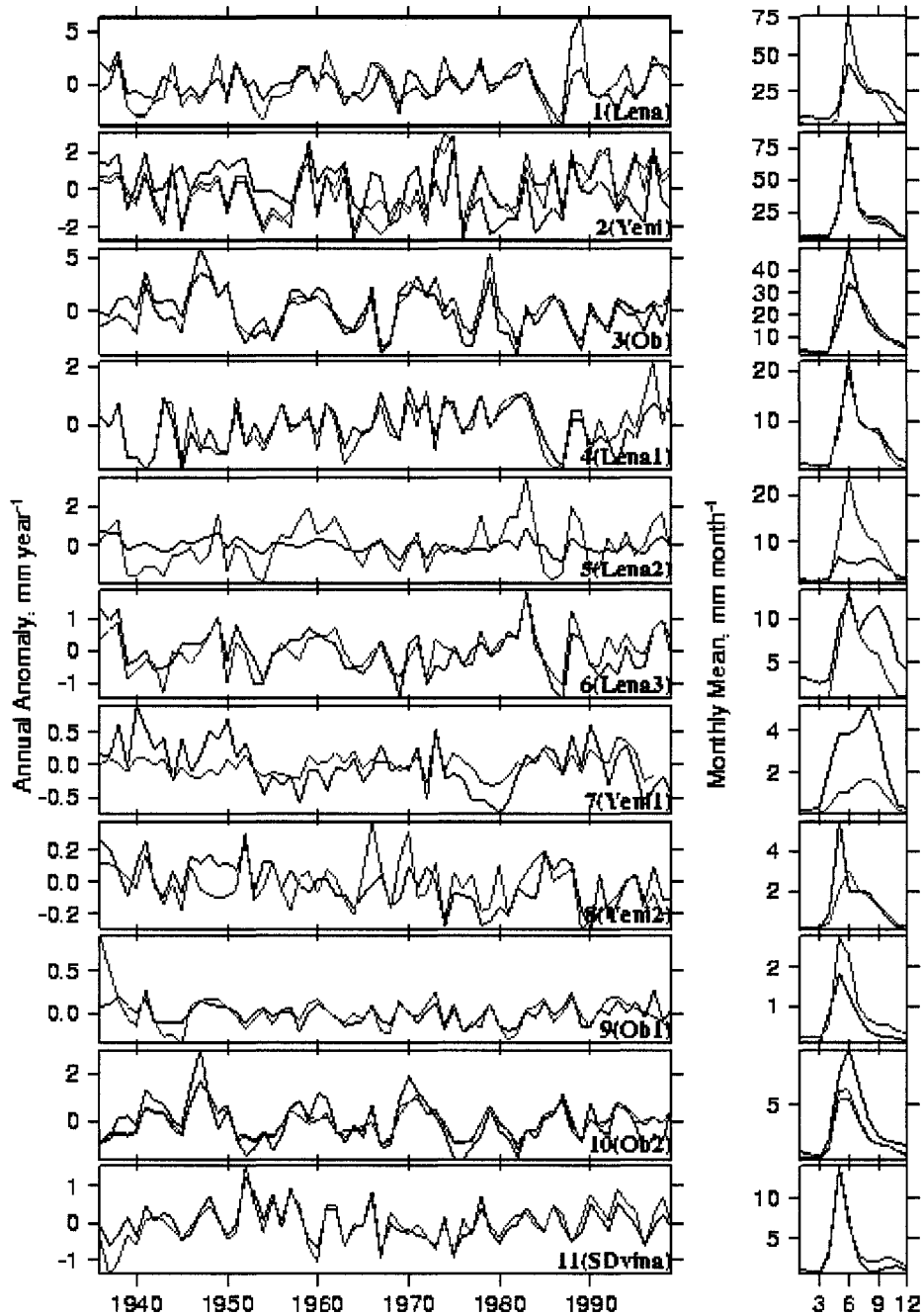


Figure 6.3 For each of the eleven study basins (see Table 3.1), basin-mean annual anomaly time-series and monthly climatologies for observed (blue line) and simulated (rouned) streamflow (red line). Also shown, for basins with reservoirs, are the annual anomaly time-series and monthly climatologies for the Adam et al. (2007) (Chapter 5) reconstructed streamflow product (green line). The monthly climatologies were calculated for the period of overlap between the period of record (see Table 3.1) and the period of analysis (1936-1999).

6.4.2. Selection of Periods and Basins for Trend Analysis

As introduced in Section 6.3.3(2), we determined a “period of captured trends” for each of the study basins as follows. For each of the periods over which the observed streamflow trend was significant at 90%, we plotted both the observed (Figure 6.4) and the simulated trend slope for routed streamflow (Figure 6.5). The length of each line in Figures 6.4 and 6.5 represents a single period, whereas the color of the line signifies the trend slope. (Note that a similar analysis of observed streamflow was performed by Adam and Lettenmaier (2007b) (cf. Figure 4.7), with the exception that the seasonal Mann-Kendall test was applied, therefore there are some differences between the results). Comparing and contrasting the line colors in Figures 6.4 and 6.5 gives an indication of the periods and time-scales over which the model was able to reproduce observed trends. For example, the model captured some of the shortest periods during the 1940s for the Lena basin, but otherwise was not able to capture significant trends prior to around 1965. For periods starting after 1965 and ending before 2000, the model captured the significant changes occurring at the outlet of the Lena basin, therefore the “period of captured trends” for this basin is 1965 to 2000. The periods of captured trends for all of the basins are given in column 3 of Table 6.5. The common characteristic of all the basins is that all trends with shorter periods (≤ 30 years) near the end of the observational record were captured (at least by correctly predicting trend sign), suggesting that the model is simulating the most important controls on streamflow generation at these shorter time-scales up through the end of the last century. Inconsistencies between observed and simulated streamflow trends exist for the early part of the observational record, for the longest periods, but only for the permafrost basins. This is not true for all the permafrost basins, however. Trend magnitudes for all periods and time-scales are captured for the Lena1 basin.

The possible explanations for the inconsistencies between simulated and observed streamflow trends include (1) inaccurate precipitation forcing data over permafrost regions and (2) remaining deficiencies in the model representation of the dynamics of

Table 6.5 Column 3: the period in which simulated (routed) streamflow captures the trends in observed streamflow (see Figures 6.4 and 6.5). Columns 4-6: "X" indicates that the analysis period overlaps with the period of captured trends, therefore trend analysis on this basin for this period may be robust. Column 7: selected periods for each basin that are used for the monthly trend analyses (Section 6.4.4). Periods were selected for which the observed streamflow trend is significant, with preference given to longer periods later in the 20th century. These periods also overlap with the period of captured trends.

ID	Basin Reference Name	Period of Captured Trends	Analysis Period I: 1936-1999	Analysis Period II: 1949-1999	Analysis Period III: 1979-1999	Basin-Specific Analysis Periods
1	Lena	1965-2000			X	1969-1984
2	Yeni	1975-2000			X	1977-1997
3	Ob	1936-2000	X	X	X	1957-1992
4	Lena1	1945-2000		X	X	1945-1990
5	Lena2	1955-1990			X*	-
6	Lena3	1955-1990			X*	1964-1999
7	Yeni1	1955-2000			X	1955-1995
8	Yeni2	1936-2000	X	X	X	-
9	Ob1	1945-2000		X	X	-
10	Ob2	1936-2000	X	X	X	1974-1999
11	SDvina	1936-2000	X	X	X	1967-1997

** Although the period of captured trends ends in 1990, we include these basins in the Period 3 analysis. No shorter periods (≤ 30 years) with significant observed trends ended between 1990 and 2000 for these basins, but because the periods beginning after 1955 captured observed streamflow trends, we inferred that the model would likely capture trends during the 1990s, were they significant.*

long-term permafrost degradation. With respect to 1), the density of meteorological stations decreases significantly from west to east and from south to north over northern Eurasia (cf. Figure 4.1 of Adam and Lettenmaier (2007b)). It is possible that the density of precipitation stations used to produce the gridded forcing data may not be adequate in permafrost regions, especially in the early decades of the study period. This may account for the fact that inconsistencies between simulated and observed streamflow exist mainly during these early decades. Conversely, we have no reason to suspect that an issue with station density would cause a negative bias in precipitation trends, thereby causing simulated streamflow trends to have a negative bias. With respect to 2), the long-term

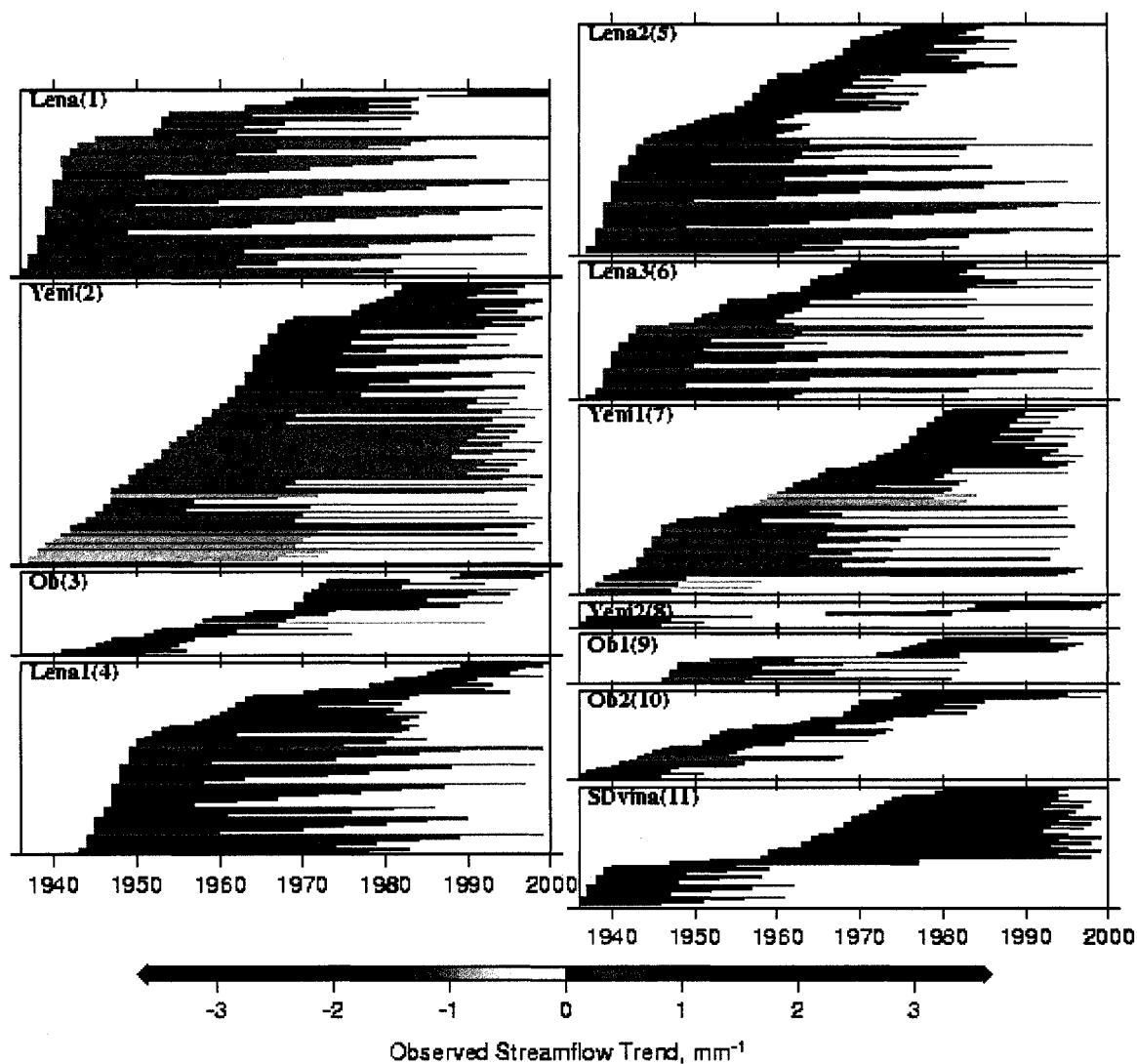


Figure 6.4 Observed streamflow trend plots for all periods with trends significant at 90% using the Mann-Kendall (Mann 1945) non-parametric test.. Each line represents a period for which the trend slope is given by the color of the line and the period length is given by the length of the line (starting and ending at the start and end of the period, respectively). Each panel is labeled according to basin reference name and ID (see Table 3.1).

dynamics of permafrost melt, particularly for excess ground ice, may not be captured for some of the permafrost basins. If the excess ground ice concentration is not correctly initialized, then both the water and energy balances of the system are affected because the melting involves a transformation of sensible heat to latent heat. Furthermore, the depth

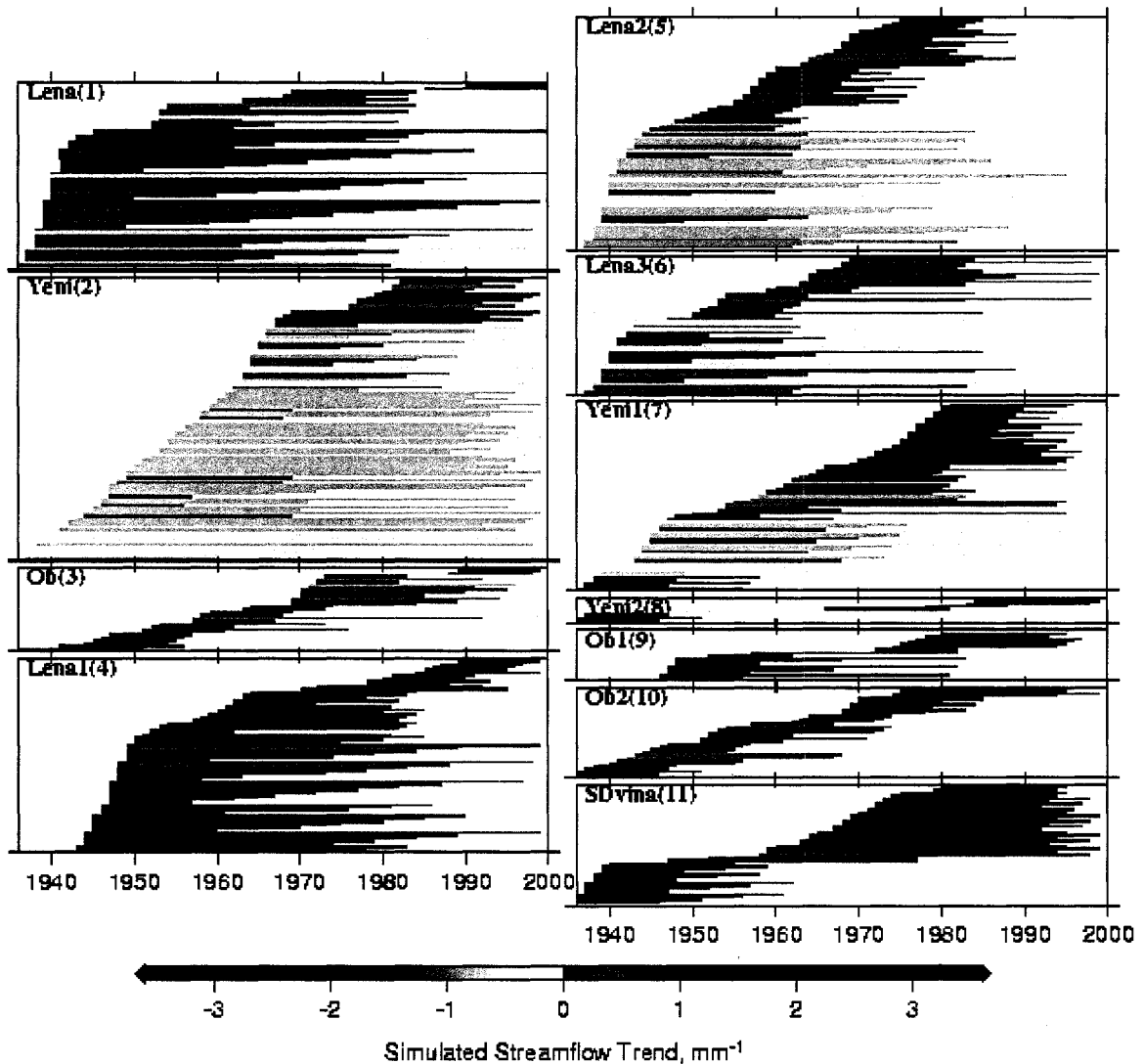


Figure 6.5 Simulated (routed) streamflow trend plots for all periods in which observed streamflow trends are significant at 90%. (See Figure 6.4 caption for further explanation).

of excess ice specification is also important. For example, if the excess ice is initialized at too shallow a depth, then ground ice melt may occur too early in the study period, causing the long-term streamflow trends to have a negative bias. This is likely to be the case for our simulations because we defined a uniform ground ice concentration for the third soil layer, which lies between the depths of 0.4 and 4 m. Once melt is initiated in the soil layer, excess ice is extracted uniformly from the entire layer, which could lead to

a bias toward early melting. A solution to this problem would be to define and simulate excess ice concentrations independently for multiple thin layers, e.g. by dividing the 3.6 m soil layer into 12 “melt” layers, allowing for a more realistic simulation of permafrost degradation. The simulation of too early a melt may be the more likely explanation for the inconsistencies between simulated and observed streamflow only for the early decades of the study period.

6.4.3. Spatial Distributions of Annual Trends

The spatial distributions of trend slopes for each water balance component, as well as for mean temperature and diurnal temperature range, are shown in Figures 6.6-6.8 for the periods 1936-1999, 1949-1999, and 1979-1999, respectively. We discuss in this section the changes in climate (P , T^{mean} , and T^{dtr}) over the entire spatial domain for each of the periods, followed by a discussion of the trends in the modulators (ET and dS/dt) and the impacts on runoff generation (Q). As mentioned in Section 6.3.3(3), the discussion of runoff trends (and the roles of the modulators) for each period is constrained to the basins for which the analysis period overlaps with the period of captured trends (see Table 6.5). Therefore, for period I (1936-1999), we constrain this discussion to one threshold basin (Yeni2) and three warm basins (Ob, Ob2, and SDvina). For the period II (1949-1999), we include one cold basin (Lena1) and another warm basin (Ob1), and all basins are included in this discussion for the period III (1979-1999).

Precipitation trends over the entire study domain have a similar distribution between the two longer periods (I and II), with widespread precipitation decreases and patchy regions of precipitation increases. The precipitation increases occur mainly over the Lena River basin (which is especially true for period I), a portion of the northern Yenisei River basin, parts of all but the central Ob' River basin, and the eastern edge of the Severnaya Dvina basin. Precipitation trends for period III, however, have a completely different pattern. Precipitation increases are much more widespread for the most recent period, possibly indicating an intensification of the hydrological cycle during the last few decades.

Regions of decreases exist over most of the Lena1 basin (a region of increasing precipitation for period I), parts of the Lena2 and Lena3 basins, parts of western Yenisei basin, a large part of the southern Ob' basin, and the southeastern Severnaya Dvina basin. Mean temperature increases are widespread over the entire domain for all three periods, with a few areas of slight increases (the far north for period I and, a portion of the northern Ob' for period III, and the very north part the Severnaya Dvina for all periods). As also shown by Adam and Lettenmaier (2007b) (cf. Figure 4.8a), warming trends are larger for the later periods, indicating an acceleration of warming trends over the Eurasian Arctic. As mean temperature increases, the diurnal temperature range may also change, e.g. Michaels et al. (1998) shows a general decrease in intra-monthly temperature variability over the United States, China, and former Soviet Union during the last 50 to 100 years of the 20th century. T^{dtr} trends also exhibit similar spatial distributions for the first two periods, with decreases over most of the domain (in agreement with the findings of Michaels et al. (1998)). Alternately, T^{dtr} increases became widespread for period III, showing a different spatial pattern from the first two periods.

Evapotranspiration may increase in response to both increased water and energy availability, or vice versa, and may be more sensitive to changes in precipitation (for moisture-limited systems) or to changes in net radiation (for energy-limited systems). In general, the spatial distribution of ET trends matches that of P, only with reduced magnitude (i.e. P changes are distributed among changes in Q, ET, and dS/dt). Notable exceptions exist for period III. Over the northeastern Yenisei, the central Lena, and the northern Severnaya Dvina River basins, strong precipitation and temperature increases occur simultaneously with ET decreases. This is a result of decreased solar irradiance, possibly associated with intensification of the hydrologic cycle (Roderick and Farquhar 2002). Although a similar pattern of change is not seen in T^{dtr} (because the VIC model uses T^{dtr} and dewpoint temperature to calculate downward solar radiation according to the algorithm of Thornton and Running (1999)), these regions are dominated by decreases in derived net shortwave radiation (not shown).

Whereas mostly negligible changes in dS/dt occur during periods I and II, dS/dt begins to play a more important role during period III. As for ET, the spatial distribution of

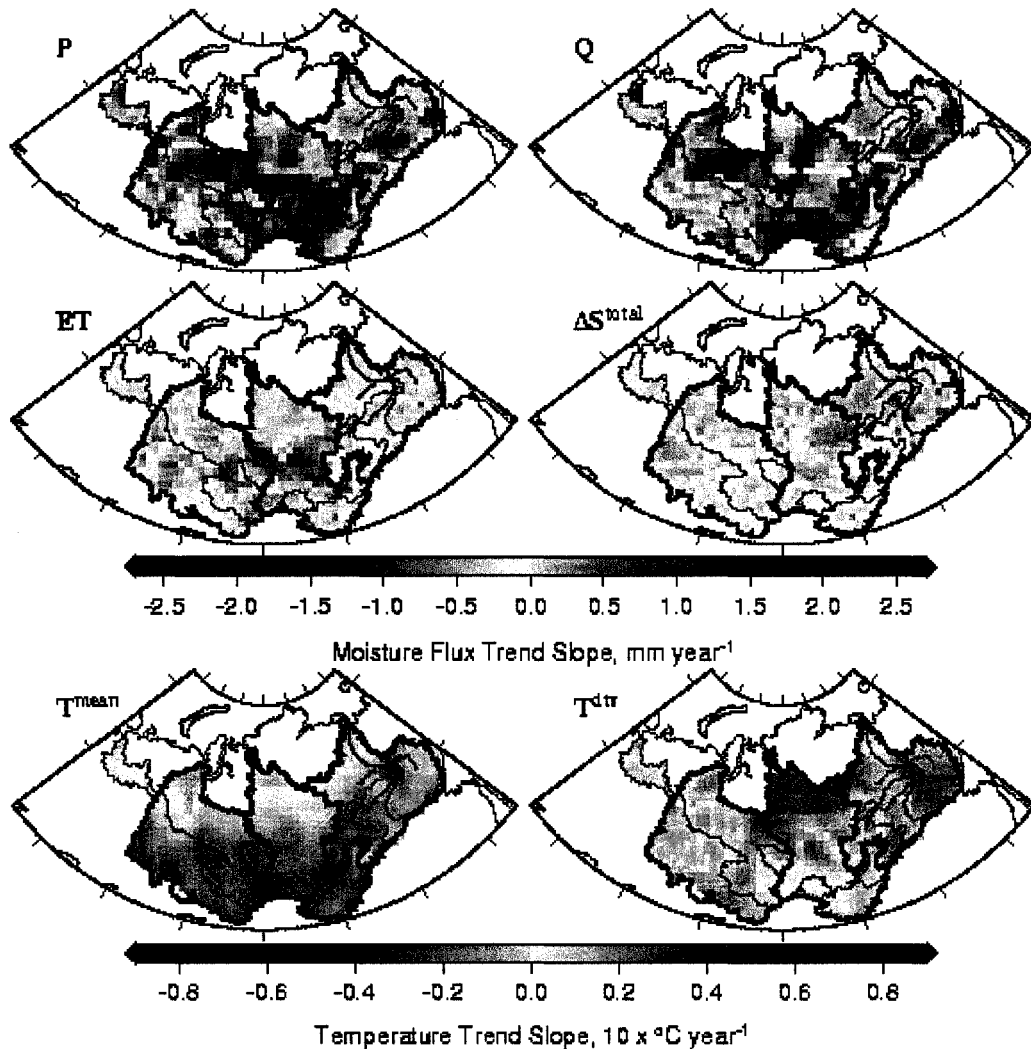


Figure 6.6 1936 to 1999 trend slopes (calculated according to Hirsch et al. (1982) for the Mann-Kendall test) for each component of the water balance (P , Q , ET , and ΔS^{total} ; see Equation 6.1, i.e. where $dS/dt = \Delta S^{total}$), mean temperature (T^{mean}), and diurnal temperature range (T^{dtr}). Whereas Q , ET , and ΔS^{total} are simulated quantities, P , T^{mean} , and T^{dtr} are observation-based gridded data (see Section 6.2.1 for details).

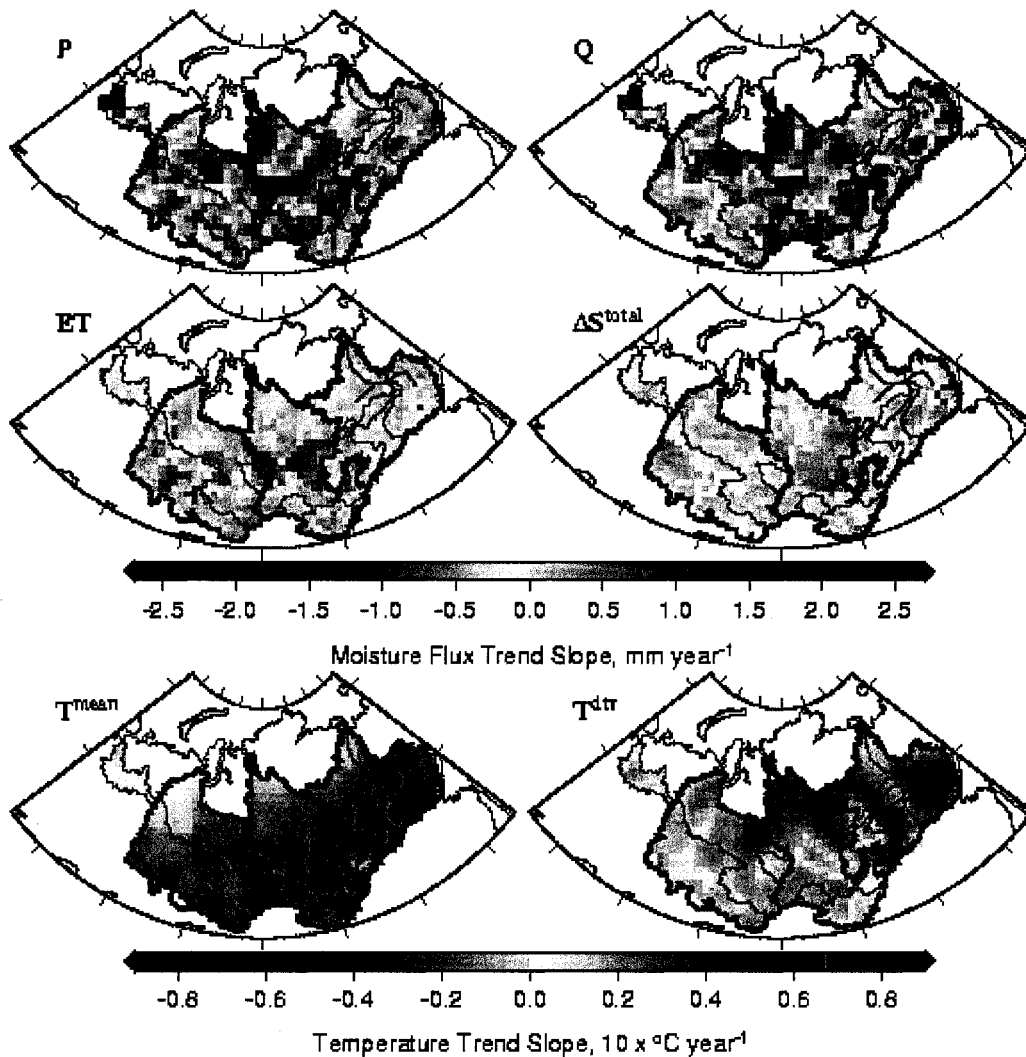


Figure 6.7 1949-1999 trend slopes. (See Figure 6.6 caption for further explanation).

changes in dS/dt generally matches that of P , although not as consistently. In some regions, dS/dt trends are negligible or negative despite strong positive trends in P , particularly over the eastern Ob' basin, the northern and southern extremes of the Yenisei basin, and the northern extreme of the Lena basin. In general, this occurred if the additional precipitation fell during the snow accumulation season or immediately after snowmelt when the ground was saturated. Therefore, most of the additional precipitation contributed directly to runoff, and soil moisture dynamics during the remainder of the year dominated the effects on dS/dt trends. Figure 6.8 also shows trends in the changes

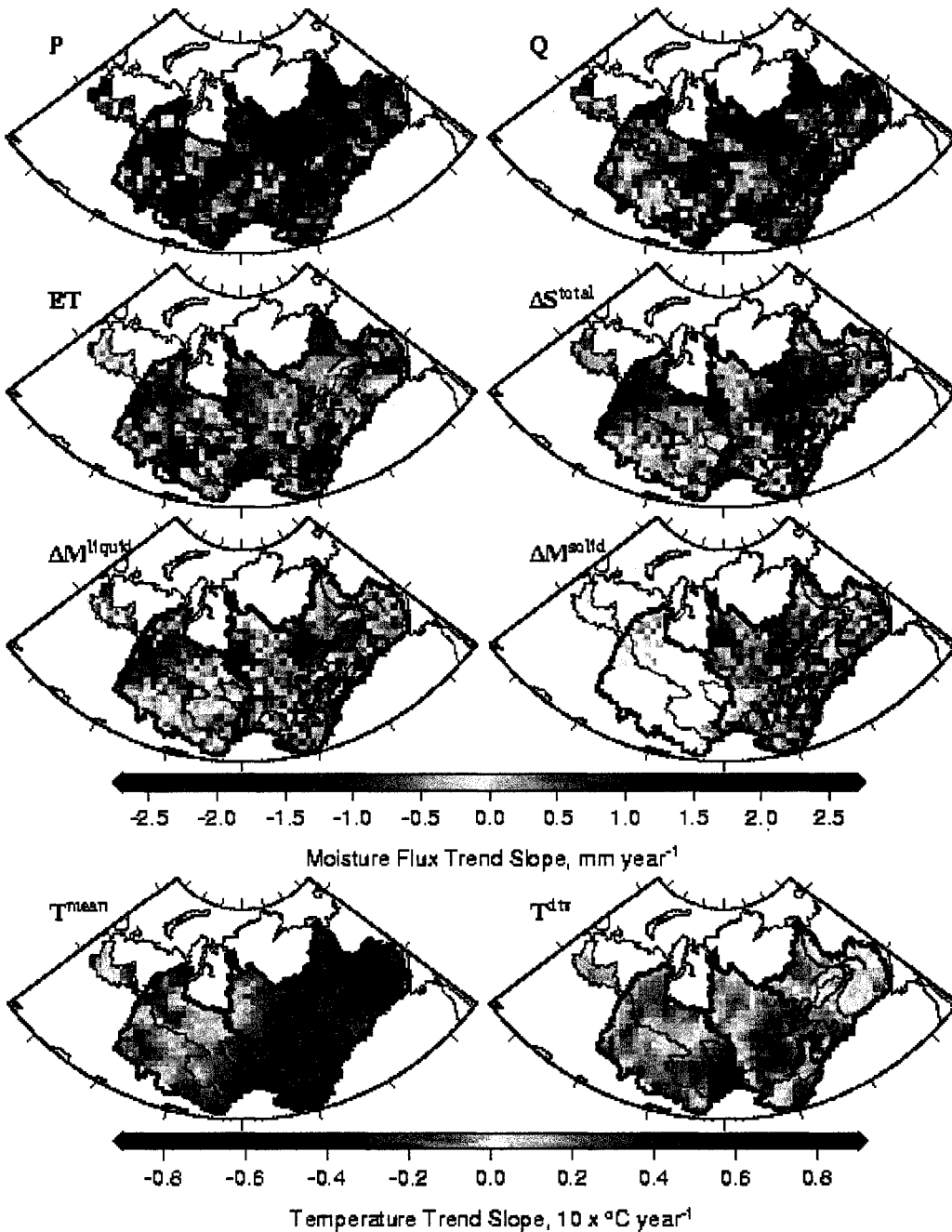


Figure 6.8 1979-1999 trend slopes. (See Figure 6.6 caption for further explanation, although also included for this period are change in liquid soil moisture storage (ΔM^{liquid}) and change in frozen soil moisture storage (ΔM^{solid}). For ΔM^{solid} , much of the Ob' and Severnaya Dvina basins are white because ice in the soil column began to accumulate after the water year began in October and completely melted before the water year ended, therefore the annual trends are necessarily zero.

in liquid soil moisture storage (ΔM^{liquid}) and frozen soil moisture storage (ΔM^{solid}). ΔM^{liquid} is most responsible for the negative dS/dt trends over the eastern Ob' basin, and northern and southern ends of the Yenisei basin, whereas ΔM^{solid} is responsible for the negative trends in dS/dt at the northern extreme of the Lena basin. Elsewhere, dS/dt trends are negligible or positive despite strong negative trends in P, e.g. the southwestern Ob' basin, and over parts of the Lena1, Lena2, and Lena3 basins. This may also occur when the largest precipitation changes, decreases in this case, occurred in the few months following snowmelt. Soil moisture dynamics during this period are dominated by changes in the timing and volume of snowmelt, therefore trends in dS/dt are most influenced by changes in winter precipitation. Large increases in dS/dt , due to changes in snowmelt, may also overwhelm negative dS/dt trends that occur later in the summer, resulting in a positive annual dS/dt trend.

The spatial pattern of Q trends is determined by the cumulative effects of trends in P, ET, and dS/dt . (Recall from the sign convention used in Equation 6.1 that increasing P, decreasing ET, and decreasing dS/dt all contribute towards increasing Q, and vice versa.) Whereas the spatial distribution of Q trends closely resembles that of P for periods I and II, suggesting that the modulators play less important roles in controlling Q trends (at least for basins that have streamflow trends that are captured by the model for these periods), Q trends are more divergent from P trends for period III. The strong increases in P over the western Ob' basin are not apparent in Q trends due to an increase in ET and dS/dt . Strong decreases in P over the south-central portion of the Ob' basin are similarly not seen in the Q trends due to decreases in ET. Although both increasing P and decreasing ET are seen over the west-central Lena basin, Q trends are negligible or negative due to increasing dS/dt . Also, a patch of increasing Q over the east-central Lena1 basin is a result of both declining ET and the melting of excess ground ice.

6.4.4. Monthly Trends in Each Water Balance Component

The monthly trend analysis results for eight of the study basins are shown in Figures 6.9 and 6.10. As mentioned in Section 6.3.3(4), the periods selected for analysis all have significant annual streamflow trends, which are positive for all basins except for the Ob'. The color of each box indicates trend slope and the number within each box indicates the level of significance passed (levels checked were 60%, 80%, 90%, 95%, 98%, and 99%; "x" indicates the trend did not pass 60% significance). Trend statistics were calculated for twelve variables. Observed and simulated basin-outlet streamflow (Obs Q and Rout Q) were included to evaluate the simulated monthly trends (recall that evaluation of the annual trends is described in Section 6.4.2, and the periods used for this analysis fall inside the "period of captured trends" for each basin). The four terms of Equation 6.1 (P, Q, ET, and dS/dt) were included to partition out the relative influences of each component on Q trends. (Recall that Obs Q and Rout Q are routed streamflow quantities, whereas Q is unrouted runoff.) To understand the causes of trends in dS/dt , we included change in snowpack (ΔS^{snow}) and change in soil moisture storage (ΔM^{total}), which was partitioned into liquid (ΔM^{liquid}) and solid (ΔM^{solid}). We also included mean temperature (T^{mean}) and diurnal temperature range (T^{dtr}). (Note that we also analyzed trends in the change in surface water storage and found that these had little effect on trends in dS/dt .) The ET and delta storage trend results (i.e. the "modulators" in Figure 2.1) are boxed in green if the following criteria are true: (1) the Q trend is significant by at least 60% and has a trend slope that is not within 10% of the P trend slope, (2) the modulator trend slope has a sign such that it can help explain the divergence between the P and Q trend slopes, and (3) the absolute value of the modulator trend slope is greater than the threshold value of 0.05 mm/year.

Although the model generally performed well in reproducing both annual and monthly streamflow trends for each of the basins and periods considered, there are exceptions. For the cold basins (the Lena and Lena1), a mismatch exists for late spring and summer

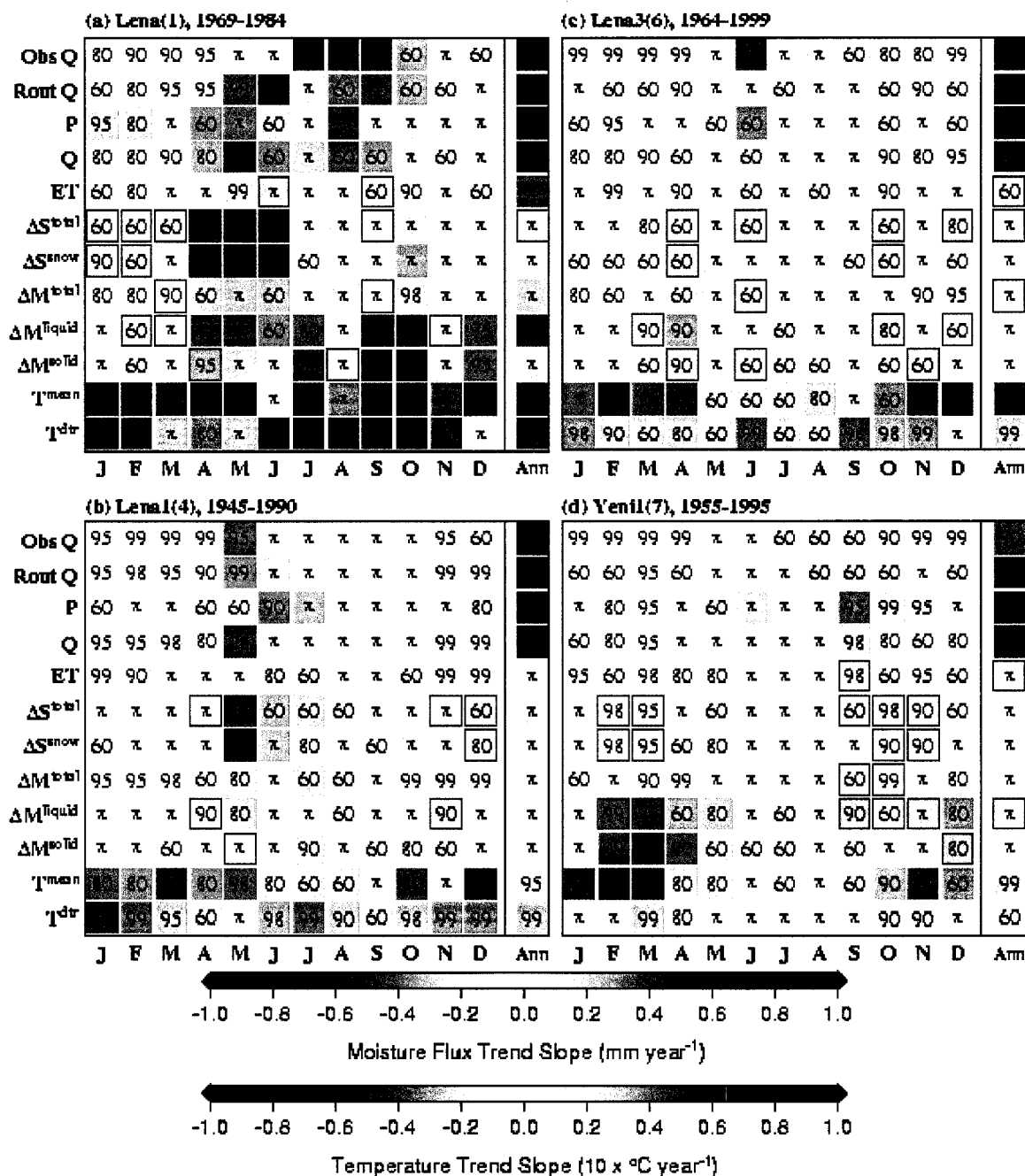


Figure 6.9 Monthly and annual trend-test results for two “cold” basins (Lena and Lena1) and two “threshold” basins (Lena3 and Yenil). The period tested for trend is according to Table 6.5 (column 7) and is given above each panel with the basin reference name and ID (see Table 3.1). See text for details.

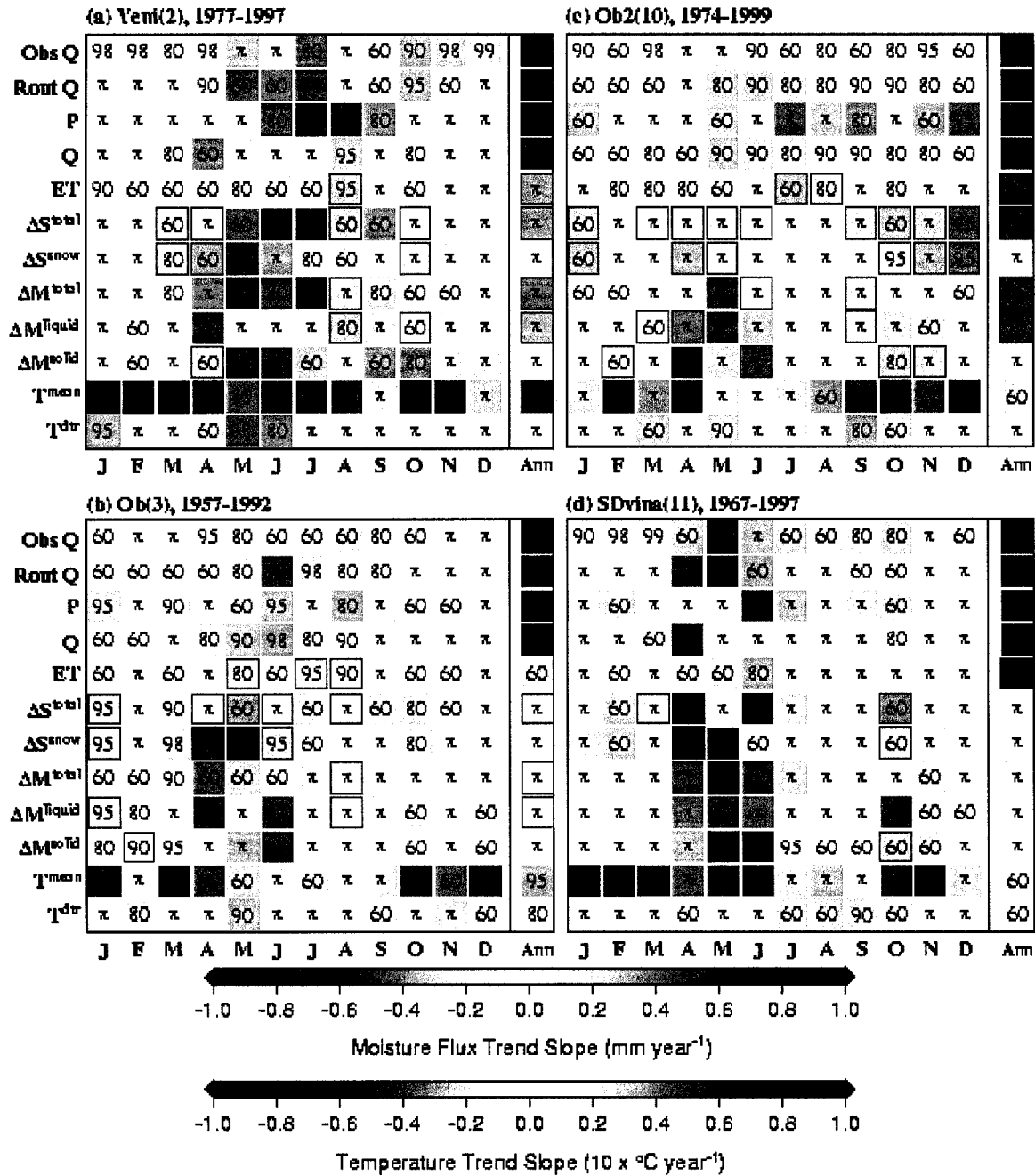


Figure 6.10 Monthly and annual trend-test results for one “threshold” basin (Yeni) and three “warm” basins (Ob, Ob2, and SDvina). The period tested for trend is according to Table 6.5 (column 7) and is given above each panel with the basin reference name and ID (see Table 3.1). See text for details.

Lena streamflow, over which time the model predicted a strong increase in flow approximately two months early. For the threshold basins (the Lena3, Yeni1, and Yeni), the model consistently under-predicted the significance of the observed streamflow trends during much of the snow accumulation season (approximately November to April). Also, the model failed to reproduce the large but weak positive trend in Lena3 June streamflow. For the warm basins (Ob, Ob2, and SDvina), the model predicted a decrease in Ob' June/July streamflow that was approximately one month early, while for the Ob2 basin, May and July trends were slightly over-simulated. Also, the model failed to reproduce small but significant increases in January to March streamflow for the SDvina basin.

Over the periods considered (which, in aggregation, spans the period of 1945 to 1999), precipitation trends were generally positive, the most notable exception being that of the Ob' basin precipitation for the period of 1957 to 1992. There is no dominant season for precipitation changes, although some of the strongest trends occurred during the summer (e.g. June to September Yeni trends and June SDvina trend). Also, other than for the Ob' basin, negative precipitation trends only occurred between April and October, with October being the most common month with negative precipitation trends. All annual mean temperature trends were positive. For the cold basins, temperature increases occurred during the months of December to March, whereas significant temperature decreases occurred from June to October. For the warm and threshold basins, temperature increases were generally strongest during the cold season (mainly January to March), whereas for some summer and fall months, temperature trends varied from strongly positive to weakly negative. All significant annual T^{dtr} trends were negative, strongly so for the Lena, Lena1, and Lena3 basins. There is no apparent dominant season of change for T^{dtr} .

Annual ET trends were positive for all basins except the Ob', which was negative due to a negative P trend. ET may have been more responsive to climatic change over the warm

basins than over the permafrost basins, particularly the cold basins. The warm basins all had ET trends that passed at least 60% significance, whereas only the Lena3 of the permafrost basins passed 60% significance. Monthly ET trends over the cooler of the eight basins (Lena, Lena1, Lena3, and Yeni1) were of small magnitude, with the largest trends having occurred during the late spring or summer due to increased P. However, small but significant ET trends occurred during the cold season for two of these basins (Lena1 and Yeni1) due to increased P and T^{mean} during these months. Monthly ET trends over the warmer of the eight basins (Yeni1, Ob, Ob2, and SDvina) were generally larger than for the cooler basins, with the largest trends having occurred between the months of May and August. These trends were the same sign as monthly P, indicating P was the likely cause for these trends. Exceptions were for the months of June and July for the Yeni basin, during which time T^{mean} may have had a greater influence on ET trends, i.e. a negative T^{mean} trend resulted in a positive ET trend, and vice versa.

Trends in the delta storage terms will be discussed in the following order: (1) ΔS^{snow} , (2) ΔM^{total} and its relationship to ΔM^{liquid} and ΔM^{solid} , and (3) dS/dt and its relationship to ΔS^{snow} and ΔM^{total} . Due to our sign convention, positive trends in ΔS^{snow} indicate either decreased melt or increased accumulation, depending on the season, and vice versa. Evident among most of the basins is an earlier snowmelt event, which can be seen by a positive ΔS^{snow} trend followed by a negative ΔS^{snow} trend during the spring or early summer. For the cold basins, snowmelt shifted from June to May. For all of the other basins except the Yeni1, snowmelt may have shifted from the May/June months to the April/May months. For the Yeni1 basin, snowmelt may have shifted from April to March. No clear snowmelt shift is evident for the Ob2 basin. In general, a later accumulation start may be indicated by positive ΔS^{snow} trends during the fall. For the two cold basins, negative ΔS^{snow} trends occurred during September and October, suggesting an earlier accumulation start as a result of late summer and fall cooling. While no clear change in the start of the accumulation season is evident for the Lena3 and Yeni1 basins, the Yeni, Ob, Ob2, and SDvina basins all had negative October ΔS^{snow} trends, suggesting

that accumulation start shifted towards November, although for the warm basins these trends may have been due to negative October precipitation trends. Changes in snow accumulation during the cold season may be due to temperature-induced changes to snow/rain partitioning or to changes in the total depth of precipitation. For all of the basins, possibly excepting the Ob', slightly positive ΔS^{snow} trends were a result of increased precipitation during those months, which would have contributed to a larger snowmelt event (a more negative spring ΔS^{snow} trend). For the Ob' basin, January increases and March decreases in snow appear to have been a result of changes in precipitation. In summary, temperature is likely to have been the controlling influence on snowmelt and accumulation onsets, whereas precipitation is likely to have been the controlling influence on snowpack accumulation and snowmelt volume.

The largest trends in ΔM^{total} began during the snowmelt period and lasted through the end of the thaw season. During snowmelt, ΔM^{total} trends were of opposite sign from ΔS^{snow} trends, i.e. increased snowmelt resulted in increased soil moisture recharge, and vice versa. During the remainder of the thaw season, ΔM^{total} trends generally followed those of P, with a few exceptions (e.g. the Lena and Ob' basins). In general, ΔM^{liquid} trends were of opposite sign from ΔM^{solid} trends, suggesting temperature influences on solid/liquid partitioning, although the change in partitioning does not appear to have been completely controlled by air temperature trends. For example, increased accumulation of snow during October for the Lena and Lena1 basins may account for an increase in the liquid/solid ratio despite negative temperature trends, i.e. the snowpack provided greater insulation from the cooling. Evidence that the ground thawed earlier can be seen for two of the warm basins (the Ob' and SDvina), i.e. a negative ΔM^{solid} trend in May was followed by a positive ΔM^{solid} trend in June. The shift towards earlier soil thaw occurred a month after the shift towards earlier snowmelt, partially due to the disappearance of the insulating snowpack. Trends in dS/dt were most influenced by ΔS^{snow} changes while a snowpack was present, otherwise dS/dt trends were most influenced by ΔM^{total} changes.

During snowmelt and at the beginning of snowpack accumulation, dS/dt trends were influenced by both ΔS^{snow} and ΔM^{total} trends.

The boxes outlined in green in Figures 6.9 and 6.10 signify modulators that contributed towards the divergence between the trends in P and Q, if there was a divergence of greater than ten percent of the P trend. Also, modulators were outlined in green only if the Q trend was significant by at least 60% because we are interested in understanding how the modulators contributed towards significant Q trends. For basins where annual Q trends were divergent from P trends, the Q trend was of smaller magnitude than the P trend in every case except for the Lena and Ob' basins. Therefore, in general, the modulators acted to diminish the influence of P changes on Q. Increases in ET and for some basins in dS/dt due to increases in ΔM^{liquid} were responsible for this effect. For the Lena basin, summer decreases in ΔM^{liquid} , possibly due to a drying-out of the summer soil column after an earlier snowmelt, caused the Q trend to be slightly larger than the P trend. For the Ob' basin, slight increases in ΔM^{liquid} may have contributed to a slightly more negative annual Q trend with respect to that of P. Note that ΔS^{snow} trends cannot have directly influenced annual Q trends because the trends were calculated over the water year, during which time the snowpack accumulated and melted completely. Also, ΔM^{solid} trends were negligible for all basins, implying that, averaged over the basins and for the periods considered, excess ground ice melt did not exert a significant influence on annual Q trends. This does not exclude the possibility that ground ice melt may have had a significant influence on annual Q trends for other periods, particularly since we intentionally neglected to analyze periods for which the model was unable to capture significant annual streamflow trends, and misrepresentation of permafrost degradation is the most likely reason for the discrepancies between observed and simulated streamflow trends (see Section 6.4.2 discussion).

Monthly Q trends diverged from P trends for a variety of reasons. ET contributed towards Q trends only between May and September, and generally more so for the

warmer basins (particularly the Yeni, Ob, and Ob2 basins). ΔS^{snow} and ΔM^{total} had distinct seasons of influence, with ΔS^{snow} influencing Q trends during the entire snow season, but primarily during snowmelt and the onset of snow accumulation. Because increases in the liquid/ice ratio results in increased cold season baseflow, an increase in the permafrost active layer depth due to summer warming may cause an increase in baseflow generation into the fall and early winter until the soil column is completely refrozen. This may be seen for two of the threshold basins, the Lena3 and Yeni1, in which positive trends in ΔM^{liquid} , coupled with negative trends in ΔM^{solid} , occurred for October and November in the Lena3 and for November and December for the Yeni (the two cold basins had cooling trends during the summer that did not lead to thickening of the active layer). Although the Q trends during these periods were slightly less positive than the P trends, most of the increased P contributed to snowpack accumulation. Therefore increases in Q during these months may have been a result of a thicker active layer.

6.5. Conclusions

Analyses of spatially-distributed annual trends were performed for three periods: (I) 1936-1999, (II) 1949-1999, and (III) 1979-1999. Also, monthly and annual basin-average trend analyses for all water balance components as well as mean temperature and diurnal temperature range were performed for periods over which annual streamflow was significant. The periods selected for analysis overlapped with the “period of captured trends” for each of the basins. A notable finding from the spatial trend analysis is that, whereas periods I and II showed similar distributions of trend for each of the water balance components, with patchy regions of positive and negative precipitation trends and similar patterns in the runoff trends, period III exhibited different characteristics. Only for this period were precipitation increases overwhelming dominant over the entire domain, an indication that the hydrologic cycle may have intensified through the end of the last century. Furthermore, in response to accelerated precipitation and temperature changes, the modulators began to play an important role, as runoff trends were more

divergent from precipitation trends for period III. The response of each of the modulators to climatic change, and the effects of this response on streamflow trends are discussed in the following paragraphs.

The spatial distribution of ET trends generally matched that of P trends, but with reduced magnitude. During period III, however, over some regions ET decreases occurred simultaneously with strong precipitation and temperature increases, causing Q trends to exceed P trends. This can be explained by negative trends in net shortwave radiation, likely due to increased cloudiness. ET generally played a greater role in Q trends for the warmer basins (the non-permafrost and the warmest of the threshold permafrost basins), with the contributions having occurred only between May and September. This result provides support for the hypothesis formulated by Adam and Lettenmaier (2007b) (Chapter 4) via correlation of mean annual temperature and streamflow, that streamflow changes will be most influenced by ET trends in the non- and threshold-permafrost basins, and only during the warm season.

Although the influences of snowpack storage on Q trends occurred during the entire snow season, the largest contributions to Q changes occurred primarily during snowmelt but also during the months of snow accumulation onset. Changes in snowmelt are a function of climatic changes that occurred during the entire snow accumulation season as well as during the snowmelt event itself. For all of the basins, except perhaps the Ob', increased precipitation during the cold season contributed to a larger snowmelt event. In response to warming winter and spring temperatures, most of the basins exhibited earlier snowmelt, shifting from June to May for the cold permafrost basins and from May/June to April/May for most of the warmer basins. An earlier snow season is evident for the two cold permafrost basins, with snow accumulation moving into September, as a result of summertime cooling over these basins. Our results also suggest that a later accumulation start may have occurred for the non-permafrost basins and for the Yenisei, with snow accumulation beginning later in October and into November.

Soil moisture dynamics exerted the greatest influence on dS/dt trends during the snow-free season. During and immediately after snowmelt, snowpack changes controlled soil moisture dynamics, whereas during the remaining months of the thaw season, trends in ΔM^{total} were generally predicted by precipitation trends. Monthly trends in ΔM^{liquid} and ΔM^{solid} were generally controlled by trends in air temperature, although exceptions include cases when snowpack changes may have had an influence, e.g. an increase in snowpack accumulation insulated the ground from October cooling trends in the cold permafrost basins. Increased subsurface water contributions to fall and winter streamflow in response to increases in active layer depth may have occurred for two of the threshold permafrost basins (contributions having occurred in November and December for the Yenisei basin and in October and November for one of the Lena sub-basins). For the basins and periods included in the monthly trend analysis, annual ΔM^{solid} trends were negligible, indicating that the melt of excess ground ice did not significantly influence annual streamflow trends. As discussed in Section 6.4.4, this does not preclude excess ground ice from being a significant factor in observed streamflow trends for the full 1936 to 2000 period.

7. Conclusions

Streamflow from the Eurasian Arctic river basins generally increased between the 1930s and the end of the 20th century, with the largest increases occurring since the 1970s.

While the largest changes in streamflow occurred during the warm season, cold season trends tended to be of a higher statistical significance. During this period precipitation generally increased (particularly over the later decades) and there were strong increases in air temperature, mainly during the winter. The primary objectives of this study were to identify, for which basins and over what periods, annual and monthly streamflow trends diverged from precipitation trends, and to investigate the roles of the remaining components of the watershed water balance in accounting for these divergences. These remaining components are termed the “modulators” and include evapotranspiration (ET) and change in the storage of water in the watershed (dS/dt). The delta storage term can be partitioned into terms related to changes in snowpack storage and changes in liquid and solid soil moisture.

Reservoirs have substantially influenced seasonal streamflow trends in many of the major rivers in the region. The signature of reservoirs on streamflow are similar to, and therefore confounded with, the effects of long-term climate change. As shown in Chapter 5, the largest effects of the reservoirs occurred during the winter and early spring, during which periods the reservoirs acted to diminish the differences in streamflow between seasons by storing streamflow during the summer season of higher flow rates and releasing additional flow during the winter low-flow season. This exchange of flow between seasons had its largest relative effect during the winter and early spring, particularly over the permafrost basins where cold season baseflow is especially small. By isolating the direct human effects on the streamflow regime, it becomes possible to examine what natural changes have occurred in order to further our understanding of how climate change has affected runoff generation in the Arctic. For example, trend analysis of the reconstructed streamflows demonstrated that the following changes were likely due

to climatic influences: long-term (spanning more than 40 years) increases in Lena and Yenisei River annual streamflow; decreases in Lena and Yenisei winter streamflow for periods starting in the 1940s and ending in the 1970s and 1980s, followed by increases for periods starting in the 1950s and 1960s and ending in the 1990s; decreases in Yenisei spring streamflow for periods starting in the 1930s and ending around 1970, followed by increases for periods starting in the 1950s and 1960s and ending in the 1990s; and increases in Yenisei summer streamflow for periods starting in the 1940s and ending in the 1970s. We detected few significant trends in Ob' seasonal or annual reconstructed streamflow, although there are some significant trends for individual months (e.g. a positive trend existed in 1938 to 1998 April streamflow).

In Chapter 4, we applied these reconstructed data to formulate a hypothesis for how precipitation and temperature changes have jointly contributed to streamflow changes in the Eurasian Arctic. First, for the coldest basins in northeastern Siberia, streamflow should be sensitive to warming primarily as a result of the melting of excess ground ice, and for these basins positive streamflow trends may exceed precipitation trends in magnitude. The melting of permafrost may be sensitive to both winter and summer temperatures, with the largest relative contributions to streamflow in fall and early winter. Second, evapotranspiration (ET) in the warmer regions of western Siberia and European Russia is sensitive to warming and increased precipitation (primarily during the warm season), therefore observed precipitation trends may exceed streamflow trends. Third, streamflow from the central Siberian basins (the "threshold" basins) should respond to both effects, therefore it is difficult to predict the degree to which streamflow trends will be consistent with precipitation trends and would depend on the state of permafrost underlying the basin, the availability of water for increased evaporation, and other factors. This hypothesis was explored by comparing precipitation and streamflow trends for periods in which streamflow trends were statistically significant. In general, the hypothesis held true, i.e. streamflow trends exceeded precipitation trends beginning in the 1950s and 1960s for the two "cold" permafrost basins, precipitation trends nearly always

exceeded streamflow trends for the “warm” non-permafrost basins, while there was no consistent discrepancy between precipitation and streamflow trends for the “threshold” basins. These results suggest that the relative roles of the “modulators” in influencing streamflow changes under a changing climate are dependent on the mean climate and permafrost state of the basin.

The improved understanding of the controls on northern Eurasian streamflow resulting from this analysis provided motivation to enhance the modeling framework used for the prediction of Arctic streamflow. For example, we now understand that permafrost most likely plays a key role in long-term streamflow variability. Most macroscale hydrologic models poorly simulate winter baseflow at high latitudes due to the presence of permafrost (Su et al. 2005), and these results provide motivation to focus our efforts on improving the permafrost algorithms in these models. Incorporation of the key physical processes into the modeling framework is crucial for the accurate prediction of future river discharge rates into the Arctic Ocean and feedbacks to the climate system, because these processes respond differently to climatic changes. For example, increased precipitation due to an accelerated hydrologic cycle will likely continue to provide additional freshwater to the system, whereas warming-induced melting of permafrost provides freshwater only until Arctic permafrost is completely melted. Therefore, we made various developments to the VIC macroscale hydrologic model’s finite-difference frozen soils algorithm. These include distributing the thermal nodes exponentially with depth to increase efficiency, using an implicit solver for unconditional stability, and incorporating an excess ground ice and ground subsidence algorithm.

In Chapter 6, we applied the VIC model to simulate 20th century streamflow trends over the Eurasian Arctic basins and evaluated the performance of the model in capturing observed streamflow trends for a large number of short and long-term periods. Over the last three decades, the model captured the most important features of streamflow trends

for both permafrost and non-permafrost basins. Discrepancies existed only for permafrost basins in the early portion of the observational record and for long-term periods that began prior to the 1960s and 1970s. Discrepancies are likely due to implementation of the excess ice algorithm, for which we specified a uniform ground ice concentration over the entire depth of the bottom 3.6 m soil layer. A current limitation to the model is that the expanded or “effective” porosity of the soil layer must be uniform in that layer. As the top portion of the layer thaws and liquid water is extracted, porosity over the entire layer is adjusted to account for thaw that occurred only in the top layer. Therefore melting of the excess ice occurred too early in the 1930 to 2000 simulation period and is the most likely explanation for our under-prediction of positive streamflow trends in permafrost basins. Over the more recent decades, the model was able to capture the key features of annual streamflow trends over both permafrost and non-permafrost basins, suggesting that precipitation changes in response to an intensification of the hydrologic cycle may have overwhelmed the contribution of permafrost melt. This is apparently in contradiction to the findings of Chapter 4, however, in which we found that precipitation and streamflow trends were divergent for some of the permafrost basins beginning in the 1950s and 1960s. One explanation for this contradiction is that the trend slope estimator applied in Chapter 4 took into account differences in seasonal change, whereas the trend slope estimator applied in Chapter 6 did not. Therefore, it is possible that the primary contribution of permafrost degradation over the last few decades is a change in seasonality (via increasing fall and winter baseflow), a contribution due primarily to a thickening permafrost active layer.

We performed annual and monthly trend analyses on the major components of the water balance for periods during which observed streamflow trends were significant. A period was selected for each basin as the longest period nearest the end of the 20th century during which time the observed streamflow trend was captured by the model (see Table 6.5). We explored the hypothesis formulated in Chapter 4, and we investigated the roles of the “modulators” (particularly evapotranspiration, snowpack storage, and soil moisture

storage) in influencing the effects of climatic change on streamflow generation. The effects of ET on annual streamflow trends support the Chapter 4 hypothesis. ET played a greater role in observed changes for the “warm” basins and some of the “threshold” basins than for the “cold” basins, with the contributions of changing ET only occurring during the warmer months of May to September. Due to current limitations in the excess ground ice algorithm, we were not able to adequately test the effects of permafrost degradation on annual streamflow trends, but the fact that discrepancies between simulated and observed trends only occurred for the permafrost basins suggests that permafrost degradation may be playing an active role in long-term annual streamflow changes. We did, however, find evidence of increased fall and winter baseflow due to a thickening active layer for some of the permafrost basins. Among the modulators, changes in the snowpack had the greatest effects on monthly streamflow trends, with the largest contributions occurring during snowmelt and the months of snowpack accumulation onset. Generally, an earlier spring snowmelt event and a shift in the onset of snow accumulation (later for many basins and earlier for basins experiencing summer cooling) were due to changes in temperature. A general increase in snowpack accumulation during the winter was a result of increased precipitation, which resulted in larger snowmelt events.

An increased understanding of the factors controlling Eurasian Arctic streamflow trends will improve our knowledge of the accuracy of and the uncertainties associated with 21st century streamflow predictions by global general circulation models (GCMs). Although precipitation changes are the primary control on streamflow changes, the modulators (in response to both temperature and precipitation changes, and other factors) are continuing to play an important role in these changes. The melting of excess ground ice is a viable explanation for discrepancies between simulated and observed streamflow trends in permafrost basins, but the magnitude of its role in streamflow changes is uncertain due both to current model deficiencies and little known information regarding the concentration, spatial distribution, and depth of ground ice. Deficiencies in land surface

process dynamics known to exist in hydrologic models will also exist in most GCMs, and GCMs are further limited by poor skill in predicting precipitation. For these reasons, GCM streamflow projections should be analyzed and discussed with the understanding that factors controlling streamflow changes, particularly precipitation and ground ice melt, have large uncertainties. To place bounds on the uncertainties, multiple GCMs and climate change scenarios, and varying ground ice concentration initializations should be applied when predicting 21st century streamflow changes.

References

- ACIA, 2005: *Arctic Climate Impact Assessment*. Cambridge University Press, NY, 1042 pp.
- Adam, J. C. and D. P. Lettenmaier, 2003: Adjustment of global gridded precipitation for systematic bias. *Journal of Geophysical Research-Atmospheres*, **108**, doi:10.1029/2002JD002499.
- , 2007a: Application of a macroscale hydrologic model to a streamflow trend attribution study in northern Eurasia. *Journal of Climate* (in preparation).
- , 2007b: Application of new long-term precipitation, temperature, and reconstructed streamflow products to a streamflow trend attribution study in northern Eurasia. *Journal of Climate* (accepted).
- Adam, J. C., E. A. Clark, D. P. Lettenmaier, and E. F. Wood, 2006: Correction of global precipitation products for orographic effects. *Journal of Climate*, **19**, 15-38.
- Adam, J. C., I. Haddeland, F. Su, and D. P. Lettenmaier, 2007: Simulation of reservoir influences on annual and seasonal streamflow changes for the Lena, Yenisei and Ob' Rivers. *Journal of Geophysical Research* (accepted).
- Andreadis, K. M., P. Storck, and D. P. Lettenmaier, 2007: Modeling the effects of canopies on snow accumulation and ablation processes. *Water Resour. Res.* (to be submitted).
- Arnell, N. W., 2005: Implications of climate change for freshwater inflows to the Arctic Ocean. *Journal of Geophysical Research-Atmospheres*, **110**, doi:10.1029/2004JD005348.
- Barnett, T. P., J. C. Adam, and D. P. Lettenmaier, 2005: Potential impacts of a warming climate on water availability in snow-dominated regions. *Nature*, **438**, 303-309.
- Beilman, D. W., D. H. Vitt, and L. A. Halsey, 2001: Localized Permafrost Peatlands in Western Canada: Definition, Distributions, and Degradation. *Arctic, Antarctic, and Alpine Research*, **33**, 70-77.

- Berezovskaya, S., D. Q. Yang, and D. L. Kane, 2004: Compatibility analysis of precipitation and runoff trends over the large Siberian watersheds. *Geophysical Research Letters*, **31**, doi:10.1029/2004GL021277.
- Berezovskaya, S., D. Q. Yang, and L. Hinzman, 2005: Long-term annual water balance analysis of the Lena River. *Global and Planetary Change*, **48**, 84-95.
- Berezovskaya, S., D. Q. Yang, and D. L. Kane, 2007: On long-term runoff variability of the largest Siberian rivers. (*in preparation*).
- Bogdanova, E. G., B. M. Ilyin, and I. V. Dragomilova, 2002a: Application of a comprehensive bias-correction model to precipitation measured at Russian North Pole drifting stations. *Journal of Hydrometeorology*, **3**, 700-713.
- Bogdanova, E. G., V. S. Golubev, B. M. Ilyin, and I. V. Dragomilova, 2002b: A new model for bias correction of precipitation measurements, and its application to polar regions of Russia. *Russian Meteorology and Hydrology*, **10**, 68-94.
- Bowling, L. C., 2002: Estimating the freshwater budget of high-latitude land areas, Ph.D. thesis, Department of Civil and Environmental Engineering, University of Washington.
- Bowling, L. C., J. W. Pomeroy, and D. P. Lettenmaier, 2004: Parameterization of blowing-snow sublimation in a macroscale hydrology model. *Journal of Hydrometeorology*, **5**, 745-762.
- Brodzik, M. J., 1997: EASE-Grid: A versatile set of equal-area projections and grids, National Snow and Ice Data Center, Boulder, CO.
- Broecker, W. S., 1997: Thermohaline circulation, the Achilles heel of our climate system: Will man-made CO₂ upset the current balance? *Science*, **278**, 1582-1588.
- Brown, J., O. J. Ferrians, J. A. Heginbottom, and E. S. Melnikov, 1998: Circum-Arctic Map of Permafrost and Ground-Ice Conditions, National Snow and Ice Data Center/World Data Center for Glaciology. Digital Media. Boulder, CO.
- Brown, R. D., 2000: Northern Hemisphere snow cover variability and change, 1915-1997. *Journal of Climate*, **13**, 2339-2355.

- Cherkauer, K. A. and D. P. Lettenmaier, 1999: Hydrologic effects of frozen soils in the upper Mississippi River basin. *Journal of Geophysical Research-Atmospheres*, **104**, 19599-19610.
- , 2003: Simulation of spatial variability in snow and frozen soil. *Journal of Geophysical Research-Atmospheres*, **108**, doi:10.1029/2003JD003575.
- Cherkauer, K. A., L. C. Bowling, and D. P. Lettenmaier, 2003: Variable infiltration capacity cold land process model updates. *Global and Planetary Change*, **38**, 151-159.
- Clark, P. U., N. G. Piasias, T. F. Stocker, and A. J. Weaver, 2002: The role of the thermohaline circulation in abrupt climate change. *Nature*, **415**, 863-869.
- Curry, R., B. Dickson, and I. Yashayaev, 2003: A change in the freshwater balance of the Atlantic Ocean over the past four decades. *Nature*, **426**, 826-829.
- Dye, D. G., 2002: Variability and trends in the annual snow-cover cycle in Northern Hemisphere land areas, 1972-2000. *Hydrological Processes*, **16**, 3065-3077.
- Dynesius, M. and C. Nilsson, 1994: Fragmentation and flow regulation of river systems in the northern third of the world. *Science, New Series*, **266**, 753-762.
- Dyrurgerov, M. B. and C. L. Carter, 2004: Observational Evidence of Increases in Freshwater Inflow to the Arctic Ocean. *Arctic, Antarctic, and Alpine Research*, **36**, 117-122.
- Fallot, J.-M., R. G. Barry, and D. Hoogstrate, 1997: Variations of mean cold season temperature, precipitation and snow depths during the last 100 years in the former Soviet Union (FSU). *Hydrological Sciences Journal*, **42**, 301-328.
- Forland, E. J. and I. Hanssen-Bauer, 2000: Increased precipitation in the Norwegian Arctic: True or false? *Climatic Change*, **46**, 485-509.
- Foster, J. L., J. W. Winchester, and E. G. Dutton, 1992: The date of snow disappearance on the Arctic tundra as determined from satellite, meteorological station and radiometric in situ observations. *IEEE Trans. on Geosci. and Rem. Sens.*, **30**, 793-798.

- Frauenfeld, O. W., T. J. Zhang, R. G. Barry, and D. Gilichinsky, 2004: Interdecadal changes in seasonal freeze and thaw depths in Russia. *Journal of Geophysical Research-Atmospheres*, **109**, doi:10.1029/2003JD004245.
- Georgievsky, V. Y., A. V. Ezhov, A. L. Shalygin, I. A. Shiklomanov, and A. I. Shiklomanov, 1996: Assessment of the effect of possible climate changes on hydrological regime and water resources of rivers in the former USSR. *Russian Meteorology and Hydrology*, **11**, 66-74.
- Groisman, P. Y., 2005: National Climatic Data Center Documentation for TD-9813, Daily and sub-daily precipitation for the Former USSR, 16 pp.
- Groisman, P. Y. and E. Y. Rankova, 2001: Precipitation trends over the Russian permafrost-free zone: Removing the artifacts of pre-processing. *International Journal of Climatology*, **21**, 657-678.
- Groisman, P. Y., T. R. Karl, and R. W. Knight, 1994a: Observed impact of snow cover on the heat-balance and the rise of continental spring temperatures. *Science*, **263**, 198-200.
- Groisman, P. Y., V. V. Koknaeva, T. A. Belokrylova, and T. R. Karl, 1991: Overcoming biases of precipitation measurement - a history of the USSR experience. *Bulletin of the American Meteorological Society*, **72**, 1725-1733.
- Groisman, P. Y., T. R. Karl, R. W. Knight, and G. L. Stenchikov, 1994b: Changes of snow cover, temperature, and radiative heat-balance over the northern-hemisphere. *Journal of Climate*, **7**, 1633-1656.
- Gutzler, D. S. and R. D. Rosen, 1992: Interannual variability of wintertime snow cover across the Northern Hemisphere. *Journal of Climate*, **5**, 1441-1447.
- Haddeland, I., D. P. Lettenmaier, and T. Skaugen, 2006a: Effects of irrigation on the water and energy balances of the Colorado and Mekong river basins. *Journal of Hydrology*, **324**, 210-223.
- Haddeland, I., T. Skaugen, and D. P. Lettenmaier, 2006b: Anthropogenic impacts on continental surface water fluxes. *Geophysical Research Letters*, **33**, doi:10.1029/2006GL026047.

- , 2007: Hydrologic effects of land and water management in North America and Asia: 1700-1992. *Hydrology and Earth System Sciences*, **11**, 1035-1045.
- Hall, D. K., 1988: Assessment of polar climate change using satellite technology. *Rev. Geophys.*, **26**, 26-39.
- Hamlet, A. F. and D. P. Lettenmaier, 2005: Production of temporally consistent gridded precipitation and temperature fields for the continental United States. *Journal of Hydrometeorology*, **6**, 330-336.
- Hamming, R. W., 1989: *Digital Filters*. Prentice Hall, 284 pp.
- Hanasaki, N., S. Kanae, and T. Oki, 2006: A reservoir operation scheme for global river routing models. *Journal of Hydrology*, **327**, 22-41.
- Hinzman, L. D. and D. L. Kane, 1992: Potential response of an arctic watershed during a period of global warming. *J. Geophys. Res.*, **97**, 2811-2820.
- Hinzman, L. D., N. D. Bettez, W. R. Bolton, F. S. Chapin, III, M. B. Dyurgerov, C. L. Fastie, B. Griffith, R. D. Hollister, A. Hope, H. P. Huntington, A. M. Jensen, G. J. Jia, T. Jorgenson, D. L. Kane, D. R. Klein, G. Kofinas, A. H. Lynch, A. H. Lloyd, A. D. McGuire, F. E. Nelson, W. C. Oechel, T. E. Osterkamp, C. H. Racine, V. E. Romanovsky, R. S. Stone, D. A. Stow, M. Sturm, C. E. Tweedie, G. L. Vourlitis, M. D. Walker, D. A. Walker, P. J. Webber, J. M. Welker, K. Winker, and K. Yoshikawa, 2005: Evidence and implications of recent climate change in northern Alaska and other arctic regions. *Climatic Change*, **72**, 251-298.
- Hirsch, R. M., 1982: A comparison of 4 streamflow record extension techniques. *Water Resources Research*, **18**, 1081-1088.
- Hirsch, R. M., J. R. Slack, and R. A. Smith, 1982: Techniques of trend analysis for monthly water-quality data. *Water Resources Research*, **18**, 107-121.
- ICOLD, 2003: *World Register of Dams*, 340 pp.
- Kalnay, E., M. Kanamitsu, R. Kistler, W. Collins, D. Deaven, L. Gandin, M. Iredell, S. Saha, G. White, J. Woollen, Y. Zhu, A. Leetmaa, and B. Reynolds, 1996: The NCEP/NCAR 40-year reanalysis project. *Bulletin of the American Meteorological Society*, **77**, 437-472.

- Kane, D. L. and J. Stein, 1983: Field evidence of groundwater recharge in interior Alaska. *Fourth International Conference on Permafrost*, Fairbanks, Alaska, Nat. Acad. Sci. - Nat. Acad. Press, 572-577.
- Kane, D. L., L. D. Hinzman, M. K. Woo, and K. R. Everett, 1992: Arctic hydrology and climate change. *Arctic Ecosystems in a Changing Climate: an Ecophysiological Perspective*, F. S. Chapin, III, R. L. Jeffries, J. F. Reynolds, G. R. Shaver, J. Svoboda, and E. W. Chu, Eds., Academic Press, 35-37.
- Korobova, D. N., 1968: Optimization by dynamic programming of hydroelectric plant operation regime during initial filling period of multiannual regulation reservoir. *Hydrotechnical Construction*, **2**, 421-425.
- Kwong, Y. T. J. and T. Y. Gan, 1994: Northward migration of permafrost along the Mackenzie Highway and climatic warming. *Climatic Change*, **26**, 399-419.
- Lammers, R. B. and A. I. Shiklomanov, 2000: R-ArcticNet, A Regional Hydrographic Data Network for the Pan-Arctic Region.
- Lammers, R. B., A. I. Shiklomanov, C. J. Vörösmarty, B. M. Fekete, and B. J. Peterson, 2001: Assessment of contemporary Arctic river runoff based on observational discharge records. *Journal of Geophysical Research-Atmospheres*, **106**, 3321-3334.
- Lawrence, D. M. and A. G. Slater, 2005: A projection of severe near-surface permafrost degradation during the 21st century. *Geophysical Research Letters*, **32**, doi: 10.1029/2005GL025080.
- Lettenmaier, D. P., 1976: Detection of trends in water quality data from records with dependent observations. *Water Resources Research*, **12**, 1037-1046.
- Lettenmaier, D. P., E. F. Wood, and J. R. Wallis, 1994: Hydro-Climatological Trends in the Continental United States, 1948-88. *Journal of Climate*, **7**, 586-607.
- Liang, X., D. P. Lettenmaier, E. F. Wood, and S. J. Burges, 1994: A simple hydrologically based model of land-surface water and energy fluxes for general-circulation models. *Journal of Geophysical Research-Atmospheres*, **99**, 14415-14428.

- Liebe, J., N. v. d. Giesen, and M. A. Andreini, 2005: Estimation of small reservoir storage capacities in a semi-arid environment: A case study in the Upper East Region of Ghana. *Physics and Chemistry of the Earth Part B-Hydrology Oceans and Atmosphere*, **30**, 448-454.
- Liston, G. E., 1999: Interrelationships among snow distribution, snowmelt, and snow cover depletion: implications for atmospheric, hydrologic, and ecologic modeling. *J. Appl. Meteor.*, **36**, 1474-1487.
- Lohmann, D., R. Nolte-Holube, and E. Raschke, 1996: A large-scale horizontal routing model to be coupled to land surface parameterization schemes. *Tellus*, **48A**, 708-721.
- Lohmann, D., E. Raschke, B. Nijssen, and D. P. Lettenmaier, 1998: Regional scale hydrology: I. Formulation of the VIC-2L model coupled to a routing model. *Hydrological Sciences Journal*, **43**, 131-141.
- Malik, L. K., N. Koronkevich, I. S. Zaitseva, and E. A. Barabanova, 2000: Briefing Paper on Development of Dams in the Russian Federation and other NIS Countries, Case Study prepared as an input to the World Commission on Dams (<http://www.dams.org/>).
- Manabe, S. and R. J. Stouffer, 1980: Sensitivity of a global climate model to an increase in CO₂ concentration in the atmosphere. *Journal of Geophysical Research-Oceans and Atmospheres*, **85**, 5529-5554.
- Mann, H. B., 1945: Nonparametric tests against trend. *Econometrica*, **13**, 245-259.
- Maurer, E. P., A. W. Wood, J. C. Adam, D. P. Lettenmaier, and B. Nijssen, 2002: A long-term hydrologically based dataset of land surface fluxes and states for the conterminous United States. *Journal of Climate*, **15**, 3237-3251.
- McClelland, J. W., R. M. Holmes, B. J. Peterson, and M. Stieglitz, 2004: Increasing river discharge in the Eurasian Arctic: Consideration of dams, permafrost thaw, and fires as potential agents of change. *Journal of Geophysical Research-Atmospheres*, **109**, doi:10.1029/2004JD004583.
- McClelland, J. W., S. J. Dery, B. J. Peterson, R. M. Holmes, and E. F. Wood, 2006: A pan-arctic evaluation of changes in river discharge during the latter half of the 20th century. *Geophysical Research Letters*, **33**.

- Mekis, E. and W. D. Hogg, 1999: Rehabilitation and analysis of Canadian daily precipitation time series. *Atmosphere-Ocean*, **37**, 53-85.
- Michaels, P. J., R. C. Balling, R. S. Vose, and P. C. Knappenberger, 1998: Analysis of trends in the variability of daily and monthly historical temperature measurements. *Climate Research*, **10**, 27-33.
- Miller, J. R. and G. L. Russell, 1992: The impact of global warming on river runoff. *Journal of Geophysical Research*, **97**, 2757-2764.
- Mitchell, T. D. and D. Jones, 2005: An improved method of constructing a database of monthly climate observations and associated high-resolution grids. *International Journal of Climatology*, **25**, 693-712.
- Nazarov, A. V., 1985: Experience in the operation of hydraulic structures and equipment of hydroelectric stations. *Power Technology and Engineering*, **19**, 154-161.
- Nelson, F. E., O. A. Anisimov, and N. I. Shiklomanov, 2001: Subsidence risk from thawing permafrost - The threat to man-made structures across regions in the far north can be monitored. *Nature*, **410**, 889-890.
- Nijssen, B., G. M. O'Donnell, A. F. Hamlet, and D. P. Lettenmaier, 2001: Hydrologic sensitivity of global rivers to climate change. *Climatic Change*, **50**, 143-175.
- Nijssen, B., D. P. Lettenmaier, X. Liang, S. W. Wetzel, and E. F. Wood, 1997: Streamflow simulation for continental-scale river basins. *Water Resources Research*, **33**, 711-724.
- Overpeck, J., K. Huguken, D. Hardy, R. Bradley, R. Case, M. Douglas, B. Finney, K. Gajewski, G. Jacoby, A. Jennings, S. Lamoureux, A. Lasca, G. MacDonald, J. Moore, M. Retelle, S. Smith, A. Wolfe, and G. Zielinski, 1997: Arctic environmental change of the last four centuries. *Science*, **278**, 1251-1256.
- Pavelsky, T. M. and L. C. Smith, 2006: Intercomparison of four global precipitation data sets and their correlation with increased Eurasian river discharge to the Arctic Ocean. *Journal of Geophysical Research-Atmospheres*, **111**, doi:10.1029/2006JD007230.
- Pavlov, A. V., 1994: Current changes of climate and permafrost in the Arctic and Sub-Arctic of Russia. *Permafrost and Periglacial Proc.*, **5**.

- Peterson, B. J., R. M. Holmes, J. W. McClelland, C. J. Vörösmarty, R. B. Lammers, A. I. Shiklomanov, I. A. Shiklomanov, and S. Rahmstorf, 2002: Increasing river discharge to the Arctic Ocean. *Science*, **298**, 2171-2173.
- Platov, V. I., 1995: Hydropower of Russia: prospects and urgent problems. *Hydrotechnical Construction*, **29**, 421-425.
- Plishkin, G. A., 1979: Possible future hydrologic budget of the Ob' river basin. *Soviet Hydrology: Selected Papers*, **18**, 332-337.
- Press, W. H., S. A. Teukolsky, W. T. Vetterling, and B. P. Flannery, 1992: *Numerical Recipes in C*. 2 ed. Cambridge University Press.
- Rawlins, M. A., C. J. Willmott, A. Shiklomanov, E. Linder, S. Froking, R. B. Lammers, and C. J. Vörösmarty, 2006: Evaluation of trends in derived snowfall and rainfall across Eurasia and linkages with discharge to the Arctic Ocean. *Geophysical Research Letters*, **33**, doi: 10.1029.2005GL025231.
- Revenge, C., S. Murray, J. Abramovitz, and A. Hammond, 1998: Watersheds of the World: Ecological value and vulnerability.
- Robinson, D. A. and K. F. Dewey, 1990: Recent secular variations in the extent of Northern Hemisphere snow cover. *Geophys. Res., Lett.*, **17**, 1557-1560.
- Robinson, D. A. and A. Frei, 2000: Seasonal variability of Northern Hemisphere snow extent using visible satellite data. *Prof. Geographer*, **52**, 307.
- Roderick, M. L. and G. D. Farquhar, 2002: The Cause of Decreased Pan Evaporation over the Past 50 Years. *Science*, **298**, 1410-1411.
- Rouse, W. R., M. S. V. Douglas, R. E. Hecky, A. E. Hershey, G. W. Kling, L. Lesack, P. Marsh, M. McDonald, B. J. Nicholson, N. T. Roulet, and J. P. Smol, 1997: Effects of climate change on the freshwaters of Arctic and Subarctic North America. *Hydrological Processes*, **11**, 873-902.
- Savelieva, N. I., I. P. Semiletov, L. N. Vasilevskaya, and S. P. Pugach, 2000: A climate shift in seasonal values of meteorological and hydrological parameters for northeastern Asia. *Progress in Oceanography*, **47**, 279-297.

- Serreze, M. C., M. P. Clark, and D. H. Bromwich, 2003: Monitoring precipitation over the Arctic terrestrial drainage system: Data requirements, shortcomings, and applications of atmospheric reanalysis. *Journal of Hydrometeorology*, **4**, 387-407.
- Serreze, M. C., D. H. Bromwich, M. P. Clark, A. J. Etringer, T. J. Zhang, and R. Lammers, 2002: Large-scale hydro-climatology of the terrestrial Arctic drainage system. *Journal of Geophysical Research-Atmospheres*, **108**, doi: 10.1029/2001JD000919.
- Serreze, M. C., J. E. Walsh, F. S. Chapin, III, T. Osterkamp, M. Dyurgerov, V. Romanovsky, W. C. Oechel, J. Morison, T. Zhang, and R. G. Barry, 2000: Observational evidence of recent change in the northern high-latitude environment. *Climatic Change*, **46**, 159-207.
- Sheffield, J., A. D. Ziegler, E. F. Wood, and Y. Chen, 2004: Correction of the high-latitude rain day anomaly in the NCEP/NCAR reanalysis for land surface hydrological modeling. *Journal of Climate*, **17**, 3814-3828.
- Shepard, D. S., 1984: Computer mapping: The SYMAP interpolation algorithm. *Spatial Statistics and Models*, G. L. Gaile and C. J. Willmott, Eds., D. Reidel, 133-145.
- Shiklomanov, A. I., R. B. Lammers, and C. J. Vörösmarty, 2002: Widespread decline in hydrologic monitoring threatens pan-Arctic research. *EOS Transactions of the American Geophysical Union*, **83**, 13.
- Shiklomanov, A. I., T. I. Yakovleva, R. B. Lammers, I. P. Karasev, C. J. Vörösmarty, and E. Linder, 2006: Cold region river discharge uncertainty - estimates from large Russian rivers. *Journal of Hydrology*, **326**, 231-256.
- Shiklomanov, I. A., 1978: Dynamics of anthropogenic changes in annual river runoff in the USSR. *Soviet Hydrology: Selected Papers*, **17**, 11-22.
- Shiklomanov, I. A. and G. M. Veretennikova, 1978: Effect of reservoirs on the annual runoff of rivers in the USSR. *Soviet Hydrology: Selected Papers*, **17**, 12-32.
- Shiklomanov, I. A., A. I. Shiklomanov, R. B. Lammers, B. J. Peterson, and C. J. Vörösmarty, 2000: The dynamics of river water inflow to the Arctic Ocean. *The Freshwater Budget of the Arctic Ocean: Proceedings of the NATO Advanced Research Workshop*, E. L. Lewis, Ed., Kluwer Acad., 281-296.

- Smith, L. C., Y. Sheng, G. M. MacDonald, and L. D. Hinzman, 2005: Disappearing Arctic lakes. *Science*, **308**, 1429-1429.
- Smith, L. C., T. M. Pavelsky, G. M. MacDonald, A. I. Shiklomanov, and R. B. Lammers, 2007: Rising minimum flows in northern Eurasian rivers suggest a growing influence of groundwater in the high-latitude water cycle. *Journal of Geophysical Research (in review)*.
- Snover, A. K., A. F. Hamlet, and D. P. Lettenmaier, 2003: Climate-change scenario's for water planning studies - Pilot applications in the Pacific Northwest. *Bulletin of the American Meteorological Society*, **84**, 1513-1518.
- Stafievskii, V. A., V. A. Bulatov, E. N. Reshetnikova, N. I. Stefanenko, L. S. Permyakova, and A. P. Epifanov, 2003: State of the dam of the Sayano-Shushenskaya hydropower plant in the last stage of reconditioning of the pressure-face concrete and contact zone of the rock bed. *Power Technology and Engineering*, **37**, 331-337.
- Storck, P. and D. P. Lettenmaier, 1999: Predicting the effect of a forest canopy on ground snow accumulation and ablation in maritime climate. *Proceedings of the 67th Snow Conference*, C. Troendle, Ed., Colorado State University, 1-12.
- Sturm, M., J. P. McFadden, G. E. Liston, F. S. Chapin, III, J. Holmgren, and M. Walker, 2001: Snow-shrub interactions in Arctic tundra: A hypothesis with climatic implications. *Journal of Climate*, **14**, 336-344.
- Su, F. G., J. C. Adam, L. C. Bowling, and D. P. Lettenmaier, 2005: Streamflow simulations of the terrestrial Arctic domain. *Journal of Geophysical Research-Atmospheres*, **110**, doi:10.1029/2004JD005518.
- Sun, S. and X. Zhang, 2004: Effect of the lower boundary position of the Fourier equation on the soil energy balance. *Advances in Atmospheric Sciences*, **21**, 868-878.
- Taylor, J. R., 1997: *An introduction to error analysis: the study of uncertainties in physical measurements*. 2 ed. University Science Books, 327 pp.
- Thie, J., 1974: Distribution and thawing of permafrost in the southern part of the discontinuous zone in Manitoba. *Arctic*, **27**, 189-200.

- Thornton, P. E. and S. W. Running, 1999: An improved algorithm for estimating incident daily solar radiation from measurements of temperature, humidity, and precipitation. *Agric. For. Meteor.*, **93**, 211-228.
- Van der Linden, S., T. Virtanen, N. Oberman, and P. Kuhry, 2003: Sensitivity Analysis of Discharge in the Arctic Usa Basin. *East-European Russia Climatic Change*, **57**, 139-161.
- Vörösmarty, C. J. and D. Sahagian, 2000: Anthropogenic disturbance of the terrestrial water cycle. *Bioscience*, **50**, 753-765.
- Vrugt, J. A., H. V. Gupta, W. Bouten, and S. Sorooshian, 2003: A Shuffled Complex Evolution Metropolis algorithm for optimization and uncertainty assessment of hydrologic model parameters. *Water Resources Research*, **39**.
- Vyruchalkina, T. Y., 2004: Lake Baikal and the Angara River before and after the construction of reservoirs. *Water Resources*, **31**, 526-532.
- Walter, K. M., S. A. Zimov, J. P. Chanton, D. Verbyla, and F. S. Chapin, III, 2006: Methane bubbling from Siberian thaw lakes as a positive feedback to climate warming. *Nature*, **443**, 71-75.
- White, D., L. Hinzman, L. Alessa, J. Cassano, M. Chambers, K. Falkner, J. Francis, W. Gutowski, M. Holland, M. Holmes, H. Huntington, D. Kane, A. Kliskey, C. Lee, J. McClelland, B. Peterson, F. Straneo, M. Stelle, R. Woodgate, D. Q. Yang, K. Yoshikawa, and T. Zhang, 2007: The Arctic freshwater system: changes and impacts. *Journal of Geophysical Research (in review)*.
- Williams, P. J. and M. W. Smith, 1989: *The frozen earth: fundamentals of geocryology*. Cambridge University Press.
- Willmott, C. J. and K. Matsuura, 2005: Arctic Land-Surface Precipitation: 1930-2004 Gridded Monthly Time Series (V. 1.03).
- Woo, M.-K., A. G. Lewkowicz, and W. R. Rouse, 1992: Response of the Canadian permafrost environment to climatic change. *Phys. Geogr.*, **134**, 287-317.
- Wood, A. W., L. R. Leung, V. Sridhar, and D. P. Lettenmaier, 2004: Hydrologic implications of dynamical and statistical approaches to downscaling climate model outputs. *Climatic Change*, **62**, 189-216.

- Wu, P. L., R. Wood, and P. Stott, 2005: Human influence on increasing Arctic river discharges. *Geophysical Research Letters*, **32**, doi: 10.1029/2004GL021570.
- Yang, D. Q., B. S. Ye, and A. Shiklomanov, 2004a: Discharge characteristics and changes over the Ob River watershed in Siberia. *Journal of Hydrometeorology*, **5**, 595-610.
- Yang, D. Q., B. S. Ye, and D. L. Kane, 2004b: Streamflow changes over Siberian Yenisei River Basin. *Journal of Hydrology*, **296**, 59-80.
- Yang, D. Q., D. Robinson, Y. Y. Zhao, T. Estilow, and Y. Baisheng, 2003: Streamflow response to seasonal snow cover extent changes in large Siberian watersheds. *Journal of Geophysical Research*, **108**, 1-14.
- Yang, D. Q., D. Kane, Z. P. Zhang, D. Legates, and B. Goodison, 2005: Bias corrections of long-term (1973-2004) daily precipitation data over the northern regions. *Geophysical Research Letters*, **32**, doi:10.1029/2005GL024057.
- Yang, D. Q., D. Kane, L. Hinzman, X. Zhang, T. Zhang, and H. Ye, 2002: Siberian Lena river hydrologic regime and recent change. *Journal of Geophysical Research*, **107**, doi:10.1029/2002JD002542.
- Ye, B. S., D. Q. Yang, and D. L. Kane, 2003: Changes in Lena River streamflow hydrology: Human impacts versus natural variations. *Water Resources Research*, **39**, 1200-1213.
- Ye, H., H. Cho, and P. E. Gustafson, 1998: The changes in Russian winter snow accumulation during 1936-83 and its spatial pattern. *Journal of Climate*, **11**, 856-863.
- Ye, H., D. Q. Yang, T. Zhang, X. Zhang, S. Ladochy, and M. Ellison, 2004: The impact of climatic conditions on seasonal river discharges in Siberia. *Journal of Hydrometeorology*, **5**, 286-295.
- Yoshikawa, K. and L. D. Hinzman, 2003: Shrinking thermokarst ponds and groundwater dynamics in discontinuous permafrost near Council, Alaska. *Permafrost and Periglacial Processes*, **14**, 151-160.

- Zhang, T., R. Barry, and D. Gilichinsky, 2001: (updated 2006) Russian historical soil temperature data. Boulder, Colorado USA: National Snow and Ice Data Center. Digital media.
- Zhang, T., M. C. Serreze, D. Yang, D. Gilichinsky, A. Etringer, H. Ye, R. G. Barry, and S. M. Chudinova, 2003: Permafrost degradation and hydrologic response in the Russian Arctic drainage basin. *Geophysical Research Abstracts*, **5**.
- Ziegler, A. D., J. Sheffield, E. P. Maurer, B. Nijssen, E. F. Wood, and D. P. Lettenmaier, 2003: Detection of intensification in global- and continental-scale hydrological cycles: temporal scale evaluation. *Journal of Climate*, **16**, 535-547.

Curriculum Vitae

EDUCATION:

University of Washington, Ph.D. Candidate, anticipated completion: June, 2007

- Department of Civil and Environmental Engineering
- Dissertation Title: "Exploration of the roles of human and climatic influences on annual and seasonal streamflow changes in the Eurasian Arctic"
- Advisor: Dr. Dennis P. Lettenmaier

University of Washington, M.S.C.E., 2002

- Department of Civil and Environmental Engineering
- Thesis Title: "Adjustment of global gridded precipitation for systematic bias"
- Advisor: Dr. Dennis P. Lettenmaier

University of Colorado, Boulder, B.S. (with distinction), 1997

- Department of Civil, Environmental, and Architectural Engineering
- Research Project Title: "The Interrelationships between ammonia and manganese removal during nitrification"
- Advisor: Dr. Marc A. Edwards (now at Virginia Tech, Blacksburg, VA)

Colorado Outward Bound Wilderness Semester, summer 1995

- 51-day mountaineering course emphasizing leadership skills

RESEARCH:

Arctic hydrological modeling and climate change, 2003 to present

- Development and parameterization of cold land processes in a large-scale hydrological modeling framework; application over land areas contributing runoff to the Arctic Ocean.
- Concurrent use of modeling and observed data to explore the relative roles of climatic and human influences on observed hydrologic changes in Arctic regions.
- Advisor: Dr. Dennis P. Lettenmaier (U. of Washington). Collaborators: Dr. Laura C. Bowling (now at Purdue U., IN), Dr. Fengge Su (U. of Washington), Dr. Daqing Yang (U. of Alaska, Fairbanks), Dr. Keith A. Cherkauer (now at Purdue U., IN)

Global-scale hydrological modeling and climate change effects on global water availability, 2005

- Applied a global-scale land surface hydrology model to delineate the regions of the world where warming-induced effects on streamflow seasonality are likely to cause increased dry season water stress.
- Collaborators: Dr. Tim P. Barnett (Scripps Inst. of Ocean, CA), Dr. Dennis P. Lettenmaier (U. of Washington)

Bias-correction of global precipitation climatology products, 2000 to 2005

- Corrected global gridded precipitation datasets for gauge under-catch and for orographic effects caused by the under-representation of precipitation

measurements in mountainous regions.

- Advisor: Dr. Dennis P. Lettenmaier (U. of Washington). Collaborators: Dr. Eric F. Wood (Princeton U., NJ), Elizabeth A. Clark (now at Stanford U., CA)

Retrospective simulation of hydrologic states and fluxes for the conterminous United States, 2000 to 2002

- Participated in a hydrologic modeling study to develop a set of spatially-distributed energy and water fluxes and states over the United States from 1950 to 2000, for use in studies where ground observations are sparse or intermittent.
- Collaborators: Dr. Dennis P. Lettenmaier (U. of Washington), Dr. Edwin P. Maurer (now at Santa Clara U., CA), Dr. Andrew W. Wood (U. of Washington), Dr. Bart Nijssen (now at 3Tier Environmental Forecasting Group, Seattle, WA)

Nitrification and manganese removal in wastewater treatment processes, 1996 to 1997

- Provided evidence that bacteria found in the nitrogen trickling filter at the City of Boulder Wastewater Treatment Plant are able to remove both ammonia and manganese from sewage, and examined possible removal mechanisms.
- Advisor: Dr. Marc A. Edwards (now at Virginia Tech, VA)

TEACHING:

Peace Corps Volunteer, 1997 to 1999

- Pawa Provincial Secondary School, Makira Province, Solomon Islands
- Courses: Years 2 and 3 mathematics, Year 2 social science
- Other duties: coordination of extracurricular projects and events, preparation of Year 3 mathematics students for the national exam, school librarian, dormitory counselor, supervision of meals and work sessions

Community Service

- TeachREACH mentor, 2005-2006 school year
 - Mentored a junior high school girl in the areas of science, technology, engineering, and mathematics.
- Women in Science and Engineering, Martin Luther King Day Event, 2001, 2002
 - Brought elementary school students on a tour of the Seattle Science Center and explored science and engineering with them.

Undergraduate Teaching Assistant, Fall 1996

- Introduction to Environmental Engineering, University of Colorado, Boulder
- Led review sessions, held office hours, and graded homework.

AWARDS and HONORS:

- Center for Water and Watershed Studies Andy Studebaker Travel Fellowship, Dec., 2006
- Climate and Cryosphere (CliC) Travel Award, Apr., 2005
- Society of Women Engineers, Outstanding Female Graduate Student, Department of Civil and Environmental Engineering, University of Washington, 2003
- Milo S. Ketchum Award for Outstanding Undergraduate, University of Colorado

Department of Civil, Environmental, and Architectural Engineering, 1997

- 1st Place Undergraduate Division, American Society of Civil Engineers Student Paper Competition, 1997
- 3rd Place Undergraduate Division, Water Environment Federation Student Paper Competition, 1997
- University of Colorado Undergraduate Research Opportunities Program Research Grant, 1996

AFFILIATIONS and PROFESSIONAL ACTIVITIES:

Student Organization

- University of Washington Program on Climate Change, 2003 to present

National Organizations

- American Geophysical Union, 2001 to present
- American Meteorological Society, 2003 to present

Honorary Societies

- Tau Beta Pi, University of Colorado chapter, 1997
- Chi Epsilon, University of Colorado chapter, 1995

Peer Review Activities

- Journals: *Atmospheric Research*, *Geophysical Research Letters*, *Journal of Geophysical Research*, *Journal of Hydrology*, *Journal of Hydrometeorology*, *Water Resources Research*
- Funding Agency: National Science Foundation

Field Activities

- Snow depth, density, and grain size sampling as part of the NASA Cold Land Processes Field Experiment (CLPX), Colorado (Spring, 2003)
- Tundra lake (water volume and quality) monitoring, Kuparuk Oil Field, Alaska (Summer, 2003)
- Permafrost active layer depth sampling and streamflow gauging, Nome, Alaska (Fall, 2003)

PUBLICATIONS:

- Adam, J.C., I. Haddeland, F. Su, and D. P. Lettenmaier, 2007. Simulation of reservoir influences on annual and seasonal streamflow changes for the Lena, Yenisei and Ob' Rivers, *Journal of Geophysical Research* (accepted).
- Adam, J.C., and D.P. Lettenmaier, 2007. Application of new long-term precipitation, temperature, and reconstructed streamflow products to a streamflow trend attribution study in Northern Eurasia. *Journal of Climate* (accepted).
- Maurer, E.P., J.C. Adam, and A.W. Wood, 2007. Climate Model based consensus on the hydrologic impacts of climate change to the Rio Lempa basin of Central America, *Hydrological Sciences Journal* (in review).
- Adam, J.C., E.A. Clark, D.P. Lettenmaier, and E.F. Wood, 2006. Correction of global precipitation products for orographic effects. *Journal of Climate* 19(1): 15-38.
- Su, F., J.C. Adam, K.E. Trenberth, and D.P. Lettenmaier, 2006. Evaluation of surface

- water fluxes of the pan-Arctic land region with a land surface model and ERA-40 reanalysis. *Journal of Geophysical Research* 111, D05110, doi:10.1029/2005JD006387.
- Barnett T.P., J.C. Adam, and D.P. Lettenmaier, 2005. Potential impacts of a warming climate on water availability in snow-dominated regions. *Nature* 438: 303-309.
- Su, F., J.C. Adam, L.C. Bowling, and D.P. Lettenmaier, 2005. Streamflow simulations of the terrestrial Arctic domain. *Journal of Geophysical Research* 110, D08112, doi:10.1029/2004JD005518.
- Adam, J.C., and D.P. Lettenmaier, 2003. Adjustment of global gridded precipitation for systematic bias. *Journal of Geophysical Research* 108, D9, doi:10.1029/2002JD002499.
- Maurer, E.P., A.W. Wood, J.C. Adam, D.P. Lettenmaier, and B. Nijssen, 2002. A long-term hydrologically-based data set of land surface fluxes and states for the conterminous United States. *Journal of Climate* 15: 3237-3251.

MEETING ABSTRACTS:

- Adam, J.C., I. Haddeland, F. Su, and D.P. Lettenmaier, 2006. Simulation of Reservoir Effects on Seasonal and Annual Streamflow for the Lena, Yenisei, and Ob' Rivers. *AGU Fall Meeting Abstracts*, San Francisco, CA, Dec. 11-15.
- Adam, J.C., and D.P. Lettenmaier, 2006. Trend Attribution of Northern Eurasian Stream Flow. Program on Climate Change Graduate Conference on Climate Change, Pack Forest, WA, Apr. 7-9.
- Lettenmaier, D.P., J.C. Adam, and T. Barnett, 2006. Sensitivity of snow-dominated hydrologic regimes to global warming. *EGU Annual Meeting Abstracts*, Vienna, Austria, Apr. 2-7.
- Adam, J.C., F. Su, and D.P. Lettenmaier, 2005. Exploring the effects of precipitation changes on the variability of pan-Arctic river discharge. *AGU Fall Meeting Abstracts*, San Francisco, CA, Dec. 5-9.
- Adam, J.C., T.P. Barnett, and D.P. Lettenmaier, 2005. Impacts of a warming climate on water availability in snow-dominated regions. *US Climate Change Science Program Workshop Abstracts*, Arlington, VA, Nov. 14-16.
- Adam, J.C., D.P. Lettenmaier, F. Su, and L.C. Bowling, 2005: Exploring the contributing effects of climate and land surface changes on the variability of pan-Arctic river discharge and surface albedo. *1st Climate and Cryosphere International Science Conference Abstracts*, Beijing, China, Apr. 11-15.
- Su, F., J.C. Adam, L.C. Bowling, and D.P. Lettenmaier, 2005: Hydrological simulations for the pan-Arctic drainage system. *1st Climate and Cryosphere International Science Conference Abstracts*, Beijing, China, Apr. 11-15.
- Adam, J.C., D.P. Lettenmaier, E. Clark, and E.F. Wood, 2005. Correction of global precipitation products for systematic bias and orographic effects. *85th AMS Annual Meeting Abstracts*, San Diego, CA, Jan. 8-14.

- Su, F., J.C. Adam, K.E. Trenberth, and D.P. Lettenmaier, 2005. Evaluation of surface water fluxes of the pan-Arctic land region with a land surface model and ERA-40 reanalysis. *85th AMS Annual Meeting Abstracts*, San Diego, CA, Jan. 8-14.
- Adam, J.C., D.P. Lettenmaier, E.A. Clark, and E.F. Wood, 2005. Correction of global precipitation products for orographic effects. *5th International Scientific Conference on the Global Energy and Water Cycle Abstracts*, Orange County, CA, Jun. 19-23.
- Adam, J.C., D.P. Lettenmaier, F. Su, and L.C. Bowling, 2004. Exploring the role of land surface changes on the variability of pan-Arctic discharge. *AGU Fall Meeting Abstracts*, San Francisco, CA, Dec. 13-17.
- Adam, J.C., D.P. Lettenmaier, E.A. Clark, and E.F. Wood, 2004. Correction of global precipitation products for orographic effects. *8th International Conference on Precipitation Abstracts*, Vancouver, BC, Aug. 8-11.
- Adam, J.C., D.P. Lettenmaier, E.A. Clark, and E.F. Wood, 2004. Correction of global precipitation products for orographic effects. *84th AMS Annual Meeting Abstracts*, Seattle, WA, Jan. 11-15.
- Adam, J.C., D.P. Lettenmaier, F. Su, L.C. Bowling, 2004. Model-based estimation of river flows to the Arctic Ocean. *AGU, CGU, and SEG Joint Meeting Abstracts*, Montreal, Quebec, May 17-21.
- Su, F., J.C. Adam, D.P. Lettenmaier, and L.C. Bowling, 2003. Streamflow simulations of the terrestrial Arctic domain. *AGU Fall Meeting Abstracts*, San Francisco, CA, Dec. 8-12.
- Adam, J.C., D.P. Lettenmaier, F. Su, and L.C. Bowling, 2003. Simulated water and energy fluxes of the pan-Arctic land region. *1st Study of Environmental Arctic Change Open Science Meeting Abstracts*, Seattle, WA, Oct. 27-30.
- Adam, J.C., and D.P. Lettenmaier, 2002. Bias correction of global gridded precipitation for solid precipitation undercatch. *AGU Fall Meeting Abstracts*, San Francisco, CA, Dec. 6-10.
- Maurer, E.P., A.W. Wood, J.C. Adam, B. Nijssen, and D.P. Lettenmaier, 2001. Derived continental U.S. land surface hydrologic fluxes and state variables, 1950-2000. *AGU Fall Meeting Abstracts*, San Francisco, CA, Dec. 10-14.
- Mullis, J.C., and M.A. Edwards, 1997. The interrelationships between ammonia and manganese removal during nitrification. *Proceedings of the CSCE/ASCE Environmental Engineering Conference*, Edmonton, Alberta, Jul. 22-26.